ABSTRACT

Title of Dissertation:	The role of consistent turbulence energetics in the representation of dry and shallow convection
	David Andrew New, Doctor of Philosophy, 2019
Dissertation directed by:	Professor Xin-Zhong Liang Department of Atmospheric and Oceanic Science

In this doctoral dissertation, the role of consistent turbulence energetics is examined in the context of sub-grid turbulence, convection, and cloud condensation parameterizations for numerical weather and climate models. The property of energetic consistency is formally defined and divided into two categories, local and non-local, and various common parameterization approaches are classified according this framework. I show theoretically that the basis of local energetic consistency is the inclusion of mean-gradient transport and buoyancy acceleration terms in the diagnostic and prognostic budget equations of all second-order statistical moments, including fluxes. Effectively, these terms account for the conversion between turbulent kinetic energy (TKE) and turbulent potential energy (TPE) under stably stratified conditions. With simple numerical experiments, I show that if local energetic consistency is not satisfied, then thermodynamic profiles cannot be

correctly predicted under stably conditions, such as in the boundary layer capping inversion. I then extend the concept of energetic consistency from local turbulent mixing to non-local convective transport. I show that the popular eddy diffusivity-mass flux (EDMF) approach for unified parameterization of turbulence and convection treats the turbulent transport of turbulent energy in two parallel but inconsistent ways: advectively and diffusively. I introduce a novel parameterization approach, inspired by EDMF, that consistently partitions all second-order moments, including TKE, between convective and non-convective parts of a grid cell and show that this approach predicts significantly more realistic depths of convective boundary layers than conventional EDMF schemes. Finally, I introduce a novel method for validating this parameterization approach, based on Langragian particle tracking in large-eddy simulations.

THE ROLE OF CONSISTENT TURBULENCE ENERGETICS IN THE REPRESENTATION OF DRY AND SHALLOW CONVECTION

by

David Andrew New

Dissertation submitted to the Faculty of the Graduate School of the
University of Maryland, College Park, in partial fulfillment
of the requirements for the degree of
Doctor of Atmospheric and
Oceanic Science
2019

Advisory Committee:
Professor Xin-Zhong Liang Chair
Professor Da-Lin Zhang
Dr. Andrea Molod
Dr. David Turner
Dr. Michael Ek
Professor Emeritus Peter Bernard

Dedication

This doctoral dissertation is dedicated to my parents, Marion and Dale, my partner, Gina Mazzuca, my advisor, Professor Xin-Zhong Liang, my close friends, Anthony Carlson and Michael Paster, and my cats, Loki and Luna. I could not have come this far without their patient love and support.

This dissertation is also dedicated to Michael J. Mazzuca (1946-2019). His wisdom lives on in those who had the privilege of knowing him.

Acknowledgements

This material is based upon work supported by the National Oceanic and Atmospheric Administration, Educational Partnership Program, U.S. Department of Commerce, under Agreement No. NA11SEC4810003.

This work was later supported by the NASA Earth and Space Sciences Fellowship (NESSF) under Grant #NNX15AN46H

Special thanks are due to Professor Xin-Zhong Liang for supporting me during my final semester at the University of Maryland.

Special thanks are also due to Professor Ann Wylie her financial support via the 2015 Green Fund Award.

Table of Contents

List of Tables

List of Figures

Figure 7.6 *The left panel depicts the mass flux profile of the "updraft particles" for the DCBL case. The rate panel depicts the corresponding entrainment and detrainment rates.*

Figure 7.7 *The left panel depicts the mass flux profile of the "updraft particles" for the DCBL case, after implementing the entrainment scheme. The rate panel depicts the corresponding entrainment and detrainment rates*

List of Abbreviations

ADHOC: *assumed distribution-high-order closure*

CBL: *convective boundary layer*

DCBL: *dry convective boundary layer*

EMDF: *eddy diffusivity-mass flux*

GCM: *general circulation model*

HOC: high-order closure

LES: *large-eddy simulation*

MLEC: *moist local energetic consistency*

TKE: *turbulent kinetic energy*

TPE: *turbulent potential energy*

TTE: *total turbulent energy*

SCM: *single-column model*

SCBL: *stratocumulus-topped boundary layer*

Chapter 1: Introduction

1.1 Motivation

The representation of boundary-layer turbulence and clouds remains among the most stubborn sources of bias and uncertainty in numerical weather and climate prediction models (Bony et al. 2015; Siebesma et al. 2004; Teixeira et al. 2011). The difficulty lies in the fact that boundary layer processes occur at scales smaller than the size of grid cells in contemporary models, so that their effects must be treated statistically as a function of the model's resolved state variables. The formulation from first principles of such sub-models, called parameterizations, is non-trivial and permits multiple alternative representations of the same physical processes. Moreover, the choice of the level of complexity for the representation of sub-grid physics is embedded in a cost-benefit analysis for how to allocate each additional CPU-hour: more complex sub-grid physics, higher spatial/temporal resolution, or more advanced data assimilation techniques. Additional physics comes at the cost of additional computational resources, numerical instability, and uncertainty as to how to model certain processes.

The original intent of my doctoral research was to address the more specific and cutting-edge problem of how to model turbulence and shallow moist convection in a unified manner. Traditionally, models have distributed the responsibility of treating these processes (along with microphysics, radiation, surface processes, etc.) across separate parameterizations, each communicating with the other primarily indirectly

through the resolved, grid-scale state. Conceptually, this is problematic, because of the unified nature of these processes. For example, cumulus clouds are simply buoyant thermals that originate near the surface and have sufficient potential energy to reach an altitude where condensation of their water vapor occurs. Practically, this is problematic however, since modeling studies have shown that this ad-hoc coupling leads to problematic interactions between parameterizations which are responsible for systematic prediction errors (Lenderink et al. 2004; Neggers et al. 2004) and unrealistic transitions between various boundary layer regimes (Teixeira et al. 2011). This has inspired a wide range of attempts over the previous two decades to unify the representation of boundary layer processes under a single parameterization (Chienet 2003, 2004; Golaz et al. 2002a,b; Köhler et al. 2011; Lappen and Randall 2001a,b,c; Siebesma and Teixeira 2000; Siebesma et al. 2007; Soares et al. 2004; Sušelj et al. 2012, 2013, 2014; Tan et al. 2018).

Thus, drawn to the importance and challenge of this problem, I proposed for my doctoral research to develop a unified turbulence-shallow convection parameterization based on my own novel method of combining two other popular methods: the eddy diffusivity-mass flux (EDMF) and assumed distribution-high order closure (ADHOC) approaches. The motivation for this design was to address certain physical inconsistencies associated with each by retaining aspects of the other, recognizing that EDMF and ADHOC can be understood as special cases of one another. However, I soon learned how difficult the problem I had undertaken was. By the time I defended by thesis prospectus, the prototype of my parameterization

was still unable to reasonably simulate a simple convective boundary layer. Moreover, while I intuitively understood the reason for certain design choices I had made, I did not have concrete reasons for them. During my prospectus defense, Professor Da-Lin Zhang, a member of my dissertation committee, asked me a question that I did not have a strong answer to: *why is it better to use a high-order closure to model turbulent mixing rather than a lower-order approach?* Essentially, this question can be restated more simply as: *why is it better to use a more complex representation of turbulence?*

This stalemate and Professor Zhang's question caused me to put the development of my parameterization on hold and led my research in a second parallel direction, with the goal of addressing two related and even more fundamental questions. First, *what does it actually mean, objectively speaking, to represent a sub-grid physical process?* For example, eddy diffusion, the simplest and most common method for modeling turbulent mixing, is justified physically in many atmospheric physics textbooks (e.g. Holton 2004) on the basis of mixing length theory. However, as I will discuss in depth in this dissertation, it can also be justified as a quasi-steady approximation of the budget equations for turbulent fluxes. Which justification, one might wonder, is objective truth and which is fantasy? The second key question I wished to address was: *what are the concrete advantages and disadvantages associated with different levels/orders of turbulence closure?* It is not always clear why model developers chose a certain level of complexity and approximation for their parameterizations, such as which turbulence state variables to make prognostic. Approximation is in

some ways the goal of numerical modeling, but when does too much or poorly chosen approximation compromise our trust in a model's predictions?

The process of addressing these questions revealed to me the different degrees to which various boundary layer parameterizations treat turbulence and convection in an energetically consistent fashion. Moreover, I came to realize that there are two types of energetic consistency: local and non-local. Local energetic consistency is closely related to Professor Zhang's question: why use a high-order closure? Non-local energetic consistency is related to the original question my research aimed at addressing of how to unify the representation of turbulence and convection. With the framework of energetic consistency guiding me, I returned to my original proposed parameterization in the final year of my doctoral study. By understanding the concrete advantages and disadvantages of different design choices, I stripped my parameterization of unnecessary complexity that compromised its robustness and numerical stability. After reworking it in this way, I finally developed a parameterization that significantly outperforms conventional approaches in simulating the depth of the convective boundary layer.

1.2 The closure problem and sub-grid process representation

At the core of the boundary-layer parameterization problem is the closure problem: how to determine sub-grid fluxes appearing in the Reynolds-averaged prognostic equations of mean wind and thermodynamic variables. Consider a simple anelastic atmospheric model with four prognostic mean state variables: two mean horizontal

winds, $\overline{u}$ and $\overline{v}$, mean liquid water potential temperature $\overline{\theta_l}$, and mean total water specific humidity $\overline{q_t}$, where overbars denote Reynold averages over the volume of a model grid cell. The prognostic equation for an arbitrary mean state variable $\overline{\phi} \in \left\{\overline{u}, \overline{v}, \overline{\theta_l}, \overline{q_t}\right\}$ is given by:

$$\frac{\partial \overline{\phi}}{\partial t} = -\overline{\mathbf{v}} \cdot \nabla \overline{\phi} - \frac{1}{\rho_0} \frac{\partial \rho_0 \overline{w'\phi'}}{\partial z} + \overline{F_\phi} \quad (1.1)$$

where primes denote deviations from the mean, and $\overline{F_\phi}$ is the sum of all mean forcings due to processes such as diabatic heating, radiation, or Coriolis acceleration. *Thus, stated formally, the closure problem is how to determine* $\overline{w'\phi'}$ *as a function of the prognostic state variables of the model.*

The complexity of a closure is typically classified according to its "order". They range from first-order schemes, which diagnose fluxes semi-empirically as a function of mean (first-order) state variables alone, to 1.5-order closures which include additional high-order moments as prognostic "turbulence state variables", to second-order (and higher) closures which treat all second-order moments including fluxes as prognostic variables. The problem driving the choice of closure order is the presence of a $n+1$-order moment in the budget equation of any nth-order moment. For example, equation (1.1) is the budget equation for the first-order moment $\overline{\phi}$, and it contains a term with the second-order moment $\overline{w'\phi'}$. The budget equation for $\overline{w'\phi'}$ is then given by:

$$\frac{\partial \overline{w'\phi'}}{\partial t} = \overline{b'\phi'} - \overline{w'^2} \frac{\partial \overline{\phi}}{\partial z} - \frac{1}{\rho_0} \frac{\partial \rho_0 \overline{w'^2 \phi'}}{\partial z} - \frac{1}{\rho_0} \overline{\phi' \frac{\partial p'}{\partial z}} - \epsilon_{w\phi} \quad (1.2)$$

This second-order budget then contains a term with the third-order moment $\overline{w'^2\phi'}$, as well as other second-order moments such as $\overline{b'\phi'}$ and $\overline{w'^2}$. Thus, not all high-order moments can be determined from their budget equations, since this would require to an infinite cascade of governing equations. Thus arises Professor Zhang's question about the level of closure: where to truncate along this cascade?

Another question arises from equation (1.2) about the physical interpretation of each term on its RHS. These terms are derived by applying the product rule to the tendency of $\overline{w'\phi'}$, so that:

$$\frac{\partial \overline{w'\phi'}}{\partial t} = \overline{w' \frac{\partial \phi'}{\partial t} + \phi' \frac{\partial w'}{\partial t}} \quad (1.3)$$

Thus, each term on the RHS of (1.2) is associated with one or more terms in the budgets of w' and ϕ'. Table (1.1) depicts these correspondences.

$\mathcal{S}$	$\mathcal{M}$	$\mathcal{T}$	$\mathcal{B}$	$\mathcal{P}$	$\mathcal{D}$
$\frac{\partial \overline{w'\phi'}}{\partial t}$	$-\overline{w'^2}\frac{\partial \overline{\phi}}{\partial z}$	$-\frac{1}{\rho_0}\frac{\partial \rho_0 \overline{w'\phi'^2}}{\partial z}$	$\overline{\phi' b'}$	$-\frac{1}{\rho_0}\overline{\phi'\frac{\partial p'}{\partial z}}$	$-\epsilon_{w\phi}$
$\frac{\partial w'}{\partial t}$		$-\mathbf{v}' \cdot \nabla w'$	b'	$-\frac{1}{\rho_0}\frac{\partial p'}{\partial z}$	$\nu \nabla^2 w'$
$\frac{\partial \phi'}{\partial t}$	$-w'\frac{\partial \overline{\phi}}{\partial z}$	$-\mathbf{v}' \cdot \nabla \phi'$			$\kappa_\phi \nabla^2 \phi'$

Table 1.1 *The rows correspond to the budget equations of $\overline{w'\phi'}$, w', and ϕ'. The columns correspond to their constituent terms and physical processes underlying them.*

Each column represents a particular physical process, denoted by an upper-case script letter which will be used throughout this dissertation to index these processes across various budget equations. These processes are the time tendency or storage ($\mathcal{S}$),

mean-gradient transport ($\mathcal{M}$), buoyancy acceleration ($\mathcal{B}$), hydrostatic-perturbation pressure gradient acceleration ($\mathcal{P}$), turbulent transport ($\mathcal{T}$), and molecular dissipation ($\mathcal{D}$). The inclusion or exclusion of terms in a modeled budget equation thereby provides an objective means to classify whether a parameterization accounts for the physical process underlying that term

1.3 Energetic consistency

The most popular high-order closure for weather and climate prediction is the TKE-l approach which utilizes a single prognostic turbulence state variable, turbulent kinetic energy (TKE) E_K, along with a diagnostic length scale to determine fluxes. TKE-l schemes are popular because they are extremely simple and computationally inexpensive and have been used for the representation of turbulence across a range of scales, from sub-filter mixing in high-resolution large-eddy simulations (LES) to boundary layer mixing in general circulation models (Lenderink et al. 2000, 2004). TKE-l schemes have successfully been combined with so-called eddy diffusivity-mass flux (EDMF) schemes to unify the representation of dry and shallow moist convection (Soares et al. 2004, Sušelj et al. 2013, 2014). Because of its usefulness across scales, the TKE-l approach the has recently been suggested as a promising means of achieving a scale-aware and scale-adaptive treatment of turbulent mixing in models with resolution approaching the convective "gray-zone" (Kurowski and Teixeira 2017).

A key problem occurs however for TKE-l schemes under stably stratified conditions whereby for a given wind shear, turbulence shuts down beyond a critical threshold of static stability (critical gradient Richardson number) (Richardson 1920), contradicting observations of turbulence persisting at very high stabilities (Kondo et al. 1978, Mahrt 1998, Mauritsen and Svensson 2007). This lead Zilitinkevich et al. (2007, 2008) to suggest total turbulent energy (TTE), the sum of TKE and turbulent potential energy (TPE), equal to the ratio of buoyancy variance to the square of static stability, as a more natural turbulence state variable for the closure problem than TKE alone. Deriving a budget equation for TPE, they showed that "buoyancy destruction" of TKE under stable conditions is in fact conversion of TKE into TPE, and that, by accounting for TPE and its role in the budget of turbulent heat flux, the critical gradient Richardson number threshold vanishes. Thus, like a pendulum, both the kinetic and potential energies of the system are required to know its state and correctly predict its evolution. Mauritsen et al. (2007) developed a turbulence closure for stable and neutral stratification based on this so-called "total energy approach", obtaining much more realistic simulations of stably stratified boundary layer (STBL).

While modeling the stable boundary layer may appear to be a much different problem than modeling convective and cloudy boundary layers, turbulence under stable stratification plays a fundamental role in each case for two reasons. First, the inversion and its stability modulate top entrainment in convective boundary layers (CBLs). Second, under and within the capping inversion is where boundary layer clouds occur. As I will show in chapter 3, cloudiness and TPE are coupled via the co-

variability of heat and moisture which determines cloud fraction and the "clear-sky" buoyancy variance, while the cloud fraction in turn determines the moist static stability and the moist buoyancy variance and thus the TPE (Bechtold et al. 1995). Just as the TKE-l closures cannot capture this coupling, total energy approach cannot either, since while its prognostic TTE variable contains information about TPE, it provides no information about the co-variability of heat and moisture and thus cloudiness. The simplest 1.5-order closures that can capture this coupling are what Mellor and Yamada (1974) dubbed "level-3" closures: those which predict four turbulence state variables: TKE along with three second-order moments making up the covariance matrix of conserved entropy and total moisture.

1.4 Novel contributions, intellectual merit, and broader impacts

In the first part of this dissertation, I compare TKE-l and level-3 closures' physical basis and performance for modeling convective and cloudy boundary layers. I show that, because the TKE-l approach does not account for the influence of TPE on turbulent mixing and the counter-gradient buoyancy fluxes it generates under stably stratified conditions, it cannot correctly simulate the shape of thermodynamic profiles in the capping inversion of convective and cloudy boundary layers. A simple level-3 closure, on the other hand, is able to correctly capture these shapes, though it under-predicts the depth of the convective boundary layer. This property of consistently accounting for TPE, its conversion from TKE, its response to phase change, and its influence on turbulent mixing, I call moist local energetic consistency (MLEC). I show that this is a local property, because the generation and conversion of turbulent

energy is driven by local physical processes. While the importance of this property has been explored thoroughly for stable boundary layers, my work is the first apply the same concepts to convective and cloudy boundary layers.

In the second part of this dissertation, I extend the concept of energetic consistency to non-local transport. The reason for the TKE-l and level-3 closures underpredicting the depth of the convective boundary layer is their inability to transport turbulent energy high enough into the capping inversion to generate sufficient top entrainment. Even when coupled to a convective mass flux scheme, making them EDMF parameterizations, the depth of the boundary layer is still underpredicted. I show that this is because of an inconsistent representation of the non-local transport of turbulent energy. Under the EDMF approach, this non-local transport is represented in two, not necessarily consistent ways: one diffusive and the other advective. I propose an alternative approach which correctly accounts for non-local transport of turbulent energy by consistently decomposing all second-order moments between the updraft plume and its environment. This then decomposes non-local transport of energy into several terms accounting for processes such as entrainment, detrainment, and mean advection of turbulent energy by the updraft plume and its subsiding environment. I show in a simulation of the convective boundary layer that his new approach yields a much more realistic prediction of boundary layer depth. While Witek et al. (2011) suggested such an approach, and Tan et al. (2018) applied it (after the my prospectus defense), scheme is locally energetically consistent (unlike Tan et al. 2018's scheme) while numerically robust due to the utilization of diagnostic thermodynamic fluxes.

Thus, my work is a novel and important step towards physically consistent unified modeling of the turbulence and dry/shallow convection.

In the final part of this dissertation, I introduce a novel numerical method for estimating the properties of surface-driven convection in large-eddy simulations (LES) via Lagrangian particle tracking (LPT). The purpose of this method is to validate the physical basis of the thermal plume model (Rio and Hourdin 2008), used in my unified turbulence and dry/shallow convection scheme. Such a method is necessary due to the thermal plume model's unique decomposition of model grid cells into an ensemble of thermal plumes and their environment. This same decomposition is used in my parameterization to derive the governing equations of sub-environmental variability which handle local turbulent mixing. Thus, my LPT scheme permits verification of the magnitude of terms in those equations using synthetic data derived from LES. This provides a quasi-empirical basis for my parameterization approach. Couvreux et al. 2008 created a similar method using an Eularian method which introduces into the LES state variables a decaying scalar/tracer with fixed surface flux. In future work, I will combine these two methods, for a more robust treatment of entrainment in the LPT-based method, while permitting analysis of the history of thermal plume air parcels which the Couvreux et al. (2008) method does not.

1.5 Organization

This dissertation is organized as follows. Chapter 2 summarizes current conventional and unified approaches to parameterizing sub-grid turbulent mixing and convection in numerical weather and climate models. Chapter 3 examines the physical basis of TKE-l closures and "level-3" high-order closures and introduces the concept of moist local energetic consistency, classifying these two closure approaches according to this criterion. Chapter 4 evaluates these closures and the importance of local energetic consistency numerically by performing single column model simulations of an idealized shear-free dry convective boundary layer (DCBL) and marine stratocumulus-topped boundary layer (SCBL). Chapter 5 introduces the concept non-local energetic consistency and evaluates, theoretically and numerically, the EDMF approach based on this criterion. Chapter 6 introduces the theoretical background and numerical formulation of my new unified turbulence-convection parameterization. This approach is evaluated numerically for the DCBL case and its performance is compared to conventional EDMF approaches. Finally, chapter 7 introduces my LES-LPT for estimating the properties of surface-driven convection.

Chapter 2: Background

2.1 Conventional vs unified approaches to modeling turbulence and convection

Before introducing my own novel research in this dissertation, the following chapter is included to provide background about current approaches to the closure problem with respect to parameterizing turbulence, shallow convection, and condensation. For shallow cumulus-topped boundary layers, I refer to the "conventional approach" as the determination of fluxes in the sub-cloud and cloud layers by separate parameterizations. In the sub-cloud layer, this parameterization is called the "turbulence parameterization", while in the cumulus cloud layer, it is called the "shallow convection parameterization" or simply the "convection parameterization". The treatment of fluxes at the boundary between these two layers is called the "cloud base closure". A third parameterization, called the "cloud parameterizations" or "microphysics parameterizations", determines cloud properties in a grid cell which are used by other model components such as the turbulence and radiation schemes.

2.2 Conventional approaches

2.2.1 Fluxes in the sub-cloud layer

By far, the most common technique for determining fluxes in the sub-cloud layer is the *eddy diffusivity approach,* whereby the turbulent flux of an arbitrary scaler ϕ is given by:

$$\overline{w'\phi'} = -K\frac{\partial\overline{\phi}}{\partial z} \quad (2.1)$$

where K is called the *eddy diffusivity coefficient*. Due to its dependency on local gradients, eddy diffusion transports air properties locally between adjacent grid cells, and due to its down-gradient formulation (negative proportionality between fluxes of local gradients), it smooths or "diffuses" vertical profiles of $\overline{\phi}$. For the same reason however, (2.1) cannot model counter-gradient fluxes that arise in the upper part of the boundary layer. Because of this, pure eddy diffusive parameterizations predict unrealistic unstable stratification throughout the depth of the boundary layer.

There are two commonly used first-order approaches for determining eddy diffusivity coefficients in numerical weather and climate models. The *Louis-type closure* determines K as an empirical function of the gradient Richardson number $Ri = N^2/S^2$, an empirical length scale l, and the vertical shear of horizontal winds S^2:

$$K = l^2 S^2 f\left(Ri\right) \quad (2.2)$$

where

$$N^2 = \frac{g}{\theta_0}\frac{\partial\overline{\theta_v}}{\partial z} \quad (2.3)$$

$$S^2 = \left(\frac{\partial\overline{u}}{\partial z}\right)^2 + \left(\frac{\partial\overline{v}}{\partial z}\right)^2 \quad (2.4)$$

Louis-type schemes are most commonly used to treat turbulence under stable stratification. For unstable and neutrally stable parts of convective boundary layers

(CBL), *K-profile closures* (Troen and Mahrt 1986) assume a quadratic similarity profile of K through the depth of the CBL:

$$K = \kappa z w_\star \left(1 - \frac{z}{z_\star}\right)^2 \quad (2.5)$$

where

$$w_\star = \left(\kappa z_\star \overline{w'b'}_s\right)^{1/3} \quad (2.6)$$

is the Deardorff convective vertical velocity scale, $z_\star$ is the height of the CBL, $\overline{w'b'}_s$ is the surface buoyancy flux, and κ is the von Karman constant. To deal with the problem of unrealistic unstable stratification through the depth of the CBL, associated with pure eddy diffusion, it is common to include a potentially counter-gradient flux correction term in conjunction with K-profile closures, so that, when ϕ is a thermodynamic variable:

$$\overline{w'\phi'} = -K\left(\frac{\partial \overline{\phi}}{\partial z} - \gamma_\phi\right) \quad (2.7)$$

where

$$\gamma_\phi \propto \frac{\overline{w'\phi'}_s}{w_\star z_\star} \quad (2.8)$$

The most common high-order closure technique for determining eddy diffusivity coefficients is the *TKE-l closure* approach, whereby K is given by the product of the square root of turbulent kinetic energy (TKE), $E_k \equiv 1/2\left(\overline{u'^2} + \overline{v'^2} + \overline{w'^2}\right)$, and a length scale L:

$$K = L E_K^{1/2} \quad (2.9)$$

TKE is treated as the sole turbulence state variable, with prognostic equation given by (Stull 1988):

$$\frac{\partial E_K}{\partial t} = -\overline{u'w'}\frac{\partial \overline{u}}{\partial z} - \overline{v'w'}\frac{\partial \overline{v}}{\partial z} + \overline{w'b'} - \frac{1}{\rho_0}\frac{\partial \overline{w'p'}}{\partial z} - \frac{1}{\rho_0}\frac{\partial \rho_0 \overline{w' E_K'}}{\partial z} - \epsilon_K \quad (2.10)$$

Momentum and thermodynamic fluxes appearing in equation (2.10) are also determined by the TKE-l eddy diffusivity approach of equations (2.1) and (2.9).

2.2.2 Fluxes in the cloud layer

Turbulent fluxes in the cloud layer are conventionally parameterized using a *mass flux approach,* in which the turbulent flux of an arbitrary thermodynamic variable ϕ is given by:

$$\rho_0 \overline{w'\phi'} = M_u \left(\overline{\phi}^u - \overline{\phi} \right) \quad (2.11)$$

where $M_u = \rho_0 a_u \overline{w}^u$ is the *mass flux* of an idealized ensemble of cloudy updraft parcels, a_u is the area fraction of the ensemble, and an over-line with superscript u denotes the mean of an intensive property, averaged over the updraft ensemble. M_u and $\overline{\phi}^u$ are determined in (2.11) by integrating from cloud base z_b to cloud top z_t the diagnostic equations of an *entraining plume model given* by:

$$\frac{1}{M_u}\frac{\partial M_u}{\partial z} = \varepsilon - \delta \quad (2.12)$$

$$\frac{\partial \overline{\phi}^u}{\partial z} = -\varepsilon \left(\overline{\phi}^u - \overline{\phi} \right) \quad (2.13)$$

where ε and δ are the *fractional rates of entrainment and detrainment* respectively. The key problem for entraining plume model is how to formulate ε and δ. The

simplest approach is to use constant values satisfying $\varepsilon < \delta$ to ensure that mass flux realistically decreases with height. Numerous others have been proposed in the literature, and de Rooy et al. (2013) provides an excellent review and analysis of them.

The lower boundary conditions at z_b of the mass flux schemes make up what is called the *cloud base closure*. Neggers et al. (2004) reviewed several of the most commonly used cloud base convective flux closures and placed them into three general categories. *Sub-cloud equilibrium closures* adjust cloud base mass flux so that shallow convection does not alter the vertical integral of either q_t or moist static energy in the sub-cloud layer. *CAPE-adjustment closures* on the other hand adjust cloud base mass flux so that compensating subsidence around shallow cumuli acts to reduce the convectively available potential energy (CAPE) over a specified time scale. Finally, *sub-cloud convective velocity closures* scale cloud base mass flux with a vertical velocity scale characteristic of sub-cloud turbulence.

The upper boundary of the cloud layer z_t is conventionally defined as the height where M_u vanishes. Since mass flux M_u is proportional to the product of area fraction a_u and vertical velocity $\overline{w}^u$, the M_u-budget given by (2.12) may be replaced by a $\overline{w}^u$-budget, where a_u is modeled instead of fractional detrainment δ. In this case, cloud top height z_t is defined as the height where $\overline{w}^u$ vanishes instead of M_u. The $\overline{w}^u$-budget is conventionally modeled as:

$$\frac{1}{2}\frac{\partial\left(\overline{w}^u\right)^2}{\partial z} = c_1\left(\overline{b}^u - \overline{b}\right) - c_2\varepsilon\left(\overline{w}^u\right)^2 \tag{2.14}$$

where c_1 and c_2 account for pressure perturbation and sub-plume turbulence effects. de Roode et al. (2012) provide an excellent summary and analysis of the parameterization of (2.14).

2.2.3 Cloud cover

Cloud parameterizations determine vertical profiles of cloud variables such as cloud fraction a_c, mean liquid water $\overline{q_l}$, liquid water flux $\overline{w'q_l'}$, and various microphysical quantities. Siebesma et al. (2003) identified three general classes of cloud parameterizations commonly found in operational models. *Relative humidity-based schemes* model cloudiness as an empirical function of mean relative humidity. *Prognostic schemes* on the other model cloud variables as prognostic variables obtained from budget equations. Lastly, *statistical schemes* diagnose cloud variables from the saturated tail of an assumed bivariate PDF of θ_l and q_t by estimating the PDF's parameters.

Except for interactions with the cloud base closure, eddy diffusivity and mass flux schemes interact indirectly through their modification of vertical profiles of grid-scale mean variables. At cloud base, this interaction plays a keys role in determining turbulent transport between the cloud and sub-cloud layers, as turbulent fluxes at cloud base are equal to the sum of contributions from each parameterization. The mechanism of the interaction is due to the fact that the mass flux scheme is not active in the sub-cloud layer, so that the fluxes it generates exhibit a discontinuity which induce flux divergences and drives a tendency for inversions to form in $\overline{\theta_l}$ and $\overline{q_t}$

profiles at cloud base. Since these gradients are inversely proportional to diffusive fluxes, the eddy diffusivity scheme responds to generate fluxes with signs opposite those generated by the mass flux scheme, so that eddy diffusion counter-acts the moistening (cooling) tendency driven by the mass flux scheme just above cloud base. When a moist turbulence parameterization is active, this local interaction can be generalized to the interior of the cloud layer by taking the derivative with respect to height of each side of (1.1). It is clear from the resulting equation that the curvature of fluxes generated by the mass flux scheme alter gradients in the interior of the cloud layer, driving the moist eddy diffusivity scheme to generate fluxes of its own. Thus, the moist eddy diffusivity scheme further counter-acts the effects of shallow convection by mixing air between the sub-cloud layer and the interior of the cloud layer.

2.4 Unified approaches

2.4.1 Eddy diffusivity-mass flux (EDMF)

EMDF schemes (Soares et al. 2004, Siebesma et al 2007) unify turbulence and shallow convection representation by extending the lower boundary of a conventional bulk mass flux scheme to the surface, so that the eddy diffusivity and mass flux schemes are both active in the sub-cloud layer. Rather than sampling idealized cloudy updraft parcels as a bulk mass flux scheme does, the EMDF mass flux scheme samples the (clear or cloudy) updraft parcels which have the strongest vertical velocities, signifying the air most likely originating in the surface layer roots of convective clouds. The onset of moist convection thus occurs without an explicit

trigger, as the upper boundary of the entraining plume model grows higher than the level of condensation. Likewise, a cloud base closure is not required, since the activity of the mass flux scheme in the sub-cloud layer completely determines the properties of convection at cloud base. An especially attractive feature of this approach is that the EDMF mass flux scheme can generate counter-gradient fluxes in the sub-cloud layer, allowing for the realistic simulation of stable stratification in the upper part of the boundary layer.

$$\rho_0 \overline{w'\phi'} \approx -\rho_0 K_\phi \frac{\partial \overline{\phi}}{\partial z} + M\left(\overline{\phi}^u - \overline{\phi}\right) \quad (2.15)$$

(2.15) can be interpreted as a scale decomposition, under which the diffusive (first) term on the right-hand-side accounts for local mixing, while the advective (second) term accounts for non-local transport by thermals (Soares et al. 2004).

The conventional EDMF approach, to be a unified treatment of turbulence and moist convection, must couple a mass flux scheme to a TKE-l closure. The TKE-l closure and mass flux scheme are coupled via the buoyancy term in the prognostic equation for TKE (equation 2.10), which, applying equation (2.15), is given by:

$$\rho_0 \overline{w'b'} = -\rho_0 K_h N^2 + M_u\left(\overline{b}^u - \overline{b}\right) \quad (2.16)$$

Although, models like the NCEP Global Forecast Model (GFS) and ECMWF Integrated Forecast Model (IFS) utilize EDMF operationally (Köhler et al. 2011; Han et al. 2015), these are not truly unified representations of turbulence and moist convection. Such parameterizations use an empirical K-profile approach (see section 2.1.1) to determine the eddy diffusivity profile. Since it is not clear how to extend

this profile into a shallow cumulus layer, the diffusive component vanishes at the top of the boundary layer in these models, so that only the mass flux component is active in the cloud layer. Thus, with few exceptions (e.g. Sušelj et al. 2014), most truly unified EDMF-based representations of turbulence and moist convection use a TKE-l closure to drive the diffusive component of turbulent fluxes (Soares et al. 2004; Sušelj et al. 2013).

Multi-plume EMDF schemes (Neggers et al. 2009; Neggers 2009; Sušelj et al. 2014) extend the conventional EDMF approach, utilizing multiple entraining plumes instead of one, each sampling from a sub-ensemble of the strongest updraft parcels. Under this approach, the turbulent flux of ϕ is approximated as

$$\rho_0 \overline{w'\phi'} = -\rho_0 K_\phi \frac{\partial \overline{\phi}}{\partial z} + \sum_i^n M_i \left(\overline{\phi}_i^u - \overline{\phi} \right) \quad (2.17)$$

The use of multiple plumes with differing properties allows for the co-existence of dry and moist plumes at the same height, such that given enough plumes and a sufficiently granular partitioning of strong updraft parcels into sub-ensembles, (2.17) can reproduce the smooth transition from dry and shallow moist convection. If K_ϕ is set to zero, then (2.17) reduces to a special class of unified turbulence-shallow convection parameterizations which represent all transport turbulent transport from the surface to cloud top with entraining plumes (Chienet 2003, 2004).

2.4.2 Assumed distribution-high order closures (ADHOC)

The second category of unified parameterizations are assumed distribution high-order closures (ADHOC) (Lappen and Randall 2001) which determine fluxes from several prognostic high-order moments. A particular family of probability distribution functions (PDFs) is assumed for the joint-variability of heat, moisture, and momentum, with the high-order moments of these properties serving as its parameters. Conversely, the PDF is used to close the budget equations of those moments by diagnosing key properties such as cloud fraction, buoyancy flux, and the turbulent transport of the moments themselves. Thus, ADHOC schemes may essentially be regarded as statistical cloud schemes in which the conventional bivariate PDF has been extended to three dimensions to account for sub-grid vertical velocity variations. ADHOC parameterizations are typified by the popular Cloud Layers Unified by Binormals (CLUBB) scheme (Golaz et al. 2002), which simulates seven high-order moments as prognostic variables – including sensible and latex heat fluxes. ADHOC schemes do not require ad-hoc cloud base closures, because dry and moist shallow convection, as well as stratiform boundary cloudiness, are all treated in an internally consistent fashion via its assumed PDF. Like EDMF, ADHOC parameterizations such as CLUBB can also simulate counter-gradient fluxes in the upper part of the CBL due to the presence of flux-correction terms in the prognostic budget equations of thermodynamic fluxes which represent the contribution of sub-grid buoyancy acceleration.

The disadvantage of the ADHOC approach is its empirical treatment of non-local transport, since third-order moments, measuring (co-)skewness, represent non-local transport of turbulent energy. In CLUBB for example, vertical velocity skewness is a prognostic variable and master skewness parameter for its analytical double-Gaussian PDF. All other third-order moments are diagnosed from this PDF in essentially an empirical fashion. Furthermore, the prognostic equation for vertical velocity skewness uses an empirical length scale to model its diffusion and dissipation. Such modeling is justified on the basis of scaling hypotheses that are on shaky physical grounds. In contrast, the entraining plume models used by mass flux and EDMF schemes treat non-local transport via a physical model of dry and shallow convection based on testable hypothesis (e.g. Siebesma et al. 1995). This analysis of EDMF and ADHOC schemes will be discussed more thoroughly in chapter 5.

2.3 Evaluating boundary layer parameterizations

2.3.1 Large-eddy simulations (LES)

"Synthetic" datasets obtained from high-resolution large-eddy simulations (LES) are a key tool for evaluating boundary layer parameterizations. While not a replacement for observations, they are a useful substitute, since they are complete in space and time, thus allowing for direct "offline" testing of closure assumptions of parameterizations and computation of statistics which are considerably more robust than those obtained from observations, including high-order moments that are often unobservable.

A key result from LES studies is the evaluation of the physical basis of the mass flux approach: the *mass flux approximation*. Its derivation and justification begins with the decomposition of a grid-cell into an updraft part and a complementary "environmental part". The linearity of Reynold's averaging operators implies that an arbitrary mean property $\overline{\phi}$ can be expressed as:

$$\overline{\phi} = a_u \overline{\phi}^u + (1 - a_u)\, \overline{\phi}^e \quad (2.18)$$

where u denotes the conditional mean over the updraft part of the grid cell and e denotes the environmental part. After some manipulation of the definition of turbulent fluxes and defining mass flux as $M_u = \rho_0 a_u \overline{w}^u$, the flux of ϕ can be expressed as

$$\rho_0 \overline{w'\phi'} = \rho_0 a_u \overline{w'\phi'}^u + \rho_0 (1 - a_u)\, \overline{w'\phi'}^e + M_u \left(\overline{\phi}^u - \overline{\phi}^e \right) \quad (2.19)$$

The three terms on the RHS are called the *sub-cloud*, *sub-environmental*, and *organized fluxes* respectively. The physical basis of a conventional mass flux convection parameterization is the *mass flux approximation*, stated formally as:

$$\rho_0 \overline{w'\phi'} \approx M_u \left(\overline{\phi}^u - \overline{\phi}^e \right) \quad (2.20)$$

It justified assuming two conditions. First, the updraft area fraction is assumed small ($a_u \ll 1$), implying that $\overline{\phi}^e \approx \overline{\phi}$ and $\rho_0 a_u \overline{w'\phi'}^u \approx 0$. Second, the sub-environmental flux is assumed negligible relative to the organized flux, so that $\rho_0 (1 - a_u)\, \overline{w'\phi'}^e \approx 0$.

Siebesma and Cuijpers (1995) evaluated the mass flux approximation by partitioning an LES domain from a simulated trade wind cumulus-topped boundary layer into cloudy updraft grid cells and their complementary environment. They found that by sampling positively buoyant cloudy updraft cells (*cloud core* sampling), the organized flux term in (2.19) could explain 80% of thermodynamic turbulent fluxes in the cloud layer, excepting the cumulus inversion where cloudy updraft parcels are predominantly negatively buoyancy. They also found best-estimates for constant fractional entrainment and detrainment rates. However, de Rooy and Siebesma (2008) argued that such constant mixing rates over-estimate convective activity for shallow cloud layers and under-estimate it for deeper ones, since they imply a unique cloud layer depth by determining the height where mass flux vanishes. In the same study, they showed that entrainment and detrainment are non-trivially dependent on environmental humidity which is also not accounted for by constant mixing rates.

Neggers et al. (2004) evaluated the three cloud base closures, described in the previous section, using an LES-generated synthetic dataset from a standard test case for the diurnal cycle of shallow convection over land. The sub-cloud equilibrium closure was found to largely over-predict cloud base mass flux due to non-negligible integrals of moisture and moist static energy tendencies in the sub-cloud layer. The CAPE adjustment closure under-predicted cloud base mass flux in the beginning of the day and over-predicted it at the end of the day. This was attributed to this closure ignoring CAPE-altering factors other than compensating subsidence and the use of a constant CAPE-relaxation time scale. Finally, the sub-cloud vertical velocity closure

was found to be superior to the previous two closures, largely capturing the phase and amplitude of cloud base mass flux.

Siebesma et al. (2003) evaluated the cloud parameterizations described in the previous section in an inter-comparison of trade wind cumulus-topped boundary layers simulated by several LES models. They found that a typical prognostic cloud fraction scheme and relative humidity-based scheme both significantly over-predicted cloud cover, though a hybrid of these two approaches performed much better. A statistical cloud scheme based on a bivariate normal PDF on the other hand significantly under-predicted cloud cover. For relative-humidity schemes, it was concluded that over-prediction was due to the lack of a clear one-to-one relationship between relative humidity and cloudiness, while for the prognostic scheme, over-prediction was attributed to strong sensitivity in the balance between sources and sinks in cloudiness budgets. For the statistical cloud scheme, it was noted that cumulus cloud layers exhibit a significant degree of skewness which a bi-normal distribution is unable to capture. The authors posited that a more realistic PDF would likely better simulate cloudiness provided reasonable estimates of the sub-grid variability of temperature and moisture. The fidelity of such estimates as modeled by various turbulence closures schemes will be discussed in chapter 3.

2.3.2 Single-column model (SCM) simulations

Single column model (SCM) simulations are another key tool for evaluating boundary layer parameterizations, as they allow for critical analysis of the behavior

and interactions of parameterizations “online” in a large-scale model while avoiding complexity associated with feedbacks from 3D simulations. SCM simulations can also be conveniently compared with LES run with identical forcings and initial conditions, thus eliminating uncertainty with how to compare large-scale model output to observations. The evaluation of various closure schemes throughout this dissertation will be performed exclusively using the SCM framework with 3D simulations left for future work.

Lenderink et al. (2004) compared simulations of the diurnal cycle of shallow convection over land (Brown et al. 2002) by single-column versions of several operational general circulation models (GCM). Compared to LES, they found that most models predicted unrealistic thermodynamic profiles in the cloud layer, too large values of cloud cover, and a high degree of numerical noise and intermittency. The occurrence of unrealistic thermodynamic profiles was associated with two classes of model behavior characterizing the relative activity of the eddy diffusivity and mass flux schemes at cloud base. The first class of models exhibited over-active (under-active) mass flux (eddy diffusion) schemes, leading to cloud layers that were too dry (warm) near cloud base and too moist (cool) in the cumulus inversion. The excess moisture in the cumulus inversion often resulted in excess stratiform cloudiness at that level characteristic of decoupled cumulus-to-stratocumulus transition regimes. This excess cloud cover was exaggerated when a prognostic cloud scheme was used, due to a strong dependency of stratiform cloudiness on detrainment by the mass flux scheme. In contrast, the second class of models exhibited over-active (under-active)

eddy diffusivity (mass flux) schemes, leading to boundary layers that were too shallow and moist which often resulted in excessive low-level stratiform cloudiness, sometimes resulting in a regime transition to a stratocumulus boundary layer.

The occurrence of either class of behavior along with the occurrence of numerical noise were in many cases the result of interactions between parameterizations which alter the relative activity of mass flux and eddy diffusivity schemes and which are amplified by a consequential positive feedback between eddy diffusivity schemes and any process that alters stability. This feedback occurs, because any increase (decrease) in the local gradient of $\overline{\theta_l}$ and $\overline{q_t}$ also increases (decreases) local stability which in turn decreases (increases) the magnitude by the eddy diffusivity coefficient by shortening (lengthening) mixing length for local stability-based schemes and decelerating (accelerating) mixing velocity for TKE-l schemes by strengthening (weakening) buoyancy production of TKE. Thus, a forcing which increases (decreases) local stability weakens the ability of the eddy diffusivity scheme to counter-act the forcing through its generation of down-gradient fluxes, thus further increasing (decreasing) stability. In the case of over-active convection, as the inversions formed by the mass flux scheme at cloud base strengthened by this feedback to the point that turbulent transport was severely weakened or, in some cases, completely shut down. It also a key cause of over-active turbulence cases via both eddy diffusivity-mass flux scheme/cloud base closure interactions and eddy diffusivity-cloud scheme interactions. The first type of interaction arose when a sub-cloud equilibrium cloud base closure was used, since any decrease in cloud base mass

flux weakens stability, thereby intensifying moisture/moist static energy fluxes generated by the eddy diffusivity and thus further decreasing cloud base mass flux to maintain sub-cloud equilibrium. The second cause of over-active turbulence occurred as moistening (drying) at cloud base by the mass flux scheme may increases (decreases) stratiform cloud fraction which increases (decreases) local stability and the absolute magnitude of buoyancy flux, driving further moistening (drying) and associated increases (decreases) in cloud fraction.

2.4 Summary

In this chapter, I first summarized the current state of the art for constructing and evaluating parameterizations of turbulence, dry/shallow convection, and condensation. I divided them into two categories of approaches, conventional and unified, and discussed the formulation and advantages/disadvantages of the members of each category. In chapters 3, 4, and 5, I will formalize and generalize the methodology for this assessment, focusing on energetic consistency. Finally, I summarized SCM and LES-based methods for parameterization evaluation. Both techniques will form the basis for parameterization evaluation throughout this dissertation.

Chapter 3: Local energetic consistency

3.1 Base model (TKE-l closure)

As a base model for the numerical experiments performed in this study, I introduce here a TKE-l-type turbulence closure and a statistical cloud parameterization, coupled to the simple anelastic single column model (SCM), introduced in chapter 1 and 2 and governed by equation (1.1). The goal is not to create a new or innovative model but one that is simple, yet representative of the typical behavior of those with turbulence closures in the TKE-l class. From this base model, the treatment of particular physical processes will be systematically included and/or excluded in order to assess their impact on the predictive skill of the SCM.

Sub-grid fluxes in a TKE-l closure are treated by an eddy diffusivity approach:

$$\overline{w'\phi'} = -K_{m,h}\frac{\partial\overline{\phi}}{\partial z} \quad (3.2)$$

where $K_{m,h}$ is the eddy diffusivity coefficient, and subscripts m and h denote coefficients for momentum variables ($\phi \in \{\overline{u}, \overline{v}\}$) and thermodynamic variables ($\phi \in \{\overline{\theta_l}, \overline{q_t}\}$) respectively. $K_{m,h}$ is given by (Kolmogorov 1941):

$$K_{m,h} = L_{m,h}E_K^{1/2} \quad (3.3)$$

where $L_{m,h}$ is a turbulent mixing length, and E_K is the turbulent kinetic energy (TKE). The momentum mixing length L_m, along with all other length scales appearing in the base model, is proportional to a master length scale L (Mellor and Yamada 1982; Golaz et al. 2002), so that $L_m = c_m L$ with $c_m = 0.516$. The

momentum and thermodynamic mixing lengths are related by the turbulent Prandtl number $Pr = L_m/L_h$, obtained by matching turbulent fluxes with fluxes in the surface layer via Monin-Obukhov similarity theory (Monin and Obukhov 1954).

Under statically unstable or neutral conditions, the master length scale is given by $L = L'$, where (Teixeira and Cheinet 2004):

$$\frac{1}{L'} = \frac{1}{\kappa z} + \frac{1}{\tau_\star E_K^{1/2}} \quad (3.4)$$

where $\tau_\star = 400\, s$ (Sušelj et al. 2013). Under statically stable conditions, L is set equal to (Brinkop and Roeckner 1995):

$$\frac{1}{L} = \frac{1}{L'} + \frac{1}{c_e N^{-1} E_K^{1/2}} \quad (3.5)$$

where N is the moist Brunt-Väisälä frequency and $c_e = 0.4$ (Lenderink et al. 2000).

The prognostic equation for E_K is given by (Stull 1988):

$$\underbrace{\frac{\partial E_K}{\partial t}}_{\mathcal{S}} = \underbrace{-\overline{u'w'}\frac{\partial \overline{u}}{\partial z} - \overline{v'w'}\frac{\partial \overline{v}}{\partial z}}_{\mathcal{M}} \underbrace{+\overline{w'b'}}_{\mathcal{B}} \underbrace{-\frac{1}{\rho_0}\frac{\partial \overline{w'p'}}{\partial z}}_{\mathcal{P}} \underbrace{-\frac{1}{\rho_0}\frac{\partial \rho_0 \overline{w'E_K'}}{\partial z}}_{\mathcal{T}} \underbrace{-\epsilon_K}_{\mathcal{D}} \quad (3.6)$$

where table (1.1) describes the physical processes each script capital-letter below the underbraces represents. The momentum fluxes appearing in the two $\mathcal{M}$-terms of (3.6) are treated by the eddy diffusivity approach given by (3.2), and $\mathcal{B}$ is modeled diffusively as well with $\overline{w'b'} = -K_h N^2$. $\mathcal{P}$ and $\mathcal{T}$ are rolled into a single eddy diffusive vertical redistribution term with diffusion coefficient $2K_m$, where the factor of 2 accounts for their joint contribution (Lenderink and Holtslag 2004). $\mathcal{D}$ is given

by $\epsilon_K = E_K/\tau_K$ where $\tau_K = E_K^{1/2}/L_K$ is the TKE dissipation time scale (Kolmogorov 1941) with $L_K = c_K L$ and $c_K = 15$ (Roeckner et al. 1996).

N^2, required for the master length scale under stable conditions as well as the buoyancy flux appearing in the TKE budget, is determined by the cloud scheme as a linear combination of the mean gradients of θ_l and q_t, with coefficients that are a function of cloud fraction. Its exact formulation and derivation are postponed until section (3.4). The statistical cloud scheme diagnoses cloud fraction by assuming a Gaussian joint-probability distribution function (PDF) for the (co-)variability of θ_l' and q_t'. It is formuted in terms of $Q = \overline{s}/\sigma_s$, where $s = q_t - q_s\left(T, p\right)$ is the saturation excess, and $\sigma_s = \overline{s'^2}^{1/2}$ is its standard deviation, so that cloud fraction is given by Gaussian cumulative distribution function:

$$a_c = \frac{1}{2}\left[1 + \mathrm{erf}\left(\frac{Q}{\sqrt{2}}\right)\right] \quad (3.7)$$

Q is determined by linearlizing saturation specific humidity q_s around the mean liquid water temperature $\overline{T_l} = \overline{\theta_l}\left(p/p_0\right)^{R_d/c_p}$, so that its numerator and denominator are given respectively by (Bechtold et al. 1995):

$$\overline{s} = A\left[\overline{q_t} - q_s\left(\overline{T_l}, p\right)\right] \quad (3.8)$$

$$\sigma_s = \left(A^2\overline{\theta_l'^2} + B\overline{q_t'^2} - 2AB\overline{\theta_l' q_t'}\right)^{\frac{1}{2}} \quad (3.9)$$

where:

$$A = \left[1 - \frac{l_v}{c_p}\frac{\partial q_s\left(\overline{T_l}, p\right)}{\partial T}\right]^{-1} \quad (3.10)$$

$$B = A\left(\frac{p}{p_0}\right)^{\frac{R_d}{c_p}} \frac{\partial q_s\left(\overline{T_l}, p\right)}{\partial T} \tag{3.11}$$

To determine σ_s, the covariance matrix of θ_l and q_t, that is $\overline{\theta_l'^2}$, $\overline{q_t'^2}$, and $\overline{\theta_l' q_t'}$, must be estimated. These three moments are obtained by assuming a quasi-steady balance between mean-gradient transport ($\mathcal{M}$) and viscous dissipation ($\mathcal{D}$) and ignoring storage ($\mathcal{S}$) and turbulent transport ($\mathcal{T}$) in their budget equations given respectively by (Stull 1988):

$$\underbrace{\frac{\partial \overline{\theta_l'^2}}{\partial t}}_{\mathcal{S}} = \underbrace{-2\overline{w'\theta_l'}\frac{\partial \overline{\theta_l}}{\partial z}}_{\mathcal{M}} \underbrace{-\frac{1}{\rho_0}\frac{\partial \rho_0 \overline{w'\theta_l'^2}}{\partial z}}_{\mathcal{T}} \underbrace{-\epsilon_{\theta_l\theta_l}}_{\mathcal{D}} \tag{3.12}$$

$$\underbrace{\frac{\partial \overline{q_t'^2}}{\partial t}}_{\mathcal{S}} = \underbrace{-2\overline{w'q_t'}\frac{\partial \overline{q_t}}{\partial z}}_{\mathcal{M}} \underbrace{-\frac{1}{\rho_0}\frac{\partial \rho_0 \overline{w'q_t'^2}}{\partial z}}_{\mathcal{T}} \underbrace{-\epsilon_{q_t q_t}}_{\mathcal{D}} \tag{3.13}$$

$$\underbrace{\frac{\partial \overline{\theta_l' q_t'}}{\partial t}}_{\mathcal{S}} = \underbrace{-\overline{w'q_t'}\frac{\partial \overline{\theta_l}}{\partial z} - \overline{w'\theta_l'}\frac{\partial \overline{q_t}}{\partial z}}_{\mathcal{M}} \underbrace{-\frac{1}{\rho_0}\frac{\partial \rho_0 \overline{w'\theta_l' q_t'}}{\partial z}}_{\mathcal{T}} \underbrace{-\epsilon_{\theta_l q_t}}_{\mathcal{D}} \tag{3.14}$$

A statistical approach is chosen because its use of budgets allows direct comparison of its physical process representation with that of the turbulence scheme via the inclusion/exclusion of various terms in these three budgets. The thermodynamic fluxes appearing in the $\mathcal{M}$-terms are determined by the turbulence scheme, and $\mathcal{D}$ is set equal to $\epsilon_{\chi\phi} = \overline{\chi'\phi'}/\tau_b$ for $\phi, \chi \in \{\theta_l, q_t\}$, where $\tau_b = L_b/E_K^{1/2}$ is the thermodynamic (co-)variance dissipation time scale and $L_b = c_b L$ with $c_b = 15$.

3.2 Background: (dry) turbulent potential energy (TPE)

In stable layers of the atmosphere, vertical velocity and buoyancy perturbations induce oscillations in the form of gravity waves and wave-like turbulence. In this way, buoyancy acceleration under stable stratification behave like a pendulum, storing turbulent energy and converting it cyclically back-and-forth between kinetic and potential states. For TKE-l closures however, potential energy is left undefined and ignored, and turbulent energy in stable layers is destroyed by this process, since the buoyancy term ($\mathcal{B}$) in the TKE budget equals:

$$\overline{w'b'} = -K_h N^2 < 0 \text{ for } N^2 > 0 \quad (3.15)$$

This energy sink is responsible for a cessation of turbulence when the gradient Richardson number $Ri = N^2 / \left[(\partial \overline{u}/\partial z)^2 + (\partial \overline{v}/\partial z)^2 \right]$ exceeds a certain threshold (Richardson 1920), contradicting observations of turbulence persisting at very large Ri (Mahrt 1998). According to such observations, a critical Ri threshold does exist, but it instead marks a transition between weakly stable and strongly stable turbulence regimes. In the first regime, turbulence actively transports momentum and heat, while in the latter, the heat flux vanishes and only the momentum transport remains.

To address this problem with the TKE-l closure, Zilitinkevich et al. (2007) introduced and derived a potential energy variable for turbulence by considering the adiabatic displacement of an air parcel from equilibrium in a dry atmosphere. Since in the absence of water vapor, buoyancy $b = (g/\theta_0)\,\theta_v = (g/\theta_0)\,\theta$ is conserved and $N^2 = \partial \overline{b}/\partial z$, the fluctuation per-unit-mass of the parcel's buoyant potential energy is obtained via integration by substitution:

$$\int_{z}^{z+\delta z} b' dz' = \frac{1}{2}\frac{\delta \overline{b'^2}}{N^2} \quad (3.16)$$

Just as TKE measures the average kinetic energy perturbation in a column layer, turbulent potential energy (TPE) E_P may be meaningfully defined by Reynolds averaging the right-hand-side of the above equation:

$$E_P = \frac{1}{2}\frac{\overline{b'^2}}{N^2} \quad (3.17)$$

To derive a budget for TPE in this idealized dry atmosphere, I begin with the (dry) buoyancy variance budget (Stull 1988):

$$\underbrace{\frac{\partial \overline{b'^2}}{\partial t}}_{\mathcal{S}} = \underbrace{-2\overline{w'b'}N^2}_{\mathcal{M}} \underbrace{-\frac{1}{\rho_0}\frac{\partial \rho_0 \overline{w'b'^2}}{\partial z}}_{\mathcal{T}} \underbrace{-\epsilon_{bb}}_{\mathcal{D}} \quad (3.18)$$

Substituting $\overline{b'^2} = 2N^2 E_p$ and dividing each side by $2N^2$, I finally obtain:

$$\underbrace{\frac{\partial E_P}{\partial t} + E_P \frac{\partial \ln N^2}{\partial t}}_{\mathcal{S}} = \underbrace{-\overline{w'b'}}_{\mathcal{M}} \underbrace{-\frac{1}{\rho_0}\frac{\partial \rho_0 \overline{w'E'_P}}{\partial z} - \overline{w'E'_P}\frac{\partial \ln N^2}{\partial z}}_{\mathcal{T}} \underbrace{-\epsilon_P}_{\mathcal{D}} \quad (3.19)$$

Zilitinkevich et al. (2007) obtained a similar equation but ignored the two terms arising due to variations of N^2 in time and space. I have included them for completeness. They argued that since the mean-gradient transport term ($\mathcal{M}$) in the TPE budget has equal magnitude but opposite sign of the buoyancy term ($\mathcal{B}$) in the TKE budget, buoyancy flux $\overline{w'b'}$ is more meaningfully interpreted in stable layers as the rate of conversion of TKE to or from TPE, depending on its sign, rather than its conventional interpretation as "buoyancy consumption" of TKE (Stull 1988). They further defined a third energy variable, total turbulent energy, equal to the sum of TKE and TPE ($E_T \equiv E_K + E_P$) and obtained its budget by summing the budgets of

these two energy states (equations 3.6 and 3.19), whereupon the conversion terms cancel. This implies that turbulent energy can only be destroyed by viscous dissipation ($\mathcal{D}$) and explains the persistence of turbulence at very large Ri.

This analysis inspired so-called total energy closure approaches (Mauritsen et al. 2007, Angevine et al. 2010) in which the sole prognostic turbulence state variable of the model is total turbulent energy, except that its TPE component is extended conceptually to neutral and unstable stratification by replacing N^2 with its absolute value in definition (3.17). Under this approach, eddy diffusivities are functions of both TKE and TPE, and the partitioning of total turbulent energy between these two states is modeled as an empirical function of Ri. In agreement with observations and LES, such closures are able to maintain turbulence under strong stability and represent both weakly and strongly stable turbulence regimes and the transition between them. Thus, total energy closures represent a tier of energetic consistency above TKE-l closures, marked by the conservation of total turbulent energy with respect to buoyancy acceleration ($\mathcal{B}$). However, this approach was created to improve the representation of stable boundary layers, where convection and condensation are not present. In the next two sections, I will generalize the concept of consistent turbulence energetics to the modeling of convective and cloudy boundary layers via high-order turbulence closures.

3.3 Role of TPE in turbulent mixing

In an inter-comparison of simulations of the diurnal cycle of shallow convection over land by SCM versions of several research and operational general circulation models (GCMs), Lenderink et al. (2004) found that for models using TKE-l closures, the turbulent energy-destroying effect of negative (downward) buoyancy flux under stable stratification was responsible for most of the systematic prediction errors. They noted that processes which modify stability, namely convection and condensation, indirectly modify the intensity of turbulent mixing by modulating the strength of the energy sink. In the stable limit for the "typical" TKE-l closure described in the previous section, the buoyancy term dissipates TKE with a timescale proportional to the inverse of the buoyancy frequency N, since the smallest length scale dominates in the harmonic average defining the master length scale (equation 3.5):

$$\overline{w'b'} \propto -\frac{E_K}{\left(\frac{N^{-1}}{lE_K^{-1/2}}\right) N^{-1}} \rightarrow -\frac{E_K}{N^{-1}} \quad \text{for } N \rightarrow \infty \text{ (3.20)}$$

For longer mixing lengths closer to the neutral limit, the above equation indicates that the dependence on N is even stronger. Since diffusive turbulent mixing tends to weaken stability, there is a positive feedback, as stability-strengthening processes weaken the ability of turbulence to counteract that strengthening. Conversely, stability-weakening processes enhance the ability of turbulence to weaken stability.

In the case of the convection parameterizations used by models in the inter-comparison, their tendency to form moisture and temperature inversions just below

cloud base was either too strong or too weak, depending on the type of cloud base closure used, so that the exaggerated strength or weakness of the inversion's stability led to turbulent mixing that was too weak or too strong respectively relative to convective transport. Either case resulted in unrealistic thermodynamic profiles in the cloud layer and too much cloud cover. For condensation schemes, the relative contributions of temperature and humidity lapse rates to moist stability, and thus the contributions of sensible and latent heat fluxes to the total buoyancy flux, are strongly dependent on cloud fraction, which is of special concern over land where the Bowen ratio can be relatively large. For some models, this effect and its positive feedback with the TKE-l closure manifested as either too much mixing and cloud cover, and for others it resulted in strong numerical instability and intermittency. Surprisingly, the authors did not address whether the poor representation of turbulent energetics by the TKE-l closure was responsible for these systematic errors, but instead recommended modifications such as the use of non-local turbulent length scales or specific types of cloud base closures to limit the most egregious errors. *The results of the Lenderink et al. (2004) model inter-comparison indicate a generalized non-physical positive feedback between turbulent mixing by TKE-l closures and any model process that modifies stability.*

To better understand and quantify the role of the turbulent energetics in this positive feedback, I examine the physical basis our "typical" TKE-l closure's formulation of turbulent fluxes by deriving it from the budget equation for (dry) buoyancy flux (Stull 1988):

$$\underbrace{\frac{\partial \overline{w'b'}}{\partial t}}_{\mathcal{S}} = \underbrace{\overline{b'^2}}_{\mathcal{B}} \underbrace{- \overline{w'^2} N^2}_{\mathcal{M}} \underbrace{- \frac{1}{\rho_0} \frac{\partial \rho_0 \overline{w'^2 b'}}{\partial z}}_{\mathcal{T}} \underbrace{- \frac{1}{\rho_0} \overline{b' \frac{\partial p'}{\partial z}}}_{\mathcal{P}} \underbrace{- \epsilon_{wb}}_{\mathcal{D}} \quad (3.21)$$

In an anelastic atmosphere, the hydrostatic pressure-perturbation field is the diagnostic solution to a Laplace equation that ensures that the acceleration field maintains mass continuity in the velocity field. Because this equation is linear, pressure perturbations can be linearly decomposed into individual responses to each acceleration process, so that $\mathcal{P}$ may be decomposed accordingly. In second-order modeling, this decomposition is traditionally treated as (Moeng and Wyngaard 1986):

$$\underbrace{- \frac{1}{\rho_0} \overline{b' \frac{\partial p'}{\partial z}}}_{\mathcal{P}} = \underbrace{- c_{\mathcal{B}} \overline{b'^2}}_{\mathcal{P}_{\mathcal{B}}} \underbrace{- \frac{\overline{w'b'}}{\tau_{wb}}}_{\mathcal{P}_{\mathcal{T}}} \quad (3.22)$$

where $\mathcal{P}_{\mathcal{B}}$ and $\mathcal{P}_{\mathcal{T}}$ denote the pressure-responses to buoyancy acceleration ($\mathcal{B}$) and momentum advection ($\mathcal{T}$) respectively. $\mathcal{P}_{\mathcal{B}}$ modifies the efficiency of $\mathcal{B}$, since $0 < c_{\mathcal{B}} < 1$, so that $\mathcal{B} + \mathcal{P}_{\mathcal{B}} = (1 - c_{\mathcal{B}}) \overline{b'^2}$ represents the buoyancy variance available for production of buoyancy flux. $\mathcal{P}_{\mathcal{T}}$ models the classic hypothesis of Rotta (1951) that hydrostatic pressure perturbations "return" turbulence to isotropy over a timescale τ_{wb}.

Assuming a quasi-steady balance between $\mathcal{B} + \mathcal{P}_{\mathcal{B}}$, $\mathcal{M}$, and $\mathcal{P}_{\mathcal{T}}$ in the buoyancy flux budget, given by equation (3.21), and substituting the definition of TPE (definition 3.17), I can solve for buoyancy flux:

$$\overline{w'b'} = -2\tau_{wb} \left[E_w - (1 - c_{\mathcal{B}}) E_P \right] N^2 \quad (3.23)$$

where $E_w = 1/2\overline{w'^2}$ is the vertical component of TKE. If I instead assumed a balance between $\mathcal{M}$ and $\mathcal{P}_\mathcal{T}$ and excluded $\mathcal{B} + \mathcal{P}_\mathcal{B}$, equation (3.23) would revert to the TKE-l closure's formulation of (dry) buoyancy flux (equations 3.2 and 3.3) (recall $N^2 = \partial\overline{b}/\partial z$ in a dry atmosphere), albeit with the assumption of a constant degree of vertical anisotropy $A_w = E_w/E_K$ and thermodynamic mixing length equal to $L_h = 2A_w\tau_{wb}E_K^{1/2}$. To help compare the realism of these two closure approaches, figure (3.1) depicts the normalized buoyancy flux and its budget for a dry, shear-free convective boundary layer (CBL), simulated by LES. The budget terms are shown for the resolved flux above the unstable layer only, since LES sub-filter fluxes near the surface are non-negligible, and it is not clear how to define their budget terms.

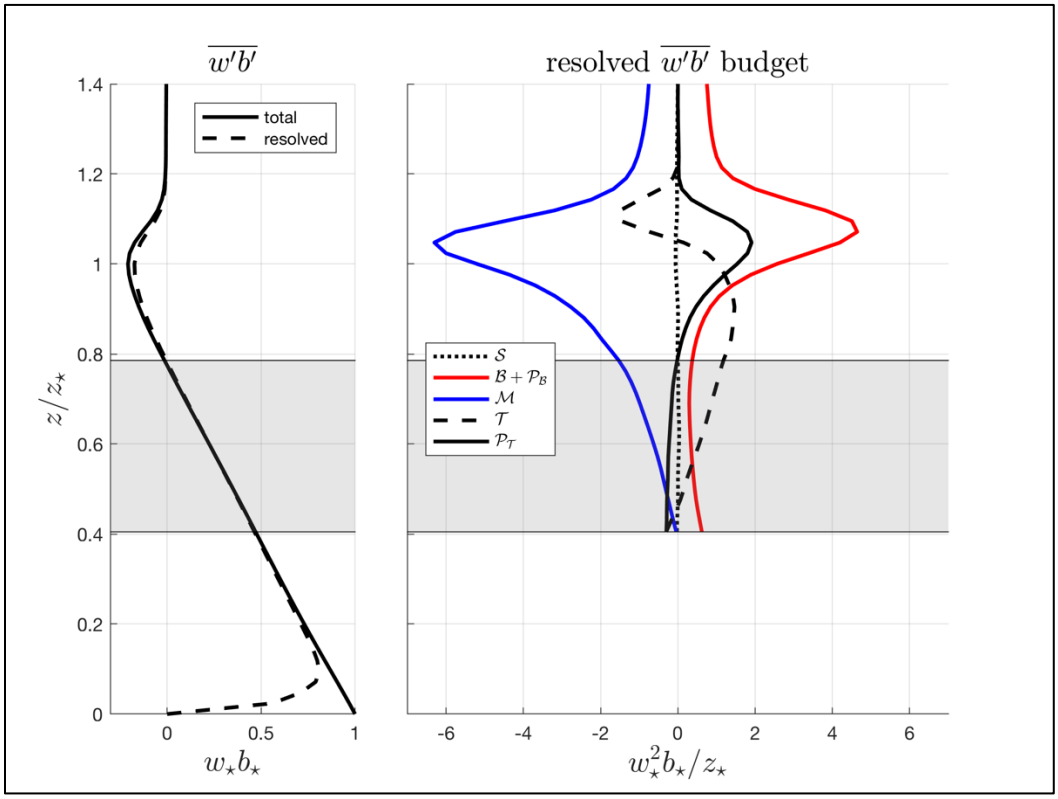

Figure 3.1 *The left panel depicts the buoyancy flux predicted by LES for the DCBL case. The right panel depicts the terms in the LES-predicted buoyancy flux budget.*

Clearly, $\mathcal{S}$ is much smaller than all other terms, justifying the quasi-steady approximation of both approaches. However, since $\mathcal{B} + \mathcal{P}_{\mathcal{B}}$ is the second largest term behind $\mathcal{M}$ in the upper part of the CBL and the only term balancing $\mathcal{M}$ in the free atmosphere, neglecting it is a poor approximation for stable stratification. Equation (3.23) implies that it is the absolute magnitude of the vertical TKE component's excess over the fraction of TPE available for flux production, $E_w - (1 - c_{\mathcal{B}})\, E_P$, rather than the vertical TKE component alone that determines the intensity of turbulent mixing. This explains why gravity waves have kinetic energy but are not responsible for thermodynamic transport (Deardorff 1972). Moreover, this excess, rather than TKE, is "consumed" in the mixing process via the conversion of TKE into TPE. Figure (3.2) depicts normalized TKE and its budget for the same LES simulation. It is apparent in this figure that turbulent transport ($\mathcal{T}$) takes TKE generated by buoyancy acceleration ($\mathcal{B}$) into the capping inversion, creating the TKE-over-TPE excess necessary to generate downward thermodynamic fluxes associated with CBL top-entrainment. The simultaneous conversion of this TKE into TPE by the $\mathcal{B}$-term is associated with the excitation of gravity waves, so that after generating downward fluxes, it becomes useless for mixing as it begins to balance TPE. Though,\ high-order closures have been applied for decades to atmospheric modeling, such analysis of their turbulence energetics is a unique contribution of this dissertation.

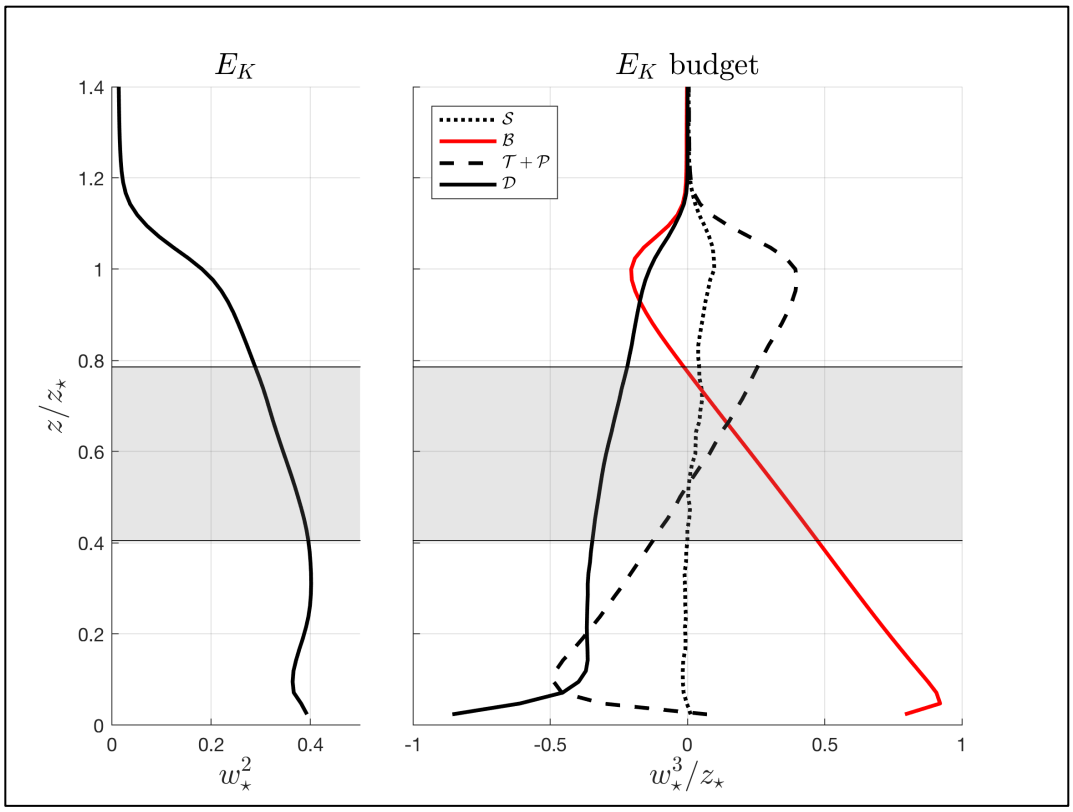

Figure 3.2 *The left panel depicts the turbulent kinetic energy predicted by LES for the DCBL case. The right panel depicts the terms in the LES-predicted TKE budget.*

The closure represented by equation (3.23), unlike TKE-l closures, can model counter-gradient buoyancy fluxes, that is, positive (upward) buoyancy fluxes in the presence of stable stratification. More specifically, TKE produces down-gradient fluxes for stable stratification, while TPE produces counter-gradient fluxes. The inability of pure eddy diffusion-based approaches to model counter-gradient fluxes is the reason they simulate unrealistic unstable stratification throughout most of the depth of the CBL (Siebesma et al. 2007). The gray shaded region in figures (3.1) and (3.2) depicts the layer of the middle of the CBL where the buoyancy flux is counter-gradient. It should be noted that the counter-gradient term associated with $\mathcal{B}+\mathcal{P}_{\mathcal{B}}$

does not represent a non-local process. Some first-order closures model buoyancy flux as (Holtslag and Moeng 1991):

$$\overline{w'b'} = -K_h \left(N^2 - \Gamma \right) \quad (3.24)$$

where $\Gamma > 0$ is an empirically-determined buoyancy gradient. This counter-gradient term is sometimes associated with non-local processes, though because it is empirical, it is not clear how to derive it from the buoyancy flux budget (Stevens 2000). Buoyancy acceleration ($\mathcal{B}$), associated with the counter-gradient term in equation (3.23), imparts vertical momentum on air parcels locally and thus produces buoyancy flux locally, while turbulent transport ($\mathcal{T}$) is the sole non-local process, carrying away excess kinetic energy produced locally by buoyancy acceleration but not converted locally into potential energy by mean-gradient transport ($\mathcal{M}$). To my knowledge, the classification of such counter-gradient flux terms as accounting for local processes has not been discussed in the turbulence modeling literature.

3.4 TPE and phase change

As discussed in section (3.3), the total energy closure approach is energetically consistent in the sense that it conserves total turbulent energy. However, if it is used in conjunction with the statistical condensation scheme detailed in section (3.2), the influence of phase change and latent heating cannot be accounted for in an energetically consistent fashion, since a second expression for TPE may be computed which is not necessarily equal to the one determined by the closure's empirical formulation. Assuming a joint-normal PDF for θ_l', and q_t', as in our base model's

cloud scheme, the linearized covariance of buoyancy and an arbitrary thermodynamic variable $\chi \in \{b, \theta_l, q_t\}$ is given by (Chen 1991):

$$\overline{\chi' b'} = \alpha\left(a_c\right) \overline{\chi' \theta_l'} + \beta\left(a_c\right) \overline{\chi' q_t'} \quad (3.25)$$

where

$$\alpha\left(a_c\right) = \frac{g}{\theta_0} \left\{ 1 - a_c B \left[\frac{l_v}{c_p} \left(\frac{p}{p_0} \right)^{-\frac{R_d}{c_p}} - \frac{R_v}{R_d} \theta_0 \right] \right\} \quad (3.26)$$

$$\beta\left(a_c\right) = \frac{g}{\theta_0} \left\{ \frac{R_d - R_v}{R_d} + a_c A \left[\frac{l_v}{c_p} \left(\frac{p}{p_0} \right)^{-\frac{R_d}{c_p}} - \frac{R_v}{R_d} \theta_0 \right] \right\} \quad (3.27)$$

Equation (3.25) implies that buoyancy variance $\overline{b'^2}$ is a function of $\overline{\theta_l' b'}$ and $\overline{q_t' b'}$, which are together functions of $\overline{\theta_l'^2}$, $\overline{q_t'^2}$, and $\overline{\theta_l' q_t'}$, so that $\overline{b'^2}$ is computed as:

$$\overline{b'^2} = \alpha\left(a_c\right)^2 \overline{\theta_l'^2} + 2\alpha\left(a_c\right) \beta\left(a_c\right) \overline{\theta_l' q_t'} + \beta\left(a_c\right)^2 \overline{q_t'^2} \quad (3.28)$$

Thus, thermodynamic fluxes determined by the total energy closure may be inserted into the budgets of these three second-order moments (equations 3.12, 3.13, and 3.14) in order to determine buoyancy variance, which, along with the moist stability, may be substituted into definition (3.17) to determine TPE.

This energetic inconsistency of the total energy closure with respect to phase change and latent heating arises because $\overline{\theta_l'^2}$, $\overline{q_t'^2}$, and $\overline{\theta_l' q_t'}$ together encode information about both cloudiness and TPE. Explicit representation of TPE is not required however to account for its influence on turbulent mixing. Consider the budgets of sensible and latent heat fluxes, given respectively by (Stull 1988):

$$\underbrace{\frac{\partial \overline{w'\theta_l'}}{\partial t}}_{\mathcal{S}} = \underbrace{\overline{\theta_l' b'}}_{\mathcal{B}} \underbrace{- \overline{w'^2} \frac{\partial \overline{\theta_l}}{\partial z}}_{\mathcal{M}} \underbrace{- \frac{1}{\rho_0} \frac{\partial \rho_0 \overline{w'^2 \theta_l'}}{\partial z}}_{\mathcal{T}} \underbrace{- \frac{1}{\rho_0} \overline{\theta_l' \frac{\partial p'}{\partial z}}}_{\mathcal{P}} \underbrace{- \epsilon_{w\theta_l}}_{\mathcal{D}} \quad (3.29)$$

$$\underbrace{\frac{\partial \overline{w'q_t'}}{\partial t}}_{\mathcal{S}} = \underbrace{\overline{q_t' b'}}_{\mathcal{B}} \underbrace{- \overline{w'^2} \frac{\partial \overline{q_t}}{\partial z}}_{\mathcal{M}} \underbrace{- \frac{1}{\rho_0} \frac{\partial \rho_0 \overline{w'^2 q_t'}}{\partial z}}_{\mathcal{T}} \underbrace{- \frac{1}{\rho_0} \overline{q_t' \frac{\partial p'}{\partial z}}}_{\mathcal{P}} \underbrace{- \epsilon_{wq_t}}_{\mathcal{D}} \quad (3.30)$$

If I multiply equation (3.29) by $\alpha\left(a_c\right)$ and equation (3.30) by $\beta\left(a_c\right)$ and then sum them together, I obtain an equation resembling the dry buoyancy flux budget (equation 3.21) discussed in the previous section. The buoyancy terms ($\mathcal{B}$) sum to exactly equal the buoyancy term in the dry buoyancy flux budget via equation (45), and the same holds for the mean-gradient transport terms ($\mathcal{M}$) if the square of the buoyancy frequency is defined as:

$$N^2 = \alpha\left(a_c\right) \frac{\partial \overline{\theta_l}}{\partial z} + \beta\left(a_c\right) \frac{\partial \overline{q_t}}{\partial z} \quad (3.31)$$

Assuming stable stratification, a quasi-steady balance between $\mathcal{B} + \mathcal{P}_{\mathcal{B}}$, $\mathcal{M}$, and $\mathcal{P}_{\mathcal{T}}$ in the flux budgets, and identical return-to-isotropy timescales (τ_{wb}) and buoyancy production efficiencies ($1 - c_{\mathcal{B}}$) for both fluxes, I obtain the following equation which resembles equation (3.23):

$$\overline{w'b'} \approx \alpha\left(a_c\right) \overline{w'\theta_l'} + \beta\left(a_c\right) \overline{w'q_t'} = -2\tau_{wb} \left[E_w - \left(1 - c_{\mathcal{B}}\right) E_P\right] N^2 \quad (3.32)$$

This equation is approximate, because buoyancy flux approximates the "Gaussian part" of the flux given some unspecified trivariate joint-PDF of w', θ_l', and q_t' (Bechtold et al. 1995), so that equation (3.25) holds when $\chi = w$. Equation (3.32) implies that retaining the buoyancy terms ($\mathcal{B}$), in addition to the mean-gradient transport terms ($\mathcal{M}$), properly accounts for the local turbulent energetics of stable

stratification and the influence of TPE on moist turbulent mixing, since, as in the dry case, the dependence of buoyancy flux on $E_K - (1 - c_{\mathcal{B}})\, E_P$ still holds.

The novel way I have defined local moist stability in equation (3.31) is physically appealing, because it is consistent with how moist buoyancy variance is formulated from equation (3.28). Typically, moist stability is treated in turbulence-condensation schemes as a linear combination, weighted by cloud fraction, of the clear-sky and in-cloud oscillation frequencies of idealized parcels that are infinitesimally perturbed from stable equilibrium (Lenderink et al. 2004). However, there is no clear reason why cloud-fraction weighting should be applied for a partially cloudy system. In fact, contradicting the implication of this method, the "slice method" of Bjerknes (1938) implies that as cloud fraction approaches zero, the stability of the system approaches the in-cloud frequency. Thus, the definition of moist stability is assumption-dependent. Equation (3.31) instead imply a more meaningful interpretation, that, for stable stratification, N^2 equals the rate of buoyancy flux production per-unit TKE-TPE excess, $E_K - (1 - c_{\mathcal{B}})\, E_P$. To my knowledge, this definition and conceptual treatment of local moist stability has not been discussed in the modeling literature.

If the buoyancy production terms ($\mathcal{B}$) are retained in the budgets of sensible and latent heat flux and determined via equation (3.25) using the same measure of the covariability of heat and moisture that is used to estimate cloud cover, then the resulting turbulence closure represents a tier of energetic consistency above that of the total energy closure approach. That is, one in which TPE is both accounted for in

moist turbulent mixing and uniquely determined by the closure. I will call this property *moist local turbulent energetic consistency*. An example of such a closure is the Mellor-Yamada Level-3 turbulence parameterization (Nakanish and Niino 2004), which has four prognostic turbulence state variables, E_K, $\overline{\theta_l'^2}$, $\overline{q_t'^2}$, and $\overline{\theta_l' q_t'}$. Hence, a turbulence closure satisfying this property is not an innovation of my study, but rather, my aim is to recognize energetic consistency as an important consideration when determining the complexity of turbulence closures to be applied in numerical model of weather or climate.

To illustrate the importance of moist local turbulent energetic consistency, I introduce here a modified version of the TKE-l closure used by my base model detailed in section (3.1), adding the least amount of complexity required to satisfy energetic consistency. I extend the number of prognostic turbulence state variables to four by including $\overline{\theta_l'^2}$, $\overline{q_t'^2}$, and $\overline{\theta_l' q_t'}$ in addition to E_K, thus making equations (3.12), (3.13), and (3.14) prognostic by retaining the storage terms ($\mathcal{S}$). For numerical stability, I also retain the transport terms ($\mathcal{T}$), modeling them diffusively with eddy diffusivity coefficients equal to K_h. The sensible and latent heat fluxes are determined by assuming a balance of the $\mathcal{B} + \mathcal{P}_{\mathcal{B}}$, $\mathcal{M}$, and $\mathcal{P}_{\mathcal{T}}$ terms in their respective budgets (equations 3.29 and 3.30), so that:

$$\overline{w'\theta_l'} = -K_h \left[\frac{\partial \overline{\theta_l}}{\partial z} - \frac{(1 - c_{\mathcal{B}})\, \overline{\theta_l' b'}}{2 A_w E_K} \right] \quad (3.33)$$

$$\overline{w' q_t'} = -K_h \left[\frac{\partial \overline{q_t}}{\partial z} - \frac{(1 - c_{\mathcal{B}})\, \overline{q_t' b'}}{2 A_w E_K} \right] \quad (3.34)$$

where the vertical anisotropy is approximated as a constant $A_w = 1/2$ and $c_{\mathcal{B}} = 1/2$. Throughout this dissertation, I will refer to this closure interchangeably as the "HOC" or "level-3 closure".

3.5 Summary

In this chapter, I introduced moist local energetic consistency as a criterion for evaluating turbulence closures. This analysis is inspired by the work of Zilitinkevich et al. (2008), who introduced the concept of TPE, as a counterpart to TKE, and raised serious concerns about its lack of representation in TKE-l closures. Their analysis forms the theoretical basis for the total energy closure approach (Mauritsen et al. 2007), which, due to its more consistent treatment of turbulent energy, addresses long standing problems with the modeling stable boundary layers. However, I show in this chapter that such an approach is not appropriate for cloudy boundary layers, since total turbulent energy does not encode sufficient information as a state variable to diagnose cloud cover and its influence on turbulent mixing. In a novel analysis, I apply the turbulence energetics concepts of Zilitinkevich et al. (2008) to the physical basis of high-order turbulence closures, showing that generalizations of the level-3-type closure of Mellor and Yamada (1974) satisfy the same energetic consistency criterion as the total energy closure approach while also accounting for the effects of phase change.

In the course of this discussion, I introduced three additional concepts that have not been previously treated in the turbulence literature. First, I show that the intensity of

turbulent mixing under stable stratification depends on the difference between TKE and TPE, not TKE alone. Second, I show that the counter-gradient flux correction present in level-3-type closures represents a local process (buoyancy acceleration), not non-local transport such as due to boundary layer thermals as is commonly assumed. Finally, I introduce an alternative definition of local moist stability that depends on the joint-distribution of heat and moisture and who's square can be conceptualized physically as the rate of buoyancy flux production per-unit TKE-TPE excess.

Chapter 4: Evaluating local energetic consistency

4.1 Experimental design

In this section, I evaluate the importance of the MLEC property, defined in the previous chapter, by performing several numerical experiments using my simple SCM. As a control for the experiments, the configuration of the SCM is that of the base model, described in section (3.1), using a TKE-l-type turbulence closure, which, as discussed in the previous chapter, does not satisfy the MLEC property. For the primary experiments, I configure the SCM with the four-variable HOC described in section (3.4) which does satisfy the MLEC property. The prognostic equations for these variables are equations (3.6), (3.12), (3.13), and (3.14), with sensible and latent heat fluxes given by equations (3.33) and (3.34) respectively. Since the TKE-l closure and HOC use the same configurations for properties like the mixing and dissipation length scales, this experimental design allows me to determine the significance of using the additional turbulence state variables to achieve local energetic consistency. To validate these experiments, I use LES, driven by identical forcings and initial conditions as the SCM experiments. The LES code used is a modified version of the UCLA-LES model (Stevens et al. 2005). UCLA-LES is an anelastic LES with a Smagorinsky-type sub-filter model. The core parts of the code are mostly unchanged, but I have written a new module for computing profile statistics, allowing the estimation of all terms in the budgets of all second-order moments. This fork from the official UCLA-LES code on GitHub can be found at http://www.github.com/davidandrewnew/uclales.

4.2 Test case #1: shear-free dry convective boundary layer (DCBL)

For the first numerical experiment, I evaluate simulations of a shear-free dry convective boundary layer (DCBL). The DCBL is a useful starting point for parameterization evaluation, since it is the boundary layer regime from which shallow cumulus convection begins. Since this idealized atmosphere lacks water vapor, the HOC reverts to a closure with two turbulence state variables: E_K and $\overline{\theta'^2} = \overline{\theta_l'^2}$. Though there is no moisture, one can still understand the two-variable HOC as a specific, dry case of the MLEC property. The DCBL test case is derived from an LES inter-comparison study by Nieuwstadt et al. (1993). The initial conditions are a uniform potential temperature lapse rate of 3.9 Kkm^{-1} and surface potential temperature of 297.2 K. The surface sensible heat flux is set equal to a constant value of 0.06 Kms^{-1}, with the simulation run for 4 hours.

Figure (4.1) depicts predictions for the DCBL case by LES, the base model SCM with the TKE-l closure, and the SCM with the HOC. What is clear for both turbulence closures is an underprediction of the height of the boundary layer by roughly 100 meters (850 meters for LES), as measured by the height of the minimum sensible heat flux. Moreover, both closures overpredict the maximum TKE by about 30%. However, the potential temperature profile from the HOC prediction is much more similar in shape to the LES prediction, despite the underprediction of boundary layer depth. That is, the unstable surface layer and stable capping inversion each make up about 10-15% of the depth of the boundary layer at its bottom and top respectively.

The middle part of the boundary layer is almost neutrally stable, with the transition point from unstable to stable stratification occurring at roughly half the height of the boundary layer. In contrast, the TKE-l closure predicts a CBL that is unstable through most of its depth with a sudden transition to unrealistically strong stratification in an unrealistically shallow capping inversion. In fact, this profile resembles that of the LES-predicted surface layer, except through the entire depth of the CBL, capped by a very strong inversion. As a consequence, the lower part of the boundary layer is too warm and its upper part is too cold.

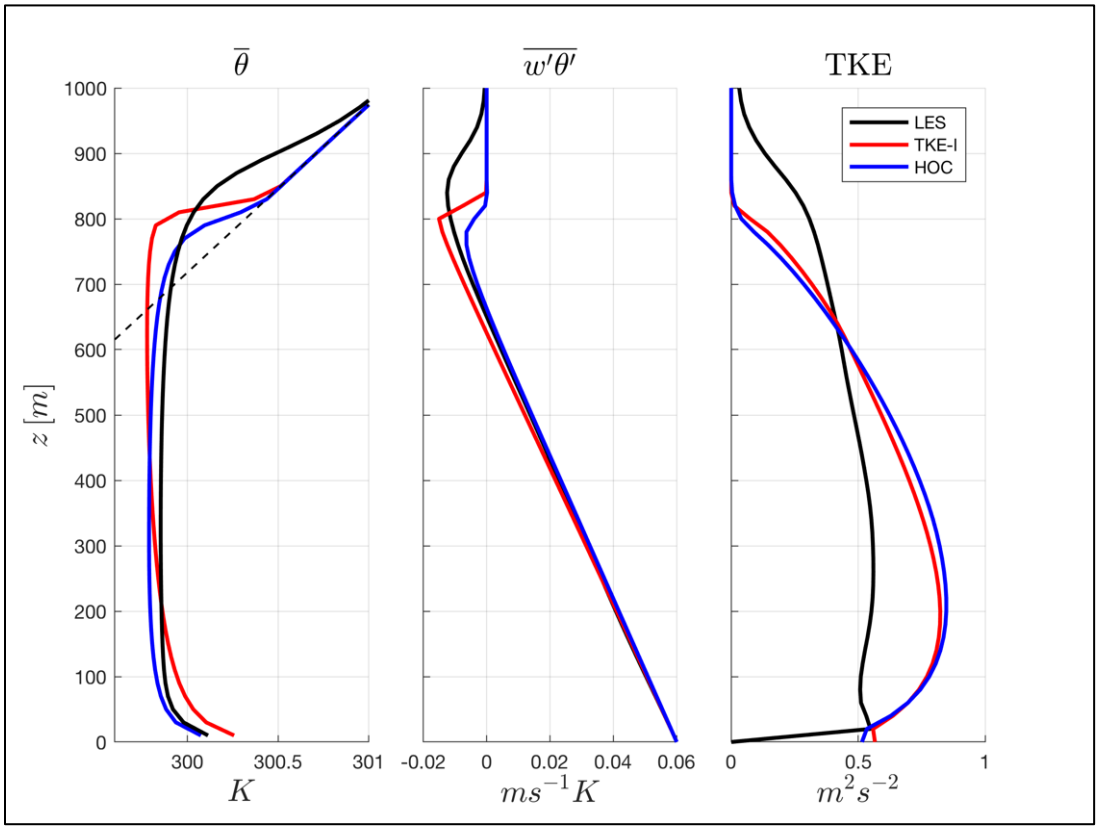

Figure 4.1 *Left panel depicts the potential temperature profiles predicted for the DCBL case by LES, the TKE-l closure, and the level-3 HOC. The middle panel depicts the corresponding potential temperature fluxes, and the right panel depicts the TKE profiles.*

To gain a better understanding of why the HOC predicts a much more realistic potential temperature profile shape than the TKE-l closure, I propose a novel method for evaluating SCM performance. Rather than comparing *predictions* of the mean state variables by SCM and LES using identical initial conditions, one can compare the flux *response* of the turbulence closure to the mean state variables predicted by the LES. For the DCBL case, this is achieved by fixing the mean potential temperature in the SCM to the LES-predicted profile, and then letting the SCM run until its turbulence state variables come to a steady state. Figure (4.2) depicts this "steady response" for the two closures.

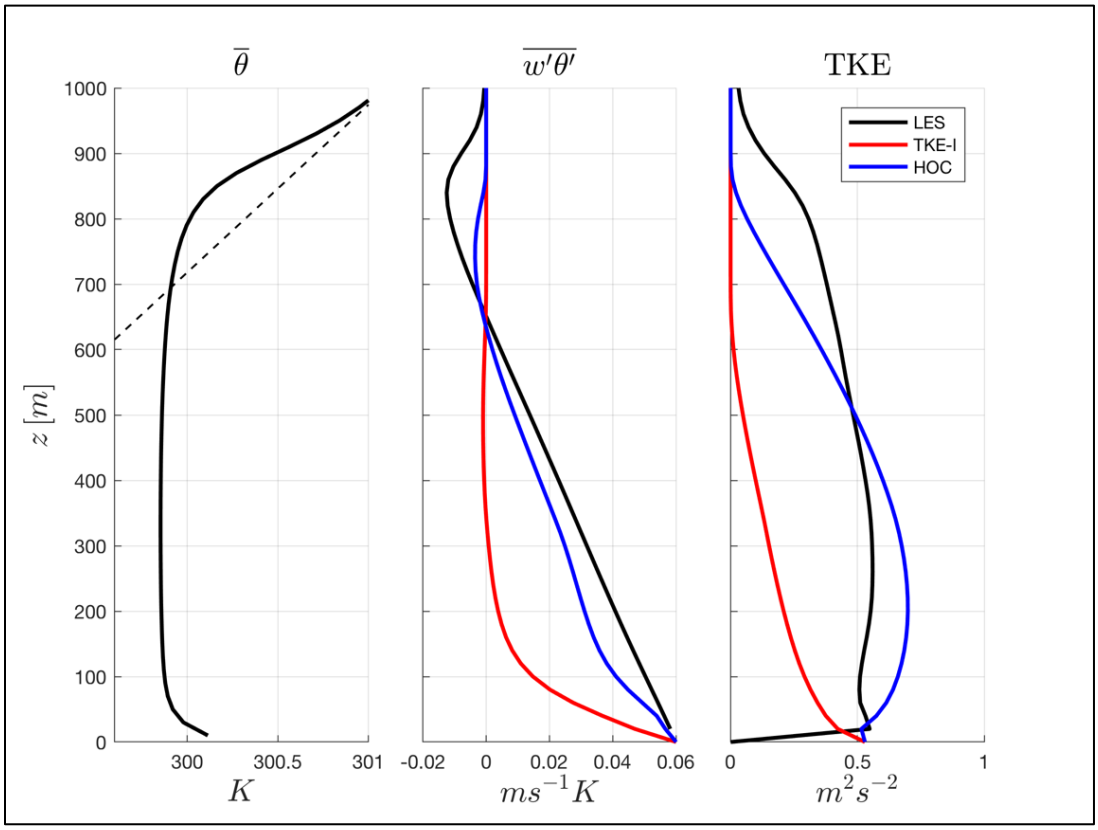

Figure 4.2 *The left panel depicts the LES-predicted potential temperature profile for the DCBL case. The middle panel depicts the corresponding potential temperature*

flux along with the quasi-steady flux responses of the TKE-l closure and the level-3 HOC. The right panel depicts the LES-predicted TKE profile and the responses of the closures.

The steady response of the sensible heat flux is concave-up in the CBL mixed layer, rather than the linear profile implied by LES, reaching zero at around 400 meters, rather than 650 meters (LES). The downward heat fluxes are almost completely negligible. Like-wise, the TKE is severely under-predicted and its profile has an unrealistic concave-up shape, vanishing at around 600 m. The degree of this under-prediction makes clear the consequences of the TKE-l closure's non-physical destruction of turbulent energy in the stable part of the potential temperature profile. Though the HOC flux response is also unrealistic in some ways, its shape is largely correct. With the exception of a small dip near the surface, the sensible heat flux profile is linear in the mixed layer and vanishes at the correct height. It exhibits a non-negligible downward heat flux at the top of the CBL, though that layer is too shallow. The TKE profile also has a realistic shape, increasing in the surface layer and then gradually decreasing until vanishing at about 850 meters, about 100-200 less that LES.

The steady response of the TKE-l closure makes clear its stark misrepresentation of the CBL's turbulence energetics. As discussed in chapter 3, TKE is effectively destroyed in the stable upper half of the CBL rather than being converted into TPE, as the buoyancy term ($\mathcal{B}$) is not included in the buoyancy flux budget. This

results in a non-physical "leaking" of turbulent energy from the system and explains the TKE-l closure's severe under-diagnoses of TKE. For the level-3 HOC on the other hand, the buoyancy term ($\mathcal{B}$) in buoyancy flux budget acts as a control value for turbulent energy, restricting the net conversion of TKE into TPE as TPE increases. TPE thus serves as a well of turbulent energy available for conversion into TKE via buoyancy acceleration ($\mathcal{B}$) so as to complement the conversion of TKE into TPE by mean-gradient transport ($\mathcal{M}$). Additionally, since TKE is required for the eddy-diffusive turbulent transport of TKE from the lower to upper half of the CBL, any scarcity of TKE in the stable upper half of the CBL hampers the efficiency of this transport, thus compounding the energy shortage manifested by the TKE-l closure.

Returning now to the "online" predictions shown in figure 4.1, both closures have very similar TKE profiles, but each achieves them with potential temperature profiles of much different shapes. The TKE-l closure predicts a profile that is unstable throughout most of the depth of the CBL, so that buoyancy flux is positive or weakly negative through that depth. In this way, it compensates for the non-physical leaking of TKE by minimizing static stability throughout the CBL. Such a profile is achieved, because there is no counter-gradient flux correction, so that TKE is used entirely for down-gradient mixing, resulting in an excess of diffusion and over-mixing. The level-3 HOC, on the other hand, can tolerate positive stability in the upper half of the CBL, since turbulent energy is not non-physically destroyed, and its counter-gradient flux correction limits the intensity of diffusion, preventing the overmixing present in the TKE-l closure's prediction.

4.3 Test case #2: marine stratocumulus-topped boundary layer (SCBL)

Here, I will test the base model and its extension for a marine stratocumulus-topped boundary layer (SCBL). This case is useful, because a convection parameterization is not required, since non-local transport is relatively negligible in stratocumulus cloud layers. Thus, it isolates and illustrates the importance of moist local energetic consistency is the presence of phase change, as discussed in section 3.4.

The setup for this case comes from LES and SCM inter-comparison study of Duynkrke et al. (1999). The initial conditions are a well-mixed layer in the first 687.5 m, with a potential temperature of $288\,K$ and specific humidity of $10.7\,gkg^{-1}$. Above that is a strong inversion measuring $5\,K$ and $1.6\,gkg^{-1}$ over $25\,m$. Above the inversion is a lapse rate in the free atmosphere of $6\,Kkm^{-1}$ and $2.4\,gkg^{-1}km^{-1}$. The surface forcing is 13 and $55\,Wm^{-2}$ sensible and latent heat fluxes, and the subsidence throughout the depth of the domain corresponds to a divergence of $1.5 \times 10^{-5}\,s^{-1}$. The zonal and meridional initial and geostrophic wind profiles are vertically uniform and southeasterly with magnitudes of 3 and $10\,ms^{-1}$ respectively. The latitude determining the geostrophic forcing is $36^{\circ}N$. A simple radiative parameterization computes the longwave radiative flux from the cloud liquid water path (LWP) as:

$$F_{longwave}\left(z\right) = F_{top}e^{-aLWP(z)} \quad (4.1)$$

where $a = 130\, m^2 kg^{-1}$ and $F_{top} = 74\, W m^{-2}$.

Figure (4.3), (4.4), and (4.5) show predictions for the SCBL case by LES, the base model SCM with the TKE-l closure, and the SCM with the level-3 HOC. Figure (4.3) depicts the total water specific humidity profiles and latent heat flux, figure (4.4) the liquid water potential temperature profiles and sensible heat flux, and figure (4.5) depicts the liquid water specific humidity and cloud fraction profiles. The LES and two SCMs predict boundary layers of similar height, with a stratiform cloud deck forming in the upper two thirds of the layer. What is striking however, is that the level-3 HOC, in agreement with LES, is able to capture the stronger tendency to form a well-mixed layer mostly within the core of the cloud deck, while the TKE-l closure tends to form a well-mixed layer through the entire depth of the boundary layer. Moreover, the level-3 HOC is able to capture the transition from neutral to strong stability at the top of the boundary layer, while the TKE-l closure forms a sharp inversion, in a similar fashion as the DCBL case. These behaviors can be explained in the same way as for the DCBL case. The TKE-l closure cannot tolerate positive stability without a collapse in its TKE profile, and it avoids such stability by over-mixing driven by the lack of a counter-gradient flux correction.

Both closures over-predict the depth of the cloud layer, with clouds too close to the surface, and both under-predict the peak cloud fraction of 100% at $700\, m$. The TKE-l closure predicts a slightly higher cloud top height and a higher cloud base height higher than the level-3 HOC's cloud base by almost $100\, m$. It also predicts an

unrealistically sharp decline in cloud fraction at the top of the boundary layer, while the level-3 HOC is better able to capture the smooth transition in cloud fraction. This difference in cloud-base height between each closure is a consequence of the over-mixing by the TKE-l closure, since more mixing results in a lower part of the SCBL that is warmer and dryer. The over-prediction of cloud-top height by the TKE-l closure can be similarly be explained by this over-mixing which results in excess boundary layer top-entrainment. The sharpness with which cloud fraction at the top of the cloud layer declines is a consequence of the sharp temperature and moisture inversions predicted by the TKE-l closure. Differences in the cloudiness profile between the level-3 closure and LES, particularly the cloud base height that is too low, is a consequence of errors in the predicted (co-)variability of heat and moisture. Though tuning of the level-3 closure would likely improve the cloudiness profile, here I am interested in differences between the TKE-l closure and level-3 HOC.

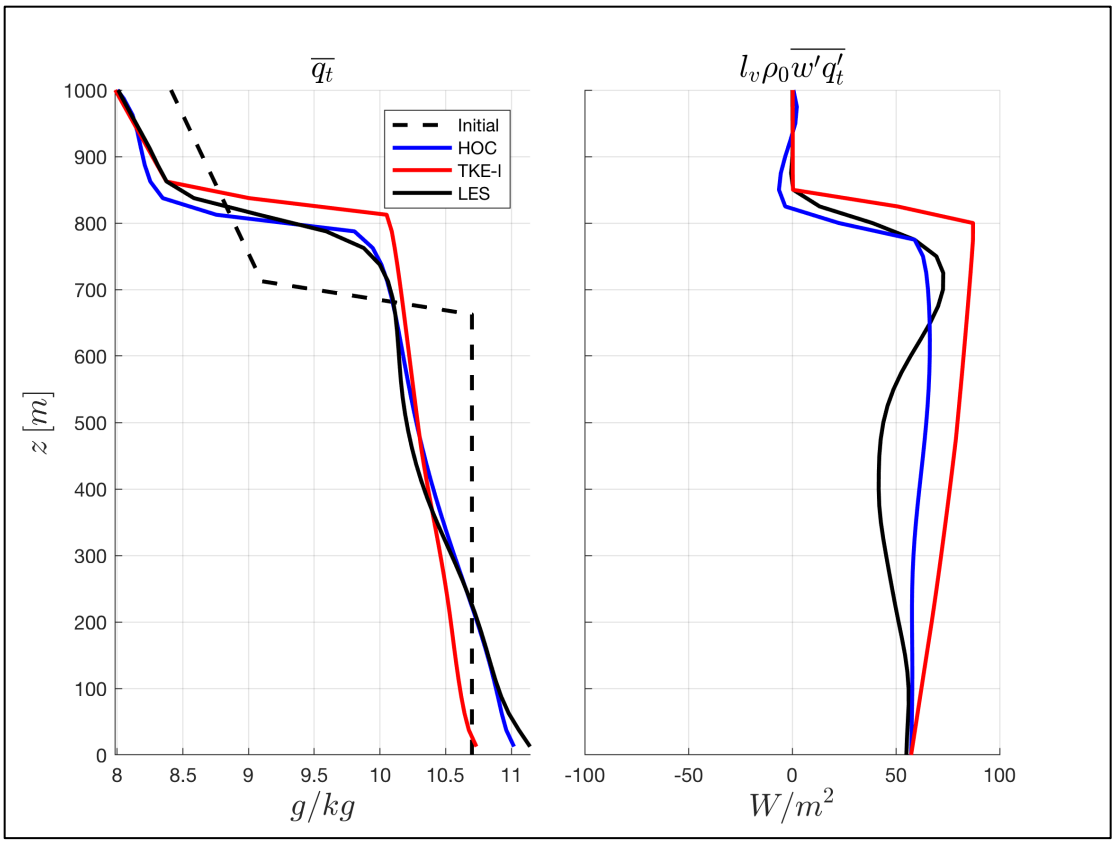

Figure 4.3 *The left panel depicts the total water specific humidity profiles for the SCBL case, predicted by LES, the TKE-l closures, and the level-3 HOC. The right panel depicts the corresponding latent heat fluxes.*

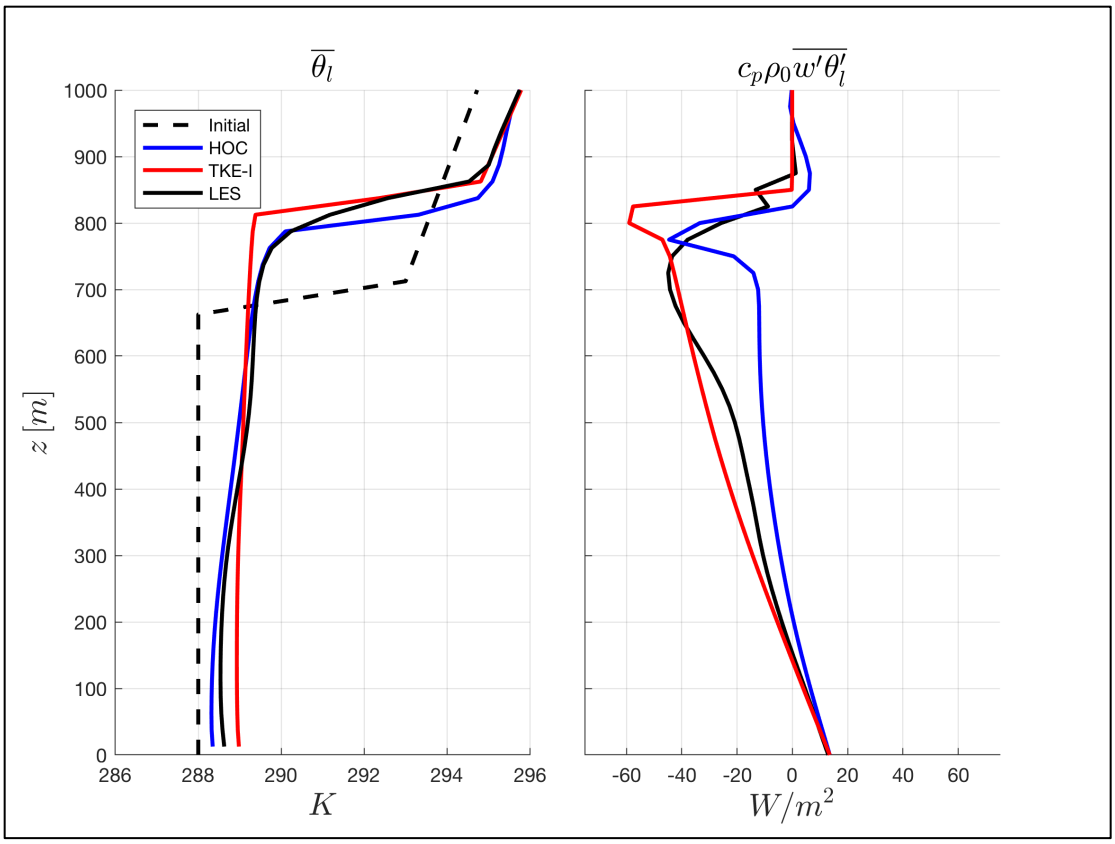

Figure 4.4 *The left panel depicts the liquid water potential temperature profiles for the SCBL case, predicted by LES, the TKE-l closures, and the level-3 HOC. The right panel depicts the corresponding latent heat fluxes.*

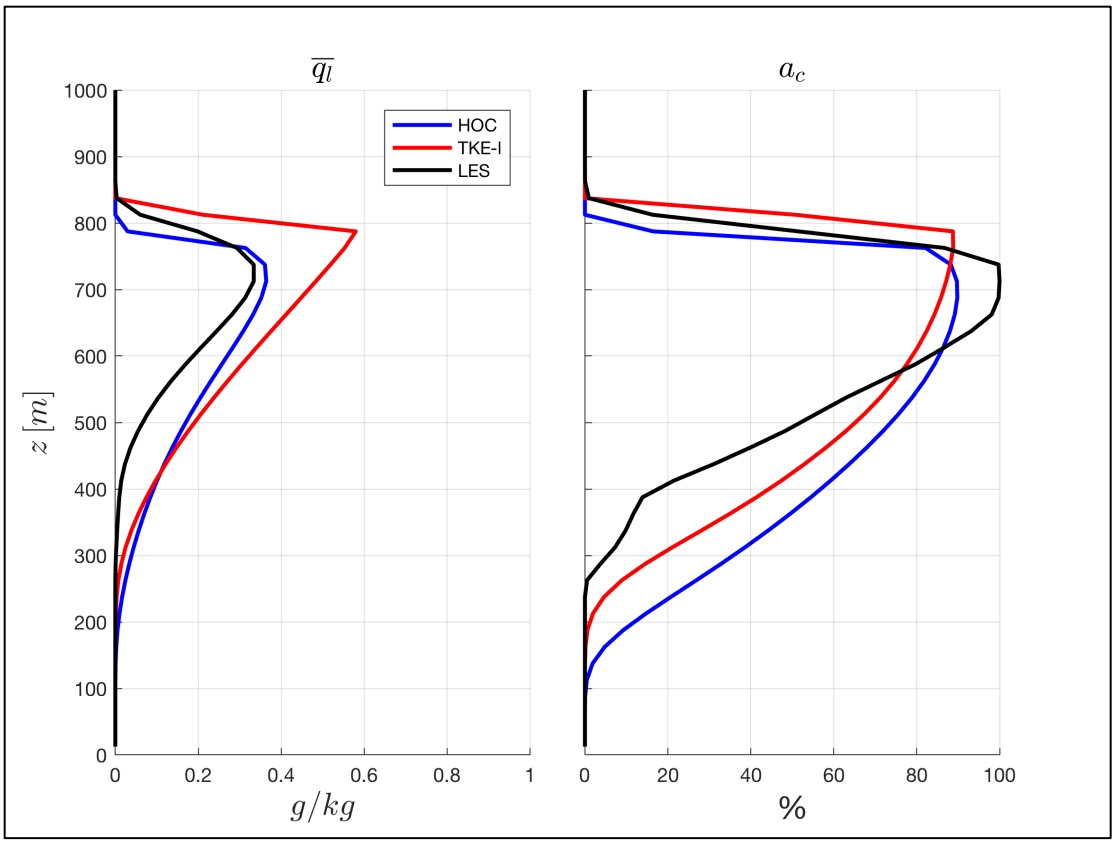

Figure 4.5 *The left panel depicts the liquid water specific humidity profiles for the SCBL case, predicted by LES, the TKE-l closure, and level-3 HOC. The right panel depicts the corresponding cloud fraction profiles.*

4.4 Summary

The DCBL and SCBL cases I use to evaluate the TKE-l closure and level-3 HOC well illustrate the importance of moist local energetic consistency in the representation of turbulent mixing I posit in chapter 3. In both cases, the level-3 HOC is correctly able to simulate the shape of thermodynamic profiles in the stably stratified capping inversion of the boundary layer, while the TKE-l closure is not.

The TKE-l closure tends to compensate by forming well-mixed layers where they do not belong, while forming inversions that are too sharp. This is because, as discussed in chapter 3, the TKE-l closure "leaks" turbulent energy under stably stratified conditions but over-mixes due to the lack of a counter-gradient flux correction. Both cases show that local energetic consistency is crucial both for dry convection and in the presence of phase change.

Chapter 5: Non-local energetic consistency

5.1 EDMF base model extension

Here, I introduce an extension to the TKE-l and level-3 HOC base models outlined in section (3.1), by including a mass flux scheme and entraining plume model to make them EMDF parameterizations. The vertical flux of $\phi \in \{\theta_l, q_t\}$ for this scheme is given by (see equation 2.16):

$$\rho_0 \overline{w'\phi'} = -\rho_0 K_h \frac{\partial \overline{\phi}}{\partial z} + M_u \left(\overline{\phi}^u - \overline{\phi}^e \right) \quad (5.1)$$

where K_h is determined using the closures described in section (3.1), while M_u and $\overline{\phi}^u$ are determined by an entraining plume model. The TKE-l closure and mass flux scheme are coupled via the buoyancy term ($\mathcal{B}$) in prognostic equation for TKE, which, applying equation (5.1) is given by

$$\rho_0 \overline{w'b'} = -\rho_0 K_h N^2 + M_u \left(\overline{b}^u - \overline{b}^e \right) \quad (5.2)$$

The HOC is coupled in a similar fashion, whereby all fluxes appearing the second-order moment budgets are specified as in equation (5.1). In a shallow cumulus-topped boundary layer, the mass flux component of the buoyancy flux generates TKE wherever the updraft is positively buoyant, that is, inside the CBL and above the level of free convection. The diffusive flux component generates TKE, as always, wherever the atmosphere is unstably stratified. Conversely, the mass flux component destroys TKE in places where the updraft is negatively buoyant, like the CBL inversion, while the diffusive component destroys TKE wherever the atmosphere is stably stratified.

The entraining plume model for the mass flux scheme is the *thermal plume model* of Rio and Hourdin (2008). The thermal plume model differs from a typical entraining plume model used by conventional mass flux and EDMF parameterizations (see section 2.2.2) in that it assumes the updraft consists of the entire ensemble of boundary layer thermals, rather than the strongest 5-10% vertical motions. For this reason, the updraft area fraction potentially approaches 50%. This type of model is used as the EDMF base model for my numerical experiments because, to my knowledge, it is the only such model formulating entrainment and detrainment in such a way as to guarantee conservation of mass. As I will show when I introduce my new parameterization, this condition becomes necessary.

The diagnostic budget equations for the thermodynamic state of the updraft are given for $\phi \in \{\theta_l, q_t\}$ by (Rio and Hourdin 2008):

$$\frac{\partial M_u \overline{\phi}^u}{\partial z} = E\overline{\phi}^e - D\overline{\phi}^u \tag{5.1}$$

where E and D are the rates of entrainment and detrainment respectively. For the updraft vertical velocity $\overline{w}^u$, the budget is given by:

$$\frac{\partial M_u \overline{w}^u}{\partial z} = -D\overline{w}^u + \rho_0 a_u \left(\overline{b}^u - \overline{b}\right) \tag{5.2}$$

where a_u is the area fraction of the updraft. The updraft mass flux M_u is governed by the updraft continuity equations, given by:

$$\frac{\partial M_u}{\partial z} = E - D \tag{5.3}$$

In the surface layer, "organized" entrainment into the updraft is assumed to be governed by convergence of the subsiding air around it. A normalized empirical profile of organized entrainment $A^\star = A/M_0$ is assumed in the surface layer, where M_0 equals the mass flux at the top of the surface layer, and A is the rate of organized entrainment. This profile is given by:

$$A^\star = \Gamma\sqrt{z}\max\left(-\frac{\partial\overline{b}}{\partial z}, 0\right) \quad (5.4)$$

where Γ is chosen so that:

$$\int_0^\infty A^\star dz = 1 \quad (5.5)$$

Above the surface layer but below the level of neutral buoyancy, detrainment is assumed to erode the area fraction of the updraft over a length scale $\lambda = 30\,m$, so that:

$$D^\star = \frac{1}{rz_tM_0}\frac{\partial\rho_0\overline{w}^u\sqrt{\lambda z}}{\partial z} \quad (5.6)$$

where $r = 2$ is the aspect ratio of the thermal plume, z_i is the height where the updraft reaches its maximum vertical velocity, and z_t is the height where its vertical velocity vanishes. In this layer, the entrainment rate is assumed to scale with, but be slightly less than, the detrainment rate, so that:

$$E^\star = \beta D^\star + A^\star \quad (5.7)$$

where $\beta = 0.4$. Above the level of neutral buoyancy, the updraft area fraction is eroded by detrainment quadratically until vanishing at z_t, so that:

$$D^{\star} = \frac{1}{M_0}\frac{\partial}{\partial z}\rho_0 a_u\left(z_i\right)\overline{w}^u\left(\frac{z_t - z}{z_t - z_i}\right)^2 \quad (5.8)$$

Following the physical arguments of Hourdin et al. (2002), the maximum vertical velocity inside the updraft is assumed equal to the maximum horizontal velocity of air entraining into it in the surface layer. After some mathematical manipulation, this implies the following closure equation for M_0:

$$M_0 = \frac{w\left(z_i\right)}{r z_t \int_0^{\infty} \frac{\left(A^{\star}\right)^2}{\rho_0} dz} \quad (5.9)$$

Once M_0 is obtained, the mass flux can be determined as $M_u = M_0 M^{\star}$. The value of the area fraction is then implied by the definition of mass flux so that:

$$a_u = \frac{M_u}{\rho_0 \overline{w}^u} \quad (5.10)$$

Since M_0 and z_t are required for several computations before they are obtained, must be computed by running the thermal plume model iteratively. The updraft vertical velocity closest to the surface is adjusted for each iteration, so that the area fraction nearest the surface equals 35% to match observations (Couvreux et al. 2010).

5.2 Energetics of non-local transport

5.2.1 The turbulent transport term

The core problem for unifying the representation of turbulence and convection is achieving a seamless treatment of local mixing and non-local transport. EDMF attempts to do this by decomposing turbulent fluxes into a diffusive component and

an advective (mass flux) component. As discussed in chapter 3 and evaluated numerically in chapter 4, an energetically consistent treatment of local mixing requires an accounting of both mean-gradient transport ($\mathcal{M}$) and buoyancy acceleration/deceleration ($\mathcal{B}$) terms in the formulation of sub-grid fluxes from their budget equations. Convection, however, is an inherently non-local processes, as boundary layer thermals and cumulus clouds transport air from the height that their air is destabilized to the height where it reaches equilibrium. In stably stratified layers, as discussed in chapter 3, this means that the rate of kinetic energy generation by buoyancy ($\mathcal{B}$) exceeds its conversion into potential energy by mean-gradient transport ($\mathcal{M}$). The communicator between these two local processes in time and space are the storage ($\mathcal{S}$) and turbulent transport ($\mathcal{T}$) terms respectively. Since, as demonstrated by the LES-estimated TKE and buoyancy flux budgets, turbulence and dry convection are effectively quasi-steady, the key process underlying non-local sub-grid transport corresponds to the turbulent transport ($\mathcal{T}$) term.

In the budgets of second-order moments, $\mathcal{T}$ is the vertical derivative of a third-order moment, and different unified turbulence-convection modeling approaches handle this term in different ways. For the simple TKE-l closure in the base model introduced in chapter 3, the turbulent flux of TKE, the only prognostic second-order moment, is treated diffusively, that is, proportional to the local gradient of TKE (see equation 3.6):

$$\mathcal{T} = -\frac{1}{\rho_0}\frac{\partial \rho_0 \overline{w' E_K'}}{\partial z} = \frac{1}{\rho_0}\frac{\partial}{\partial z}\rho_0 K_E \frac{\partial E_K}{\partial z} \quad (5.11)$$

As demonstrated in the DCBL experiment of chapter 4, this treatment cannot transport turbulent energy high enough into the inversion to generate enough top-entrainment to match the LES-predicted boundary layer height.

To compare the treatment of non-local transport by the mass flux approach with the two closures, I need to be able to compare the turbulent transport terms ($\mathcal{T}$) for their second-order moment budgets. However, the governing equations of the thermal plume model in an EDMF scheme (equations 5.1 and 5.2) are budgets for first-order updraft-averaged properties. De Roode et al. (2000) took these equations and, after strenuous mathematical manipulation and retaining time tendencies for completeness, derived budgets equations for second-order moments:

$$\underbrace{\rho_0 \frac{\partial a_u \left(1-a_u\right) \left(\overline{w}^u - \overline{w}^e\right)^2}{\partial t}}_{\mathcal{S}} = \underbrace{2M_u \left(\overline{b}^u - \overline{b}^e\right)}_{\mathcal{B}} \underbrace{- \frac{\partial \left(1-2a_u\right) M_u \left(\overline{w}^u - \overline{w}^e\right)^2}{\partial z} - \left(E+D\right)\left(\overline{w}^u - \overline{w}^e\right)^2}_{\mathcal{T}} \tag{5.12}$$

$$\underbrace{\rho_0 \frac{\partial a_u \left(1-a_u\right) \left(\overline{\phi}^u - \overline{\phi}^e\right)^2}{\partial t}}_{\mathcal{S}} = \underbrace{-2M_u \left(\overline{\phi}^u - \overline{\phi}^e\right) \frac{\partial \overline{\phi}}{\partial z}}_{\mathcal{M}} \underbrace{- \frac{\partial \left(1-2a_u\right) M_u \left(\overline{\phi}^u - \overline{\phi}^e\right)^2}{\partial z} - \left(E+D\right)\left(\overline{\phi}^u - \overline{\phi}^e\right)^2}_{\mathcal{T}} \tag{5.13}$$

$$\underbrace{\frac{\partial M_u \left(\overline{\phi}^u - \overline{\phi}^e\right)}{\partial t}}_{\mathcal{S}} = \underbrace{\rho_0 a_u \left(1-a_u\right) \left(\overline{b}^u - \overline{b}^e\right)\left(\overline{\phi}^u - \overline{\phi}^e\right)}_{\mathcal{B}} \underbrace{- M_u \left(\overline{w}^u - \overline{w}^e\right) \frac{\partial \overline{\phi}}{\partial z}}_{\mathcal{M}} \underbrace{- \frac{\partial \left(1-2a_u\right) M_u \left(\overline{w}^u - \overline{w}^e\right)^2}{\partial z} - \left(E+D\right)\left(\overline{w}^u - \overline{w}^e\right)^2}_{\mathcal{T}} \tag{5.14}$$

Though these equations are not explicitly integrated by the thermal plume model, they are mathematically equivalent and provide a useful perspective to illustrate the treatment of turbulent energetics by mass flux schemes.

Three comments are in order about these equations. First, entrainment and detrainment effects are turbulent transport processes ($\mathcal{T}$), since they are derived from advection terms in the underlying perturbation budgets. De Roode et al. (2000) associated entrainment and detrainment with dissipation, but only because these terms are strictly negative. This is because the mass flux approximation assumes that the interior of the updraft and environment are uniform with respect to dynamic and thermodynamic properties, so that, cooler/dryer/slower environmental, air entrained into the updraft, must be warmed/moistened/accelerated in order for the updraft to remain uniform with respect to heat/moisture/momentum. This amounts to an effective dissipation of variance, though viscous dissipation ($\mathcal{D}$) is not explicitly accounted for. Second, since the equations of the thermal plume model (equations 5.1 and 5.2) are diagnostic, the storage terms ($\mathcal{S}$) in equations (5.12), (5.13), and (5.14) are neglected. Third, though the mass flux approach is considered inherently non-local, it still accounts for local processes via mean-gradient transport **(**$\mathcal{M}$**)** and buoyancy acceleration **(**$\mathcal{B}$**)** terms in these equations.

5.2.2 Parallel treatments of non-local transport in EMDF approach

Non-local transport in EDMF parameterizations are represented in two parallel but not necessarily consistent ways. First, it is determined in the mass flux scheme via

the advective treatment of the turbulent transport terms ($\mathcal{T}$) in equations (5.12), (5.13), and (5.14). Second, it is determined in the TKE-l closure or level-3 HOC by the diffusive turbulent transport term ($\mathcal{T}$) in the TKE budget. In a third, somewhat vague sense, non-local transport is treated by the coupling of the mass flux scheme and the closures, since, for example, updraft buoyancy may be non-locally transported by mass flux scheme from one height to another, where both closures use it to generate/destroy TKE.

The energetic inconsistency lies in two facts. First, the organized TKE associated with the updraft vertical velocity is rolled into the prognostic TKE variable. This can lead to a contradiction, whereby, at some heights, the organized TKE associated with the updraft vertical velocity is non-zero, but the total TKE, according to the TKE-l closure or HOC, equals zero, so that:

$$0 < \frac{1}{2} a_u \left(1 - a_u\right) \left(\overline{w}^u - \overline{w}^e\right)^2 > E_K = 0 \tag{5.15}$$

Second, both closures transport TKE diffusively, while the mass flux approach transports TKE advectively. It seems unlikely that diffusion can "keep up" with advection and transport TKE high enough into the inversion to match the organized TKE of the mass flux scheme.

5.3 Evaluating the EDMF approach

Figure (5.1) depicts simulations of the DCBL experiment from chapter 4, using the TKE-l and HOC-based EMDF extensions to the base model, along with LES.

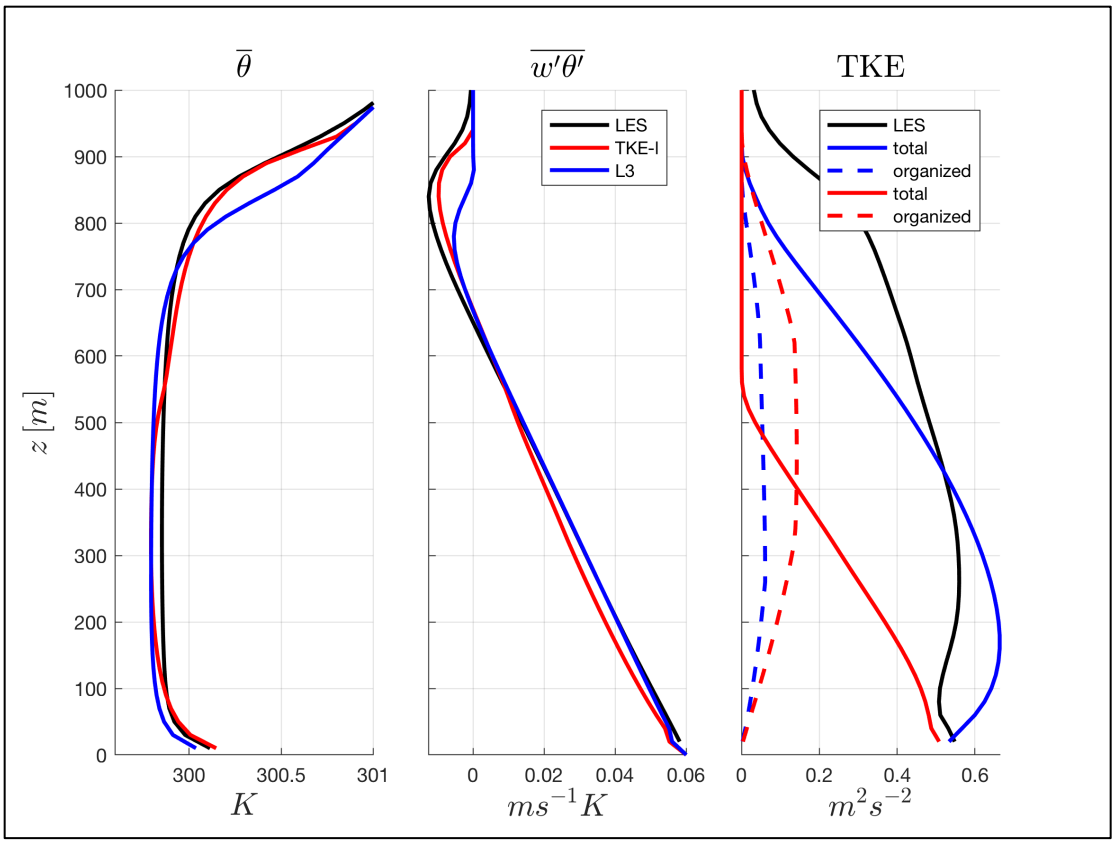

Figure 5.1 *The left panel depicts the potential temperature profiles for the DCBL case, predicted the LES and the TKE-l-based and HOC-based EDMF schemes. The middle panel depicts the corresponding potential temperature flux profiles. The right panel depicts the corresponding total TKE profiles, along with the organized TKE profiles for each mass flux scheme.*

As hypothesized as a possibility in the previous section, the prognostic TKE of the TKE-l closure vanishes at around 500 m, below the top of the updraft at around 900 m, implying the contradiction of inequality (5.15). This leads to a peculiar "bump" in the predicted potential temperature profile where TKE vanishes. In contrast, the HOC's TKE vanishes around the same height at the top of the updraft at around 850

m, and the potential temperature profile has a similar shape as the LES-predicted profile. This is easily explained by the fact that the HOC, with its counter-gradient buoyancy flux correction, does not non-physically "leak" TKE under stably stratified conditions, as discussed in chapter 3 and 4. For the TKE-l closure this problem is exacerbated by the fact that the downward organized buoyancy flux associated with the updraft also destroy TKE. However, the local energetic consistency gained from the counter-gradient flux correction causes the downward buoyancy flux, and thus the top-entrainment, to be too small, resulting in a boundary layer that is too shallow by roughly 100 m. The TKE-l-based EMDF scheme actually over-predicts the height of the boundary layer by a few tens of meters.

Chapter 6: A new approach: consistent partitioning of second-order moments

6.1 Non-local energetic consistency

As shown in chapter 5, a contradiction can occur for EDMF parameterizations, whereby the total TKE predicted by the TKE-l closure may vanish in the CBL inversion, while the organized (updraft) TKE diagnosed by the mass flux scheme is positive. At the root of this contradiction is the inconsistent partitioning of second-order moments and a fundamental difference in treatment of the turbulent transport term ($\mathcal{T}$) in the second-order moment budgets, whereby the diffusive treatment by the TKE-l closure or HOC cannot match the advective treatment by the mass flux scheme. This is because the EMDF approximation applies the updraft-environment decomposition only to sub-grid fluxes, but not to other second-order moments such as TKE. This suggests an alternative approach, whereby second-order moments are separated consistently between the sub-environmental and organized components, while still neglecting all sub-updraft second-order moments, so that an arbitrary variance is given by:

$$\overline{\phi'^2} \approx (1-a_u)\,\overline{\phi'^2}^e + a_u\,(1-a_u)\left(\overline{\phi}^u - \overline{\phi}^e\right)^2 \tag{6.1}$$

The organized (second) term continues to be diagnosed by the mass flux scheme and thermal plume model, while the sub-environmental (first) term becomes a prognostic variable. This ensures that the total variances is always positive when either of its components are positive. Tan et al. (2018) proposed applied a similar decomposition

after I introduced it in my prospectus defense, though their approach is not locally energetically consistent, since it treats sub-environmental fluxes using a TKE-l closure.

In general, if I expand the third-order moment underlying the turbulent transport term for the budget of an arbitrary second-order moment $\overline{\phi'^2}$, I obtain (after strenuous mathematical manipulation):

$$\begin{aligned}\rho_0\overline{w'\phi'^2} &= M_u\left(1-2a_u\right)\left(\overline{\phi}^u-\overline{\phi}^e\right)^2 \\ &+ 2M_u\left(\overline{\phi'^2}^u-\overline{\phi'^2}^e\right) \\ &+ \rho_0 a_u\left(1-a_u\right)\left(\overline{\phi}^u-\overline{\phi}^e\right)\left(\overline{w'\phi'}^u-\overline{w'\phi'}^e\right) \\ &+ \rho_0\left[a_u\overline{w'\phi'^2}^u+\left(1-a_u\right)\overline{w'\phi'^2}^e\right]\end{aligned} \tag{6.2}$$

Then, neglecting sub-updraft second-order moments, the turbulent transport term ($\mathcal{T}$) in the budget of $\overline{\phi'^2}$ becomes:

$$\begin{aligned}\mathcal{T}=-\frac{\partial\rho_0\overline{w'\phi'^2}}{\partial z} &\approx -\frac{\partial M_u(1-2a_u)\left(\overline{\phi}^u-\overline{\phi}^e\right)^2}{\partial z} \\ &+ \frac{\partial M_u\overline{\phi'^2}^e}{\partial z} \\ &+ 2\frac{\partial\rho_0 a_u(1-a_u)\left(\overline{\phi}^u-\overline{\phi}^e\right)\overline{w'\phi'}^e}{\partial z} \\ &- \frac{\partial\rho_0(1-a_u)\overline{w'\phi'^2}^e}{\partial z}\end{aligned} \tag{6.3}$$

Thus, I obtain a consistent partitioning of non-local transport. The first term on the RHS represents the organized turbulent transport of organized variance by the updraft. This same term appears in equation (5.13), the budget equation for the $\overline{\phi'^2}$ when only the mass flux scheme is active. The last term in the RHS represents turbulent transport of the $\overline{\phi'^2}$ within the environment. The remaining two terms

represent transport, in a coupled sense, due to both organized and sub-environmental transport.

6.2 Budgets equations for sub-environmental second-order moments

6.2.1 First-order moments

To derive budgets for sub-updraft and sub-environmental second-order moments, it will be helpful to begin with the standard derivation of first-order moments budgets, following Siebesma (1998). Consider an idealized model grid cell with cross-sectional area A_g and containing an updraft ensemble with cross-sectional area $A_u(z,t)$. The ratio of these two areas yields the updraft area fraction:

$$a_u(z,t) \equiv \frac{A_u(z,t)}{A_g} \tag{6.4}$$

The area-weighted Reynolds average of ϕ over the updraft cross-sectional area U is then given by:

$$\overline{\phi}^u = \frac{1}{A_u} \int \int_U \phi dA \tag{6.5}$$

Now, consider the flux-form prognostic equation for ϕ, given by:

$$\rho_0 \frac{\partial \phi}{\partial t} = -\rho_0 \nabla_h \cdot \mathbf{v}\phi - \frac{\partial \rho_0 w \phi}{\partial z} + \rho F_\phi + \rho_0 k_\phi \nabla^2 \phi \tag{6.6}$$

where ∇_h is the horizontal gradient operator, and k_ϕ is the rate of molecular diffusion for ϕ. I neglect molecular diffusion, integrate both sides of this equation over U, divide by A_g, and apply Gauss' and Leibniz' theorems to yield the flux-form budget equation for $\overline{\phi}^u$:

$$\rho_0 \frac{\partial a_u \overline{\phi}^u}{\partial t} = -\frac{\partial M_u \overline{\phi}^u}{\partial z} + E_\phi - D_\phi - \frac{\partial \rho_0 \overline{w'\phi'}^u}{\partial z} + \rho_0 a_u \overline{F_\phi}^u \quad (6.7)$$

Where E_ϕ and D_ϕ are the entrainment and detrainments rates of ϕ respectively.

The diagnostic budgets for the thermal plume model, equations (5.1) and (5.2), are obtained in three steps. First, ignore the time tendency and sub-updraft flux convergence terms. Second, define the following two averaging operators.

$$\overline{\phi}^E \equiv \frac{E_\phi}{E} \quad (6.8)$$

$$\overline{\phi}^D \equiv \frac{D_\phi}{D} \quad (6.9)$$

These represent the conditional mean, averaged over the air entraining into and detraining out of the updraft. Finally, assume the mean flux approximation (Siebesma 1998), that air entraining into or out of the updraft has the same properties as the grid cell and updraft respectively, so that:

$$\overline{\phi}^E \approx \overline{\phi} \quad (6.10)$$

$$\overline{\phi}^D \approx \overline{\phi}^u \quad (6.11)$$

For convenience, I restate equations (5.1) and (5.2) here:

$$\frac{\partial M_u \overline{\phi}^u}{\partial z} = E\overline{\phi}^e - D\overline{\phi}^u$$

$$\frac{\partial M_u \overline{w}^u}{\partial z} = -D\overline{w}^u + \rho_0 a_u \left(\overline{b}^u - \overline{b}\right)$$

To obtain the updraft continuity equation, substitute $\phi = 1$, yielding:

$$\rho_0 \frac{\partial a_u}{\partial z} = -\frac{\partial M_u}{\partial z} + E - D \quad (6.12)$$

As before, to obtain the diagnostic continuity equation for the thermal plume model (equation 5.3), ignore the time tendency to obtain:

$$\frac{\partial M_u}{\partial z} = E - D \tag{6.13}$$

6.2.2 Sub-updraft second-order moments

To derive budget equation for sub-environmental second-order moments, I first derive sub-updraft second-order moments. I first need the advective form of the updraft budget equations. Multiplying both sides of (6.12) by $\overline{\phi}^u$ and subtracting the resulting equation (6.7) yields:

$$\rho_0 a_u \frac{\partial \overline{\phi}^u}{\partial t} = -M_u \frac{\partial \overline{\phi}^u}{\partial z} + E\left(\overline{\phi}^E - \overline{\phi}^u\right) - D\left(\overline{\phi}^D - \overline{\phi}^u\right) - \frac{\partial \rho_0 \overline{w'\phi'}^u}{\partial z} + \rho_0 a_u \overline{F_\phi}^u \tag{6.14}$$

Now, consider the flux form prognostic equation for ϕ^2, obtained by multiplying both sides of equation (6.6) by 2ϕ, yielding:

$$\rho_0 \frac{\partial \phi^2}{\partial t} = -\rho_0 \nabla_h \cdot \mathbf{v}\phi^2 - \frac{\partial \rho_0 w \phi^2}{\partial z} + \rho F_{\phi^2} + \rho_0 k_\phi \nabla^2 \phi^2 \tag{6.15}$$

Integrating this equation over U and dividing both sides by A_g, then multiplying (6.14) by $2\overline{\phi}^u$ and subtracting the two resulting equations yields the advection form prognostic equation for $\overline{\phi'^2}^u$:

$$\begin{aligned}
\rho_0 a_u \frac{\partial \overline{\phi'^2}^u}{\partial t} \quad = \quad & - \quad M_u \frac{\partial \overline{\phi'^2}^u}{\partial z} - \frac{\partial \rho_0 a_u \overline{w'\phi'^2}^u}{\partial z} \\
& + \quad E(\overline{\phi'^2}^E - \overline{\phi'^2}^u) + E(\overline{\phi}^E - \overline{\phi}^u)^2 \\
& - \quad D(\overline{\phi'^2}^D - \overline{\phi'^2}^u) - D(\overline{\phi}^D - \overline{\phi}^u)^2 \\
& - \quad 2\rho_0 a_u \overline{w'\phi'}^u \frac{\partial \overline{\phi}^u}{\partial z} + 2\rho_0 a_u \overline{\phi' F'}^u \\
& - \quad \rho_0 a_u \epsilon^u_{\phi^2}
\end{aligned} \tag{6.16}$$

where $\epsilon^{e}_{\phi^2}$ is the rate of dissipation for $\overline{\phi'^2}^u$. To obtain the flux-form version of this equation, multiply equation (6.12) by $\overline{\phi'^2}^u$ and subtract it from (6.16) to obtain:

$$\begin{aligned}
\rho_0 \frac{\partial a_u \overline{\phi'^2}^u}{\partial t} &= - \frac{\partial M_u \overline{\phi'^2}^u}{\partial z} - \frac{\partial \rho_0 a_u \overline{w'\phi'^2}^u}{\partial z} \\
&+ E\overline{\phi'^2}^E + E(\overline{\phi}^E - \overline{\phi}^u)^2 \\
&- D\overline{\phi'^2}^D - D(\overline{\phi}^D - \overline{\phi}^u)^2 \\
&- 2\rho_0 a_u \overline{w'\phi'}^u \frac{\partial \overline{\phi}^u}{\partial z} + 2\rho_0 a_u \overline{\phi' F'}^u \\
&- \rho_0 a_u \epsilon^u_{\phi^2}
\end{aligned} \tag{6.17}$$

6.2.3 Sub-environmental second-order moments: budgets and interpretation

Almost identical derivation as from the previous section yields the flux-form budget of the sub-environmental second-order moments. For my proposed parameterization, I need budgets for $\overline{w'^2}^e$, $\overline{\phi'^2}^e \in \left\{\overline{\theta_l'^2}^e, \overline{q_t'^2}^e\right\}$, and $\overline{w'\phi'}^e \in \left\{\overline{w'\theta_l'}^e, \overline{w'q_t'}^e\right\}$. These are given by:

$$\begin{aligned}
\underbrace{\rho_0 \frac{\partial \left(1-a_u\right) \overline{w'^2}^e}{\partial t}}_{\mathcal{S}} &= \underbrace{+ \frac{\partial M_u \overline{w'^2}^e}{\partial z} - \frac{\partial \rho_0 \left(1-a_u\right) \overline{w'^3}^e}{\partial z}}_{\mathcal{T}} \\
&\underbrace{- E\overline{w'^2}^E - E(\overline{w}^E - \overline{w}^e)^2}_{\mathcal{T}} \\
&\underbrace{+ D\overline{w'^2}^D + D(\overline{w}^D - \overline{w}^e)^2}_{\mathcal{T}} \\
&\underbrace{- 2\rho_0 \left(1-a_u\right) \overline{w'^2}^e \frac{\partial \overline{w}^e}{\partial z}}_{\mathcal{M}} \underbrace{+ 2\rho_0 \left(1-a_u\right) \overline{w'b'}^e}_{\mathcal{B}} \\
&\underbrace{- \rho_0 \left(1-a_u\right) \epsilon^e_{w^2}}_{\mathcal{D}+\mathcal{P}}
\end{aligned} \tag{6.18}$$

$$\underbrace{\rho_0 \frac{\partial \left(1-a_u\right) \overline{\phi'^2}^e}{\partial t}}_{\mathcal{S}} = \underbrace{+ \frac{\partial M_u \overline{\phi'^2}^e}{\partial z} - \frac{\partial \rho_0 \left(1-a_u\right) \overline{w'\phi'^2}^e}{\partial z}}_{\mathcal{T}} \underbrace{- E\overline{\phi'^2}^E - E(\overline{\phi}^E - \overline{\phi}^e)^2}_{\mathcal{T}} \underbrace{+ D\overline{\phi'^2}^D + D(\overline{\phi}^D - \overline{\phi}^e)^2}_{\mathcal{T}} \underbrace{- 2\rho_0 \left(1-a_u\right) \overline{w'\phi'}^e \frac{\partial \overline{\phi}^e}{\partial z}}_{\mathcal{M}} \underbrace{- \rho_0 \left(1-a_u\right) \epsilon^e_{\phi^2}}_{\mathcal{D}} \tag{6.19}$$

$$\underbrace{\rho_0 \frac{\partial \left(1-a_u\right) \overline{w'\phi'}^e}{\partial t}}_{\mathcal{S}} = \underbrace{+ \frac{\partial M_u \overline{w'\phi'}^e}{\partial z} - \frac{\partial \rho_0 \left(1-a_u\right) \overline{w'^2\phi'}^e}{\partial z}}_{\mathcal{T}} \underbrace{- E\overline{w'^2}^E - E(\overline{w}^E - \overline{w}^e)(\overline{\phi}^E - \overline{\phi}^e)}_{\mathcal{T}} \underbrace{+ D\overline{w'\phi'}^D + D(\overline{w}^D - \overline{w}^e)(\overline{\phi}^D - \overline{\phi}^e)}_{\mathcal{T}} \underbrace{- \rho_0 \left(1-a_u\right) \overline{w'^2}^e \frac{\partial \overline{\phi}^e}{\partial z} - \rho_0 \left(1-a_u\right) \overline{w'\phi'}^e \frac{\partial \overline{w}^e}{\partial z}}_{\mathcal{M}} \underbrace{+ \rho_0 \left(1-a_u\right) \overline{\phi' b'}^e}_{\mathcal{B}} \underbrace{- \rho_0 \left(1-a_u\right) \epsilon^e_{w\phi}}_{\mathcal{D}+\mathcal{P}} \tag{6.20}$$

In the sub-environmental flux and vertical velocity variance budgets, pressure ($\mathcal{P}$) and viscous dissipation ($\mathcal{D}$) effects have been rolled into a single "effective dissipation" term. This is because the consistent partitioning of second-order moments expands pressure and dissipation into several terms.

These equations are physically appealing, because they well illustrate the turbulent energetics within the environment of the updraft. Turbulent transport ($\mathcal{T}$) is now

decomposed into 6 terms. First term, $\partial M_u \overline{w'^2}^e / \partial z$, accounts for the advection of sub-environmental TKE by the subsidence of the environment around the updraft. The second term, $-\partial \rho_0 \left(1 - a_u\right) \overline{w'^3}^e / \partial z$, accounts for turbulent transport within the environment. Entrainment and detrainment processes are each included as two terms respectively. In the case of detrainment, for example, the first term, $D\overline{w'^2}^D$, represents the detrainment of sub-updraft TKE into the environment. In other words, it accounts for how turbulence within the updraft is transferred into the environment. The second term, $D\left(\overline{w}^D - \overline{w}^e\right)^2$, represents detrainment of TKE into the environment in a bulk sense, that is, due to the difference between mean vertical velocities of the updraft and the environment. The two entrainment terms are similarly interpreted as detrainment.

Examining these new equations, a process level interpretation emerges for the turbulent energy cycle of convection in the CBL. Suppose, I define the updraft as the ensemble of buoyant thermals originating in the surface layer, as implied by the thermal plume model, so that detrainment by definition occurs when air in a thermal loses its buoyancy in the CBL inversion. Now, when the air inside a thermal detrains into the inversion, it still has a positive vertical velocity at that point, and so it detrains TKE associated with this "overshooting" into the environment via the bulk detrainment term in equation (6.18). This sub-environmental TKE, contributed by the updraft, now generates downward heat flux and upward moisture flux via the mean-gradient transport term ($\mathcal{M}$), $-\rho_0 \left(1 - a_u\right) \overline{w'^2}^e \partial \overline{\phi}^e / \partial z$, in the sub-environmental flux budget (equation 6.20). Meanwhile, this sub-environmental TKE is converted into

sub-environmental TPE via the mean-gradient transport term ($\mathcal{M}$), $-2\rho_0 \left(1 - a_u\right) \overline{w'\phi'}^e \partial\overline{\phi}^e / \partial z$, in a similar fashion as discussed in chapter 3. Simultaneously, this TKE is also advected by subsidence of the environment back into the CBL via the turbulent transport term ($\mathcal{T}$), $\partial M_u \overline{w'^2}^e / \partial z$.

6.3 Considerations for modeling budgets of sub-environmental second-order moments

If equations (6.18), (6.19), and (6.20) are to be used as the basis for the new parameterization I am proposing, two special considerations are in order, not required for a conventional EDMF scheme. First, recall that the entraining plume model of a "typical" EDMF mass flux scheme, described in chapter 2, treats detrainment implicitly and does not need to formulate it. Its budget equations (equations 2.12 and 2.14) are repeated here for convenience:

$$\frac{\partial \overline{\phi}^u}{\partial z} = -\varepsilon \left(\overline{\phi}^u - \overline{\phi} \right)$$

$$\frac{1}{2} \frac{\partial \left(\overline{w}^u\right)^2}{\partial z} = c_1 \left(\overline{b}^u - \overline{b} \right) - c_2 \varepsilon \left(\overline{w}^u\right)^2$$

In these entraining plume models, the area fraction, a_u, of the updraft ensemble is assumed to be constant, so given the definition mass flux, $M = \rho_0 a_u \overline{w}^u$, the vertical variations in $\overline{w}^u$ determine the detrainment rate via the updraft continuity equation in the thermal plume model (equation 5.3). However, if the entrainment rate is formulated carelessly, the implied detrainment rate can be potentially negative.

Though this is unphysical, since the updraft is not conserving mass, the consequences are masked. However, given the use of consistently-partitioned sub-environmental budgets (equations 6.18, 6.19, 6.20) in my proposed parameterization, this becomes a problem. It then becomes possible, for example, for detrainments to be a sink of TKE in the CBL inversion and thus generate unrealistic upward heat fluxes. This is why the thermal plume model of Rio and Hourdin (2008) was chosen, since the updraft area fraction is allowed to vary vertically, while detrainment is formulated as a (positive) fraction of entrainment.

The second consideration is the fact that the mean-gradient transport term ($\mathcal{M}$), $-\rho_0 \left(1 - a_u\right) \overline{w'^2}^e \partial \overline{\phi}^e / \partial z$ in the sub-environmental flux budgets are proportional to vertical gradient of the sub-environmental mean $\overline{\phi}^e$. However, recall from the discussion in chapter 3 that the advantage having diagnostic sensible and latent heat fluxes is the numerical stability gained by opportunity to use implicit diffusion. This is because the fluxes are derived from quasi-steady budgets of grid-cell averaged fluxes, so that the mean-gradient transport terms ($\mathcal{M}$), $-\rho_0 \overline{w'^2} \partial \overline{\phi} / \partial z$, are proportional to the vertical gradient of the total grid cell-averaged mean $\overline{\phi}$. Since these are state variables of the model, the appearance of their gradients permits diffusion. For the initial prototype of my proposed parameterization, I chose for sub-environmental fluxes to be prognostic, so that the storage terms ($\mathcal{S}$) in theirs budgets (equation 6.20) is retained. However, in practice, this leads to serious issues with robustness and numerical instability.

6.4 New approach

6.4.1 Modified sub-environmental second-order moment budgets

It is possible to manipulate the sub-environmental moment budgets (equations 6.18, 6.19, and 6.20) in such a way as to replace the vertical gradients of $\overline{\phi}^e$ with vertical gradients of $\overline{\phi}$. This allows for sub-environmental fluxes to utilize implicit numerical diffusion after making their budgets (equation 6.20) diagnostic by neglecting the storage terms ($\mathcal{S}$. Recall the thermodynamic variance budget for a conventional mass flux scheme, derived by de Roode et al. (2000) (equation 5.14). I repeat it here for convenience:

$$\underbrace{\rho_0 \frac{\partial a_u \left(1-a_u\right)\left(\overline{\phi}^u - \overline{\phi}^e\right)^2}{\partial t}}_{\mathcal{S}} = \underbrace{-2M_u\left(\overline{\phi}^u - \overline{\phi}^e\right)\frac{\partial \overline{\phi}}{\partial z}}_{\mathcal{M}}$$
$$\underbrace{-\frac{\partial \left(1-2a_u\right) M_u \left(\overline{\phi}^u - \overline{\phi}^e\right)^2}{\partial z} - \left(E+D\right)\left(\overline{\phi}^u - \overline{\phi}^e\right)^2}_{\mathcal{T}}$$

Their derivation begins with the flux-form budgets of $\overline{\phi}^u$ (equation 6.7) and $\overline{\phi}^e$ but neglects sub-updraft and sub-environmental flux convergence term. If I retain the sub-environmental flux convergence, an additional term appears on the RHS in the variance budget, equal to:

$$\begin{aligned} 2a_u\left(\overline{\phi}^u - \overline{\phi}^e\right)\frac{\partial \rho_0 (1-a_u)\overline{w'\phi'}^e}{\partial z} \quad &= \quad 2\frac{\partial \rho_0 (1-a_u)\left(\overline{\phi}^u - \overline{\phi}^e\right)\overline{w'\phi'}^e}{\partial z} \\ &+ \quad \rho_0\left(1-a_u\right)\overline{w'\phi'}^e \frac{\partial \overline{\phi}^e}{\partial z} \\ &- \quad \rho_0\left(1-a_u\right)\overline{w'\phi'}^e \frac{\partial \overline{\phi}}{\partial z} \end{aligned} \tag{6.21}$$

Then, I take the sub-environmental variance budget (equation 6.18), solve for the mean-gradient transport term ($\mathcal{M}$), $-\rho_0\left(1-a_u\right)\overline{w'^2}^e \partial\overline{\phi}^e/\partial z$, and substitute it into

equation (6.21). Finally, assuming quasi-equilibrium for the organized variance, as implied by the diagnostic thermal plume model, I obtain a new form of the sub-environmental variance budget:

$$\underbrace{\rho_0 \frac{\partial \left(1-a_u\right) \overline{\phi'^2}^e}{\partial t}}_{\mathcal{S}} = \underbrace{-\frac{\partial M_u \left(1-2a_u\right) \left(\overline{\phi}^u - \overline{\phi}^e\right)^2}{\partial z}}_{\mathcal{T}} \underbrace{+\frac{\partial M_u \overline{\phi'^2}^e}{\partial z} + 2\frac{\partial \rho_0 \left(1-a_u\right) \left(\overline{\phi}^u - \overline{\phi}^e\right) \overline{w'\phi'}^e}{\partial z}}_{\mathcal{T}} \underbrace{-\frac{\partial \rho_0 \left(1-a_u\right) \overline{w'\phi'^2}^e}{\partial z} - E\overline{\phi'^2}^e}_{\mathcal{T}} \underbrace{-2\left[\rho_0 \left(1-a_u\right) \overline{w'\phi'}^e + M_u \left(\overline{\phi}^u - \overline{\phi}^e\right)\right] \frac{\partial \overline{\phi}}{\partial z}}_{\mathcal{M}} \underbrace{-\rho_0 \left(1-a_u\right) \epsilon^e_{\phi^2}}_{\mathcal{D}} \tag{6.22}$$

Budgets can be derived similarly for $\overline{w'^2}^e$ and $\overline{w'\phi'}^e \in \left\{\overline{w'\theta'_l}^e, \overline{w'q'_t}^e\right\}$ and are given by:

$$\underbrace{\rho_0 \frac{\partial \left(1-a_u\right) \overline{w'^2}^e}{\partial t}}_{\mathcal{S}} = \underbrace{-\frac{\partial M_u \left(1-2a_u\right)\left(\overline{w}^u - \overline{w}^e\right)^2}{\partial z}}_{\mathcal{T}} \underbrace{+3\frac{\partial M_u \overline{w'^2}^e}{\partial z}}_{\mathcal{T}} \underbrace{-\frac{\partial \rho_0 \left(1-a_u\right)\overline{w'^3}^e}{\partial z} - E\overline{w'^2}^e}_{\mathcal{T}} \underbrace{-2\left[\rho_0\left(1-a_u\right)\overline{w'b'}^e + M_u\left(\overline{b}^u - \overline{b}^e\right)\right]}_{\mathcal{B}} \underbrace{-\rho_0\left(1-a_u\right)\epsilon^e_{w^2}}_{\mathcal{D}+\mathcal{P}} \quad (6.23)$$

$$\underbrace{\rho_0 \frac{\partial \left(1-a_u\right) \overline{w'\phi'}^e}{\partial t}}_{\mathcal{S}} = \underbrace{-\frac{\partial M_u \left(1-2a_u\right)\left(\overline{w}^u - \overline{w}^e\right)\left(\overline{\phi}^u - \overline{\phi}^e\right)}{\partial z}}_{\mathcal{T}} \underbrace{+2\frac{\partial M_u \overline{w'\phi'}^e}{\partial z} + \frac{\partial \rho_0 \left(1-a_u\right)\left(\overline{\phi}^u - \overline{\phi}^e\right)\overline{w'^2}^e}{\partial z}}_{\mathcal{T}} \underbrace{-\frac{\partial \rho_0 \left(1-a_u\right)\overline{w'^2\phi'}^e}{\partial z} - E\overline{w'\phi'}^e}_{\mathcal{T}} \underbrace{+\rho_0\left[\left(1-a_u\right)\overline{b'\phi'}^e + a_u\left(1-a_u\right)\left(\overline{b}^u - \overline{b}^e\right)\left(\overline{\phi}^u - \overline{\phi}^e\right)\right]}_{\mathcal{B}} \underbrace{-\rho_0\left[\left(1-a_u\right)\overline{w'^2}^e + a_u\left(1-a_u\right)\left(\overline{w}^u - \overline{w}^e\right)^2\right]\frac{\partial \overline{\phi}}{\partial z}}_{\mathcal{M}} \underbrace{-\rho_0\left(1-a_u\right)\epsilon^e_{w\phi}}_{\mathcal{D}+\mathcal{P}} \quad (6.24)$$

The equations, compared to their alternate form (equations 6.18, 6.19, and 6.20), have some appealing properties. First, note that the turbulent transport terms ($\mathcal{T}$) in equation (6.22) now contain the decomposition of $\mathcal{T}$ described in the beginning of the chapter by equation (6.3). Also, all the entrainment and detrainment terms vanish,

except for one. This remaining term (with coefficient E) accounts for the fact that sub-updraft variability is assumed negligible, so that any sub-environmental variability entrained into the updraft is instantly "dissipated". Conveniently, the total vertical velocity variance, including the organized component due to the updraft, is included in the mean gradient transport term ($\mathcal{M}$), so that if equation (6.24) is taken as diagnostic, the mass flux scheme will actually contribute numerically stabilizing diffusion.

6.4.2 Numerical implementation

The prognostic variables of my new parameterization are $(1-a_u)\,\overline{w'^2}^e$, $(1-a_u)\,\overline{\theta_l'^2}^e$, $(1-a_u)\,\overline{q_t'^2}^e$, and $(1-a_u)\,\overline{\theta_l' q_t'}^e$. In the absence of the thermal plume and mass flux schemes, their budget equations are treated mostly the same way as the level-3 HOC from chapter 3. The thermal plume model is run first, to obtain the updraft properties required to be substituted into equations (6.9), (6.10), and (6.11). An additional "entrainment time scale" is included to account for its dissipating effect on sub-environmental variances:

$$\tau_E = \frac{\rho_0\,(1-a_u)}{E} \tag{6.25}$$

This time scale is harmonically averaged with the primary dissipation time scale to compute an effective total dissipation time scale. Fluxes are determined by neglecting the time tendency in equation (6.11). These fluxes are then used to update the mean state variables ($\overline{\theta_l}, \overline{q_t}$). The turbulent transport terms containing third-order sub-environmental moments are treated to as to diffuse the underlying second-order

moments, just as they do in the TKE-l and level-3 HOC from chapter 3. The fluxes and mean gradients appearing in the sub-environmental variance budgets (equation 6.22) are then treated implicitly, aiding numerical stability and ensuring that diffusion always diminishes variance.

6.5 Evaluating the new approach

Figure (6.1) shows the performance of my new parameterization compared to LES and the HOC-based EDMF scheme. Both schemes produce the correct shape of the CBL potential temperature profile, but the new scheme significantly outperforms the HOC-MF scheme in predicting the depth of the boundary layer by around $75\,m$. Moreover, the downward heat flux at the top of the boundary layer is much larger and closer to LES, thereby explaining the correct improved boundary layer depth.

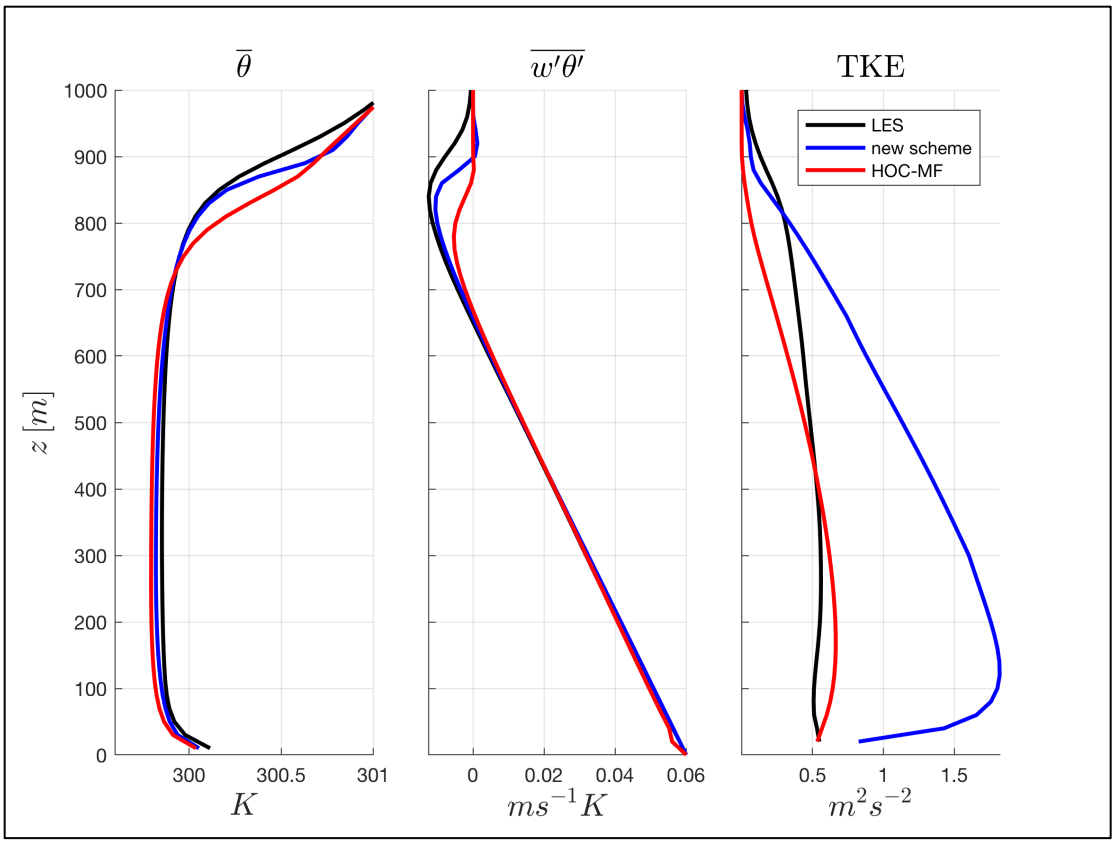

Figure 6.1 *Left panel depicts the potential temperature profiles predicted for the DCBL case by LES, the level-3 HOC, and my new parameterization. The middle panel depicts the corresponding potential temperature fluxes, and the right panel depicts the TKE profiles.*

Oddly however, the new scheme overpredicts the peak TKE in the boundary layer by a factor of 3.5. The cause of this over-prediction is not yet known, and debugging is still required given how recently the scheme was developed. The correct prediction of mean profiles despite the overprediction of TKE can be explained by the simultaneous over-prediction of potential temperature variance. Figure (6.2) depicts the TKE, potential temperature variance, and heat flux profiles predicted by LES and

the new scheme for the DCBL case. Also shown is the organized component of each second-order moment to illustrate their partitioning. As discussed in chapter 3, the buoyancy flux depends on the difference between the vertical velocity and buoyancy variance (proportional to potential temperature variance), so that the over-prediction of both compensate each other and yields a correct flux response. Ultimately, validation of this new closure approach requires real estimates of the magnitude of terms in the budgets of sub-environmental second-order moments (equations 6.22, 6.23, and 6.24). The LES-based evaluation methods used so far cannot provide such estimates. Chapter 7 will introduce a novel method for achieving this goal.

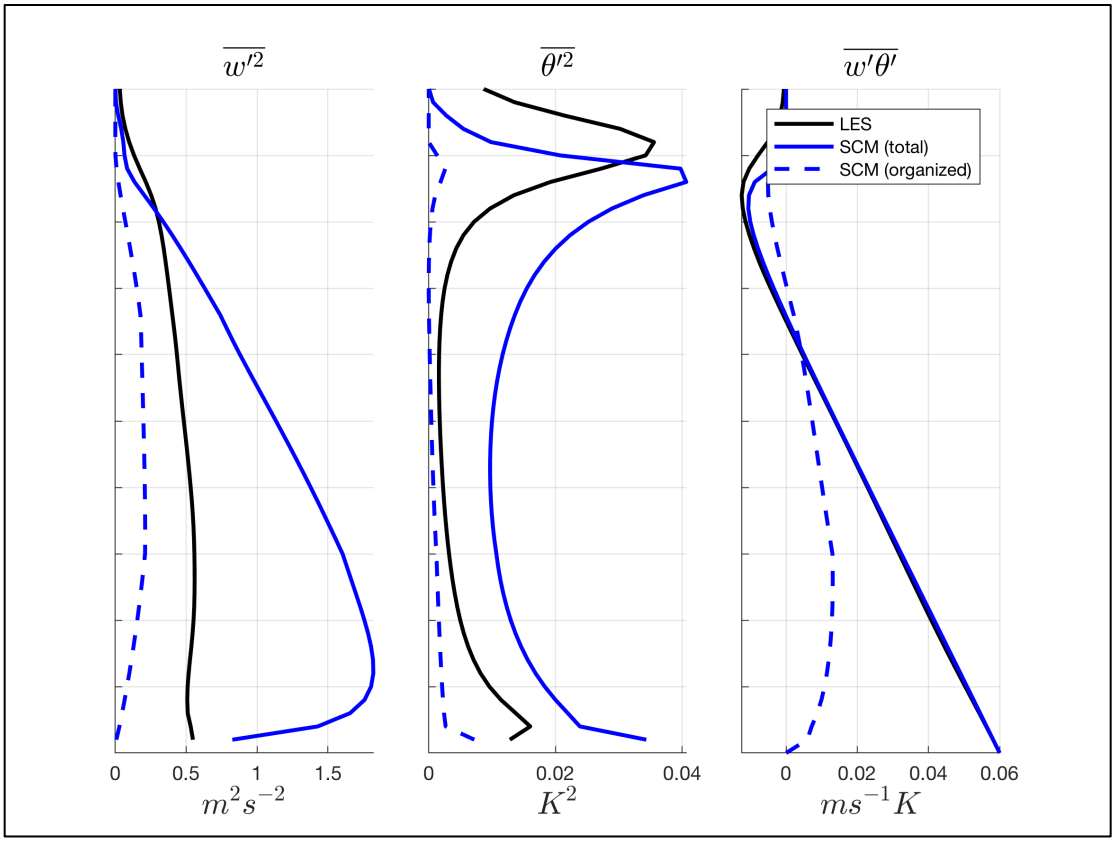

Figure 6.2 *Left panel depicts the TKE profiles predicted for the DCBL case by LES and my new parameterization, along with the organized TKE component for the*

updraft-environment decomposition. The middle panel depicts the corresponding potential temperature variance profiles, and the right panel depicts the heat flux profiles.

Chapter 7. An LES-based method for estimating the properties of surface-driven convection

7.1 Motivation

The thermal plume model used in my new parameterization models the ensemble of convective thermals present in a convective boundary layer. To validate my parameterization with LES from a process level, some method is required to determine the properties of such thermals. One available method is to sample grid cells in the LES domain that are considered part of the thermal, conditionally averaging atmospheric properties over these grid cell. However, the question arises as to how to the define the thermal. A naïve way would be to sample grid cells with positive buoyancy and positive vertical velocity. Figure (7.1) depicts such a sampling using the modified UCLA-LES code to simulate the DCBL case. It becomes clear from this figure that in addition to sampling grid cells belonging to convective thermals, this method also samples upward buoyant motions due to gravity waves in the free atmosphere. This is clear, because the area fraction of the "updraft" approaches 25% in the free atmosphere limit, rather than vanishing.

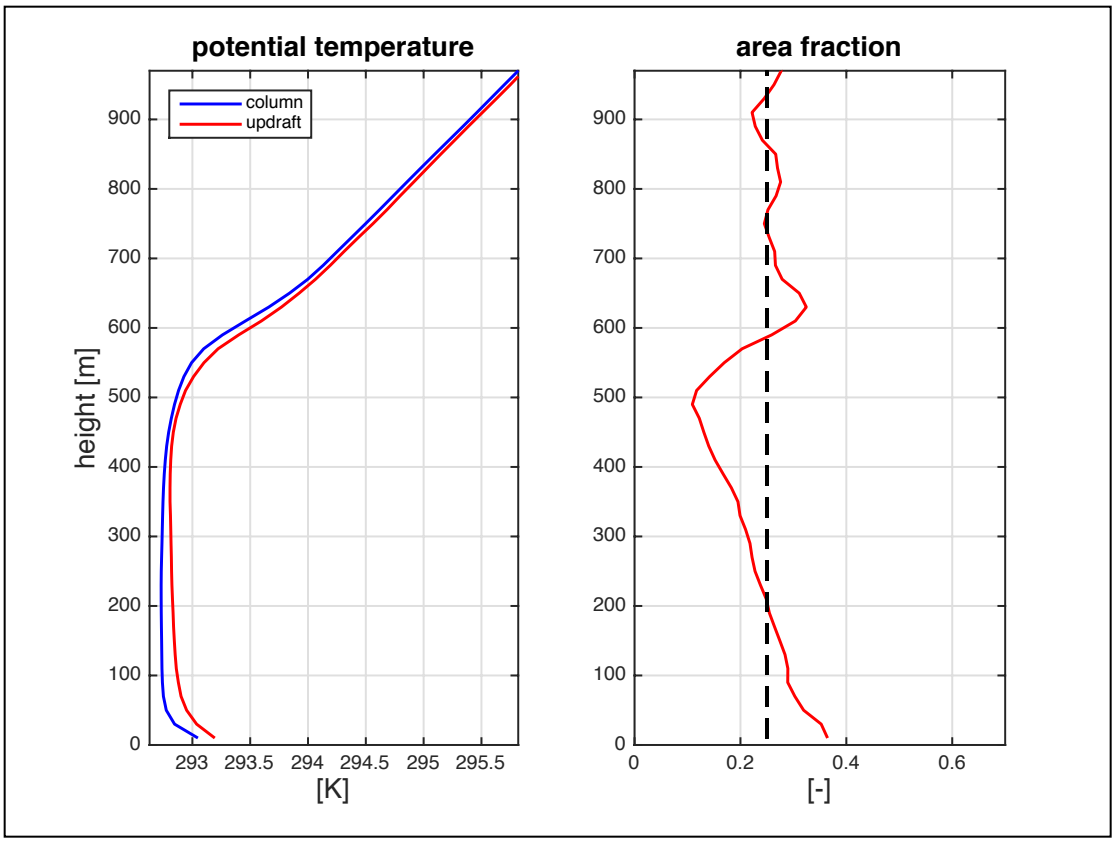

Figure 7.1 *The left panel depicts the potential temperature profile predicted by LES for the DCBL case, along with the conditional mean, averaged over LES grid cells with positive buoyancy and vertical velocity. The right panel depicts the area fraction associated with these grid cells.*

What is required for this analysis, is a method of determining which grid cells are considered inside the thermals and which are not. One consideration is that thermal air originates near the surface where positive buoyancy fluxes drive convective circulations. This suggests an approach, whereby thermal air is defined as air, originating near the surface, that has had positive buoyancy and vertical velocity since it left the surface. However, applying an approach to the LES domain requires

knowledge about the history of air. To account for the history of air in a model domain requires Lagrangian particle tracking (LPT) (Heus et al. 2008).

7.2 Methodology

The UCLA-LES model has an LPT feature, whereby a pre-set number of massless particles are placed randomly in the LES domain. On each time step, the vertical velocity from the LES Eulerian is interpolated to the location of each particle. The location of each particle is then updated based on this velocity. Thermodynamic profiles can be computed by averaging thermodynamic properties, interpolated to the location of each particle, across all particles in bins corresponding to grid cells at the same height. I have modified the UCLA-LES LPT code, so that each particle includes a flag designating it as either an "updraft particle" and "environmental particle". An environmental particle can become an updraft particle if it enters the grid cell closest to the surface and attains positive buoyancy. From that point, it remains an updraft particle until its vertical velocity or buoyancy stops being positive. Profiles of updraft properties can then be estimated by bin-averaging over updraft particles only.

7.3 Numerical experiments

Figure (7.2) depicts a 3D view of the locations of updraft particles in the LES domain for the DCBL case. Clear in this figure is the structure of convective thermals. Figure (7.3) depicts the LES-predicted potential temperature profiles for the DCBL case,

including the bin average over the updraft particles, along with the updraft area fraction. In contrast to the Eularian sampling of figure (7.1), the area fraction vanishes at the top of the boundary layer.

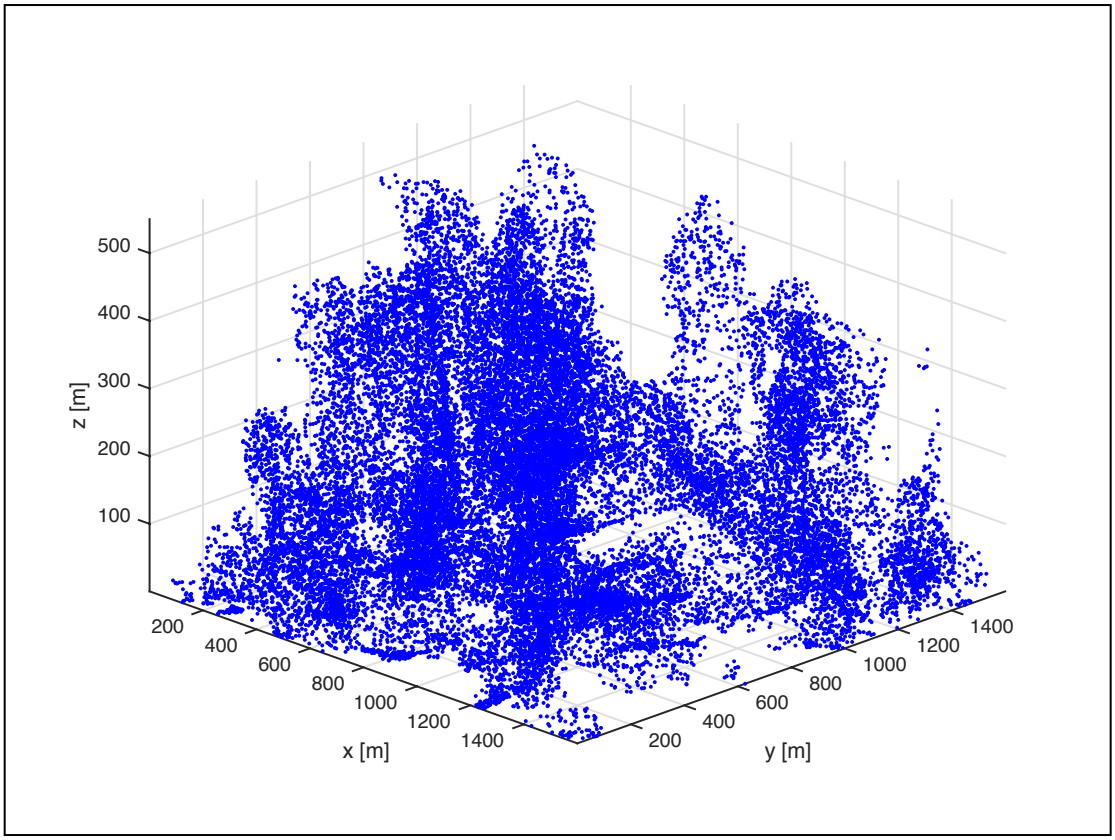

Figure 7.2 *The particles in the DCBL LES-domain marked as "updraft particles". Note the convective thermal structures present in the organization of the particles.*

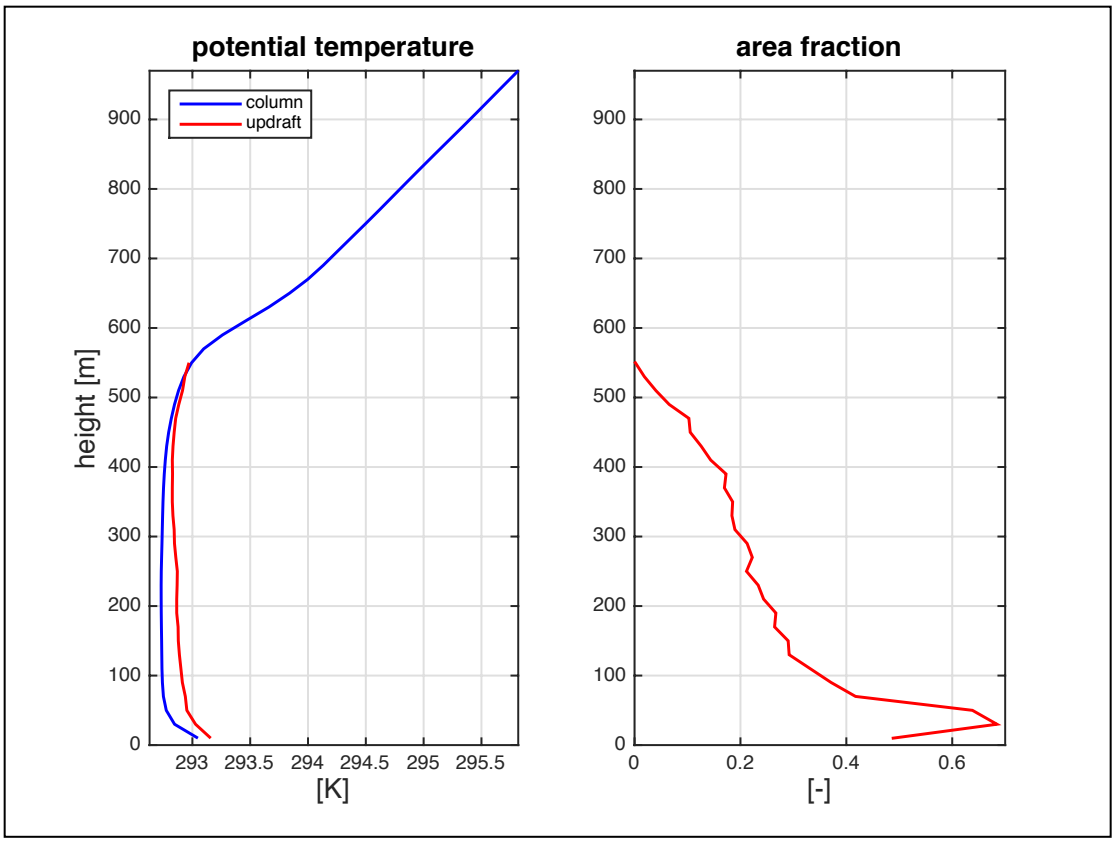

Figure 7.3 *The left panel depicts the potential temperature profile predicted by LES for the DCBL case, along with the conditional mean, bin-averaged over the particles marked as "updraft particles". The right panel depicts the area fraction associated with these particles.*

Figure (7.4) depicts a 3D view of updraft particles for the BOMEX marine trade cumulus LES case (Holland and Rasusson 1973, Siebesma and Cuijpers 1995). Figure (7.5) depicts these locations from a lateral view, along with the mean liquid water potential temperature profile to indicate to the location of the mixed layer and cloud layer. The lateral view makes clear the structure of thermals and cumulus

clouds. The dry thermals are dense within the mixed layer, while the cumulus clouds are relatively sparse within cloud layer but rooted in the mixed layer.

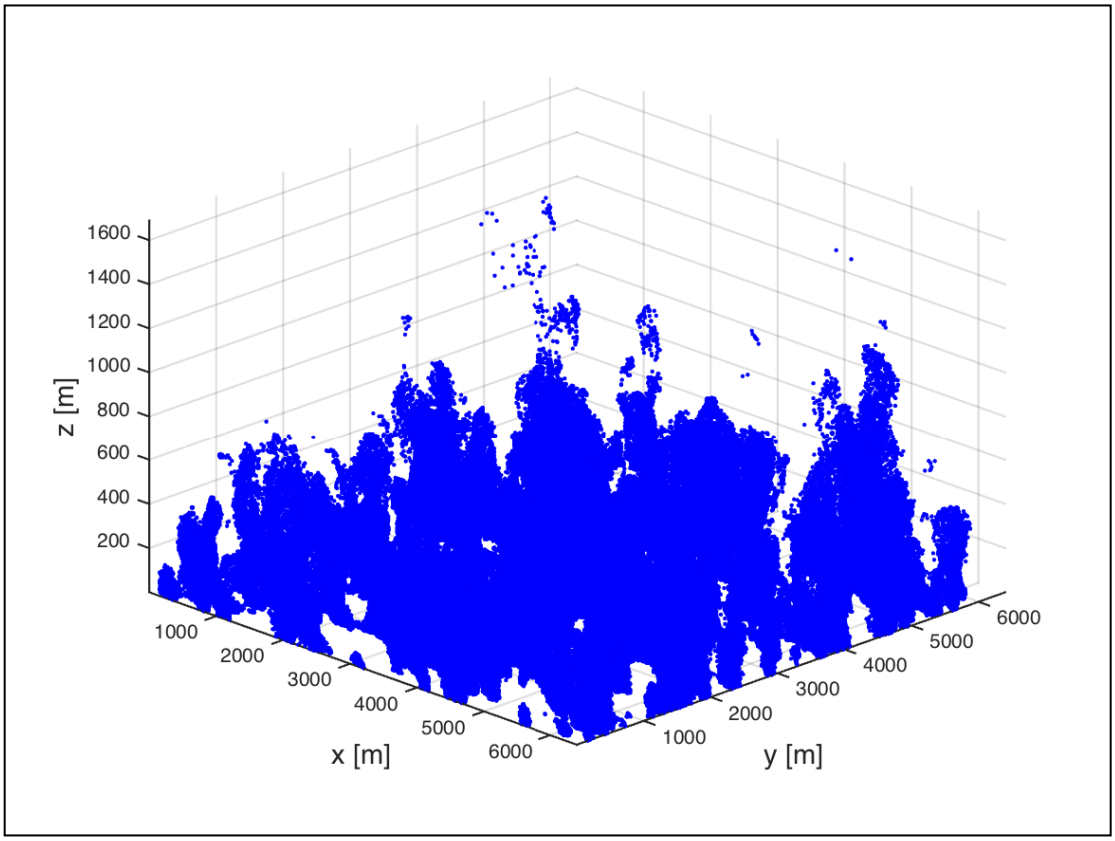

Figure 7.4 *The particles in the BOMEX LES-domain marked as "updraft particles". Note the convective thermal and cumulus cloud structures present in the organization of the particles.*

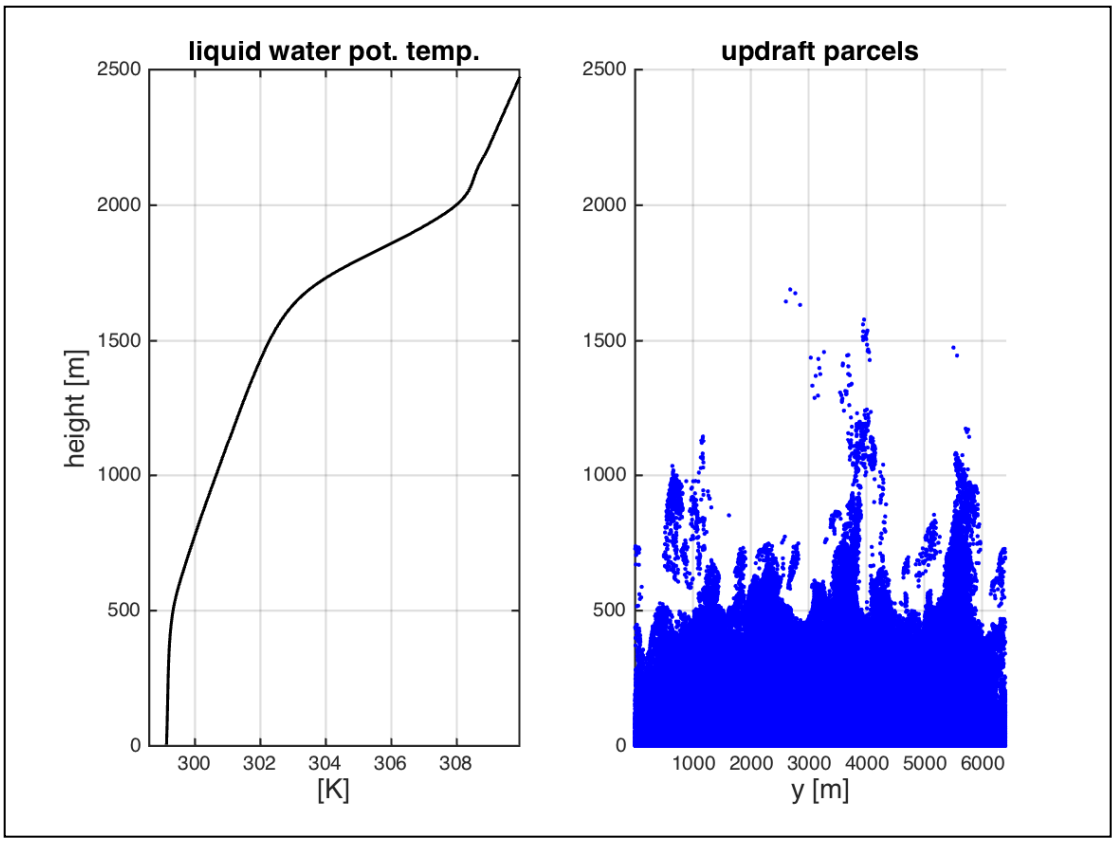

Figure 7.5 *The left panel depicts the liquid water potential temperature profile for the BOMEX case. The right panel depicts a lateral view of the particles marked "updraft particles".*

It is possible to estimate entrainment and detrainment rates for the thermal ensemble via the updraft continuity equation (equation 6.12), by counting the number of updraft particles entering and exiting the vertical bins on each time step, along with the number of particles gaining and losing updraft status. Figure (7.6) depicts the updraft mass flux profile and entrainment/detrainment rates. This figure indicates a key problem for this particle tracking method. Because particles can only become updraft particles in the grid cell closest to the surface, entrainment can only happen at this

level. However, entrainment is a process that should occur throughout the depth of the thermal ensemble.

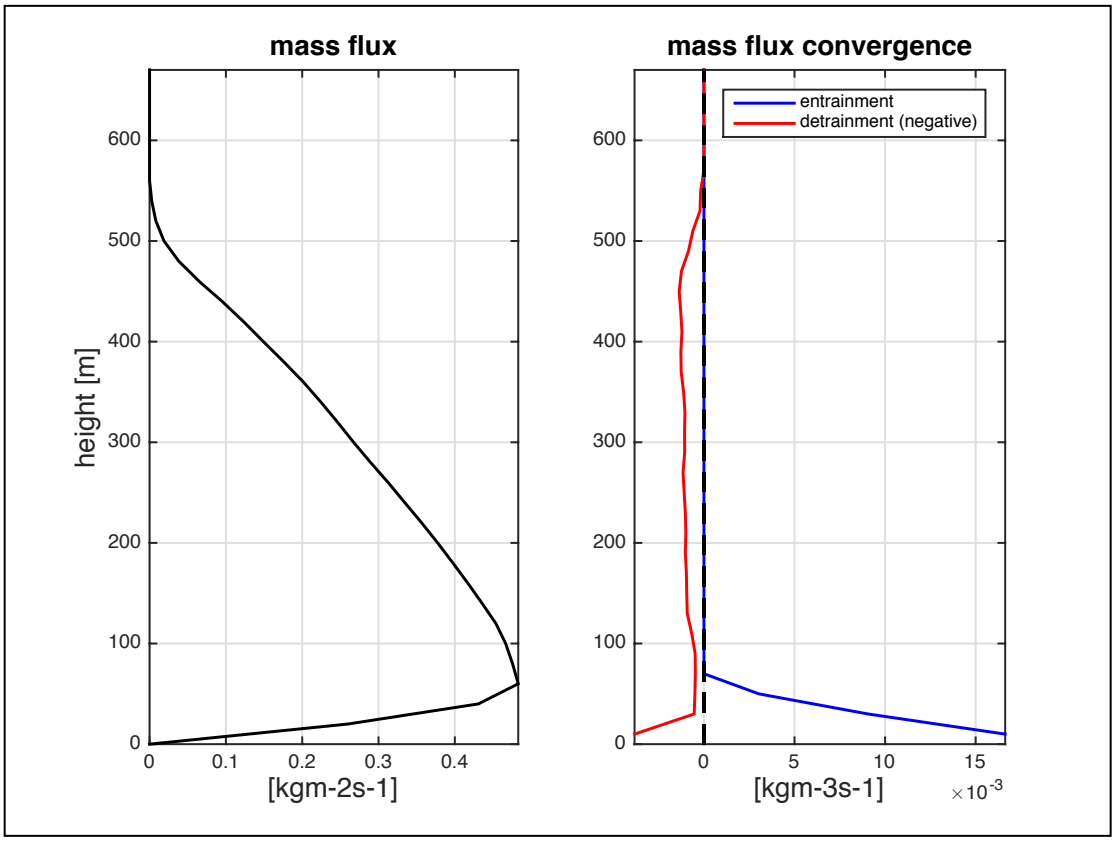

Figure 7.6 *The left panel depicts the mass flux profile of the "updraft particles" for the DCBL case. The rate panel depicts the corresponding entrainment and detrainment rates.*

To address this problem, I have modified my thermal particle tracking method by including a way to define entrainment away from the surface. If a grid cell contains an updraft particle, it is marked as an updraft grid cell. Then, if an environmental particle enters that grid cell while having positive vertical velocity and positive buoyancy, it becomes an updraft particle. Figure (7.7) depicts the mass flux and

entrainment/detrainment profiles for this new method. Now, entrainment extends through the depth of the boundary layer, just like detrainment.

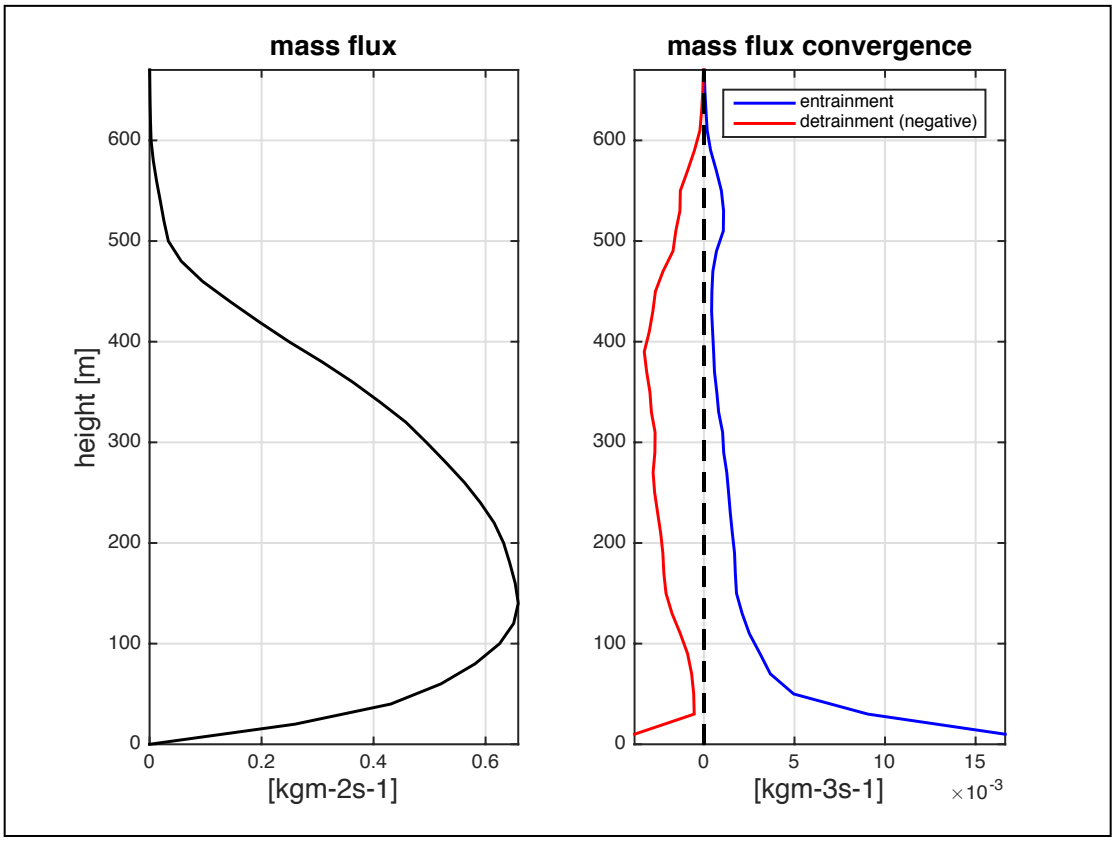

Figure 7.7 *The left panel depicts the mass flux profile of the "updraft particles" for the DCBL case, after implementing the entrainment scheme. The right panel depicts the corresponding entrainment and detrainment rates*

An alternative method for treating entrainment would be to combine my Lagrangian method with the Eularian of Couvreux et al. (2008). The basis of their method is to introduce a decaying scalar/tracer with fixed surface flux, so that thermals can be defined based on a threshold concentration of this scalar. By applying this threshold to the updraft particle definition, entrainment could be defined without the resolution

dependence likely present with my current entrainment method. Moreover, it would improve upon the Couvreux et al. (2008) method be permitting analysis of the history of air parcels. Such an approach is left for future work.

Chapter 8. Summary and major contributions

In the first part of the dissertation, I compared the physical bases of TKE-l closures and level-3-type HOCs and evaluated the consequence of their choice of physical process representation. In chapter 3, I showed that the level-3 closure is energetically consistent with respect to local physical processes, because it conserves turbulent energy, in contrast to the TKE-l closure. Essentially, I extended the analysis of Zilitinkevich et al. (2008) to high-order turbulence closures and convective/cloudy boundary layers. In the course of this discussion, I made three novel contributions to the understanding of the atmospheric closure problem. First, I showed that the intensity of turbulent mixing under stable stratification depends on the difference between TKE and TPE, not TKE alone. Second, I show that the counter-gradient flux correction present in level-3 HOCs represents a local process (buoyancy acceleration), not non-local transport such as due to boundary layer thermals as is commonly assumed. Finally, I introduced an alternative definition of local moist stability that depends on the joint-distribution of heat and moisture and who's square can be conceptualized physically as the rate of buoyancy flux production per-unit TKE-TPE excess.

In chapter 4, I compared SCM simulations of a simple dry convective boundary layer and stratocumulus-topped boundary layer using each closure type. I showed that the local energetic inconsistency of the TKE-l closure results in unrealistic thermodynamic profile predictions in both test case. To show why, I introduced a

novel method for evaluating turbulence closures, whereby LES-predicted thermodynamic profiles are fixed, and the closures are allowed to run until their turbulence state variables reach a steady state. This method makes clear how the non-conservation of turbulent energy causes a severe under-diagnosis of TKE by the TKE-l closure, since it cannot maintain realistic turbulent energy in the stably stratified parts of the boundary layer. When the TKE-l closure is run "online", it over-mixes thermodynamic profiles, resulting in more realistic TKE profiles at the expense of realistic static stability. This over-mixing is a consequence of the lack of a counter-gradient flux correction which is present in the level-3 HOC but not in the TKE-l closure.

In the second part of this dissertation, I extend the criterion of energetic consistency to non-local transport. In chapter 5, I formally define non-local transport of turbulent energy and show that EDMF parameterizations represent such transport in two parallel but inconsistent ways: diffusively and advectively. I then couple the two closures defined and evaluated in chapters 3 and 4 to a thermal plume model, making them EDMF(-like) closures. I show using the DCBL SCM test case that, when the EDMF scheme combines with the TKE-l closure, TKE vanishes far below the top of the boundary layer as defined by the activity of the thermal plume model. This creates two artificial layers within the boundary layer and an unrealistic stable "kink" at their interface. This effect is due to the non-physical destruction of turbulent energy discussed in chapter 3, enhanced by the plume model's negative buoyancy flux near the top of the CBL. In the case of the level-3 HOC-EDMF closure, this

unrealistic effect is not present, but the height of the boundary layer is essentially the same as without thermal plume model: too shallow. I explain this by the EDMF approach's dual diffusive-advective treatment of non-local transport.

In chapter 6, I introduce a novel closure approach which correctly accounts for non-local transport of turbulent energy by consistently decomposing all second-order moments between the thermal updraft plume and its environment. This approach decomposes non-local transport of turbulent energy into several terms accounting for processes such as entrainment, detrainment, and mean advection by the updraft plume and its subsiding environment. I show using the DCBL SCM test case that it yields a much more realistic prediction of boundary layer depth than the level-3 HOC-based EDMF scheme evaluated in chapter 5. This is because the advective transport by the thermal plume model is a source of sub-environmental turbulent energy and is better capable of transporting it high into the inversion. Tan et al. (2018) applied a similar decomposition in their own scheme (after I introduced it in my prospectus defense), my scheme is locally energetically consistent (which theirs is not) while numerically robust due to the utilization of diagnostic thermodynamic fluxes. I believe that the utilization of this concept is an important step towards physically consistent unified modeling of the turbulence and dry/shallow convection.

In the final part of this dissertation (chapter 7), I introduce a novel numerical method for estimating the properties of surface-driven convection in LES using Lagrangian particle tracking (LPT). The purpose of this method is to validate the physical basis

of my new closure scheme by allowing estimates of the magnitude of terms of its budget equations for sub-environmental second-order moments. I show results for first-order moments using the DCBL case as promising proof of concept. In future work, I will apply this method to second-order moments. I will also combine it with the Eularian method of Couvreux et al. (2008) for a more robust treatment of entrainment into thermals.

Bibliography

Arakawa, A., and W. H. Schubert, 1974: Interaction of a Cumulus Cloud Ensemble with the Large-Scale Environment, Part I. *J. Atmos. Sci.*, **31**, 674–701

Bechtold, P., J. W. M. Cuijpers, P. Mascart, and P. Trouilhet, 1995: Modeling of Trade Wind Cumuli with a Low-Order Turbulence Model: Toward a Unified Description of Cu and Se Clouds in Meteorological Models. *J. Atmos. Sci.*, **52**, 455–463

Bjerknes, J., 1938: Saturated-adiabatic ascent of air through dry-adiabatically descending environment. *Quart. J. Roy. Meteor. Soc.*, **64**, 325–330.

Blackadar, A. K., 1962: The vertical distribution of wind and turbulent exchange in a neutral atmosphere. *Journal of Geophysical Research*, **67**, 3095–3102

Brinkop, S., and E. Roeckner, Sensitivity of a general circulation model to parameterizations of cloud–turbulence interactions in the atmospheric boundary layer. *Tellus A*, **47**, 197–220

Brown, A. R., and Coauthors, 2002: Large-eddy simulation of the diurnal cycle of shallow cumulus convection over land. *Q.J.R. Meteorol. Soc.*, **128**, 1075–1093

Chen, J.-M., 1991: Turbulence-Scale Condensation Parameterization. *J. Atmos. Sci.*, **48**, 1510–1512

Cheinet, S., 2003: A Multiple Mass-Flux Parameterization for the Surface-Generated Convection. Part I: Dry Plumes. *J. Atmos. Sci.*, **60**, 2313–2327

Cheinet, S., 2004: A Multiple Mass Flux Parameterization for the Surface-Generated Convection. Part II: Cloudy Cores. *J. Atmos. Sci.*, **61**, 1093–1113

Clark, R.H., Dyer, A.J., Brook, R.R., Reid, D.G., and Troup, A.J., 1971: The Wangara experiment: Boundary layer Data. Tech. Paper 19, Division of Meteorological Physics, CSIRO, Australia.

Couvreux, F., F. Hourdin, and C. Rio, 2010: Resolved Versus Parametrized Boundary-Layer Plumes. Part I: A Parametrization-Oriented Conditional Sampling in Large-Eddy Simulations. *Boundary-Layer Meteorol*, **134**, 441–458

Deardorff, J. W., 1970: Convective Velocity and Temperature Scales for the Unstable Planetary Boundary Layer and for Rayleigh Convection. *J. Atmos. Sci.*, **27**, 1211–1213

Deardorff, J. W., 1972: Theoretical expression for the countergradient vertical heat flux. *Journal of Geophysical Research*, **77**, 5900–5904

Deardorff, J. W., 1974: Three-dimensional numerical study of the height and mean structure of a heated planetary boundary layer. *Boundary-Layer Meteorol*, **7**, 81–106

de Roode, S. R., P. G. Duynkerke, and A. P. Siebesma, 2000: Analogies between Mass-Flux and Reynolds-Averaged Equations. *J. Atmos. Sci.*, **57**, 1585–1598

de Roode, S. R., A. P. Siebesma, H. J. J. Jonker, and Y. de Voogd, 2012: Parameterization of the Vertical Velocity Equation for Shallow Cumulus Clouds. *Mon. Wea. Rev.*, **140**, 2424–2436

de Rooy, W. C., and A. P. Siebesma, 2008: A Simple Parameterization for Detrainment in Shallow Cumulus. *Mon. Wea. Rev.*, **136**, 560–576

de Rooy, W. C., and Coauthors, 2013: Entrainment and detrainment in cumulus convection: an overview. *Q.J.R. Meteorol. Soc.*, **139**, 1–19

Duynkerke, P. G., and Coauthors, 1999: Intercomparison of Three- and one-Dimensional Model Simulations and Aircraft Observations of Stratocumulus. *Boundary-Layer Meteorology*, **92**, 453–487

Golaz, J.-C., V. E. Larson, and W. R. Cotton, 2002: A PDF-Based Model for Boundary Layer Clouds. Part I: Method and Model Description. *J. Atmos. Sci.*, **59**, 3540–3551

Golaz, J.-C., V. E. Larson, and W. R. Cotton, 2002: A PDF-Based Model for Boundary Layer Clouds. Part II: Model Results. *J. Atmos. Sci.*, **59**, 3552–3571

Guichard, F., and Coauthors, 2004: Modelling the diurnal cycle of deep precipitating convection over land with cloud-resolving models and single-column models. *Q.J.R. Meteorol. Soc.*, **130**, 3139–3172

Han, J., M. L. Witek, J. Teixeira, R. Sun, H.-L. Pan, J. K. Fletcher, and C. S. Bretherton, 2015: Implementation in the NCEP GFS of a Hybrid Eddy-Diffusivity Mass-Flux (EDMF) Boundary Layer Parameterization with Dissipative Heating and Modified Stable Boundary Layer Mixing. *Wea. Forecasting*, **31**, 341–352

Holland, J. Z., and E. M. Rasmusson, 1973: Measurements of the Atmospheric Mass, Energy, and Momentum Budgets Over a 500-Kilometer Square of Tropical Ocean. *Mon. Wea. Rev.*, **101**, 44–55

Heus, T., G. van Dijk, H. J. J. Jonker, and H. E. A. Van den Akker, 2008: Mixing in Shallow Cumulus Clouds Studied by Lagrangian Particle Tracking. *J. Atmos. Sci.*, **65**, 2581–2597

Holtslag, A. a. M., and C.-H. Moeng, 1991: Eddy Diffusivity and Countergradient Transport in the Convective Atmospheric Boundary Layer. *J. Atmos. Sci.*, **48**, 1690–1698

Hourdin, F., F. Couvreux, and L. Menut, 2002: Parameterization of the Dry Convective Boundary Layer Based on a Mass Flux Representation of Thermals. *J. Atmos. Sci.*, **59**, 1105–1123

Köhler, M., M. Ahlgrimm, and A. Beljaars, 2011: Unified treatment of dry convective and stratocumulus-topped boundary layers in the ECMWF model. *Q.J.R. Meteorol. Soc.*, **137**, 43–57

Kolmogorov, A., 1941: The Local Structure of Turbulence in Incompressible Viscous Fluid for Very Large Reynolds' Numbers. *Akademiia Nauk SSSR Doklady*, **30**, 301–305.

Lappen, C.-L., and D. A. Randall, 2001: Toward a Unified Parameterization of the Boundary Layer and Moist Convection. Part I: A New Type of Mass-Flux Model. *J. Atmos. Sci.*, **58**, 2021–2036

Lappen, C.-L., and D. A. Randall, 2001: Toward a Unified Parameterization of the Boundary Layer and Moist Convection. Part II: Lateral Mass Exchanges and Subplume-Scale Fluxes. *J. Atmos. Sci.*, **58**, 2037–2051

Larson, V. E., J.-C. Golaz, and W. R. Cotton, 2002: Small-Scale and Mesoscale Variability in Cloudy Boundary Layers: Joint Probability Density Functions. *J. Atmos. Sci.*, **59**, 3519–3539

Larson, V. E., and J.-C. Golaz, 2005: Using Probability Density Functions to Derive Consistent Closure Relationships among Higher-Order Moments. *Mon. Wea. Rev.*, **133**, 1023–1042

Lenderink, G., and A. a. M. Holtslag, 2004: An updated length-scale formulation for turbulent mixing in clear and cloudy boundary layers. *Quarterly Journal of the Royal Meteorological Society*, **130**, 3405–3427

Rio, C., and F. Hourdin, 2008: A Thermal Plume Model for the Convective Boundary Layer: Representation of Cumulus Clouds. *J. Atmos. Sci.*, **65**, 407–425

Roeckner, E., and Coauthors, 1996: The atmospheric general circulation model ECHAM4: Model description and simulation of present-day climate. *Max-Planck-Institut für Meteorologie*

Mailhot, J., and R. Benoit, 1982: A Finite-Element Model of the Atmospheric Boundary Layer Suitable for Use with Numerical Weather Prediction Models. *J. Atmos. Sci.*, **39**, 2249–2266

Mellor, G. L., and T. Yamada, 1974: A Hierarchy of Turbulence Closure Models for Planetary Boundary Layers. *J. Atmos. Sci.*, **31**, 1791–1806

Mellor, G. L. and T. Yamada, 1982: Development of a Turbulence Closure Model for Geophysical Fluid Problems, *Rev. Geophys. Space Phys.*, **20**, 851–875.

Mahrt, L., 1998: Nocturnal Boundary-Layer Regimes. *Boundary-Layer Meteorology*, **88**, 255–278

Mauritsen, T., G. Svensson, S. S. Zilitinkevich, I. Esau, L. Enger, and B. Grisogono, 2007: A Total Turbulent Energy Closure Model for Neutrally and Stably Stratified Atmospheric Boundary Layers. *J. Atmos. Sci.*, **64**, 4113–4126

Moeng, C.-H., and J. C. Wyngaard, 1986: An Analysis of Closures for Pressure-Scalar Covariances in the Convective Boundary Layer. *J. Atmos. Sci.*, **43**, 2499–2513

Monin, A.S., and A.M. Obukhov, 1954: Main characteristics of the turbulent mixing in the atmospheric surface layer. *Trudy Geophys. Inst. AN SSSR*, **24**, 1553-187

Nakanishi, M., and H. Niino, 2004: An Improved Mellor–Yamada Level-3 Model with Condensation Physics: Its Design and Verification. *Boundary-Layer Meteorology*, **112**, 1–31

Neggers, R. a. J., A. P. Siebesma, and H. J. J. Jonker, 2002: A Multiparcel Model for Shallow Cumulus Convection. *J. Atmos. Sci.*, **59**, 1655–1668

Neggers, R. a. J., A. P. Siebesma, G. Lenderink, and A. a. M. Holtslag, 2004: An Evaluation of Mass Flux Closures for Diurnal Cycles of Shallow Cumulus. *Mon. Wea. Rev.*, **132**, 2525–2538

Neggers, R. A. J., M. Köhler, and A. C. M. Beljaars, 2009: A Dual Mass Flux Framework for Boundary Layer Convection. Part I: Transport. *J. Atmos. Sci.*, **66**, 1465–1487

Nieuwstadt, F. T. M., P. J. Mason, C.-H. Moeng, and U. Schumann, 1993: Large-Eddy Simulation of the Convective Boundary Layer: A Comparison of Four Computer Codes. *Turbulent Shear Flows 8*, F. Durst, R. Friedrich, B.E. Launder, F.W. Schmidt, U. Schumann, and J.H. Whitelaw, Eds., Springer Berlin Heidelberg, 343–367.

Richardson L. F. 1920. The supply of energy from and to atmospheric eddies. Proc. R. Soc. London A 97: 354–373.

Rotta, J.C., 1951: Statistische theorie nichthomogener turbulenz. *Z. Phys.*, **129**, 47-72

Siebesma, A. P., and J. W. M. Cuijpers, 1995: Evaluation of Parametric Assumptions for Shallow Cumulus Convection. *J. Atmos. Sci.*, **52**, 650–666

Siebesma, A. P., 1998: Shallow Cumulus Convection. *Buoyant Convection in Geophysical Flows*, E.J. Plate, E.E. Fedorovich, D.X. Viegas, and J.C. Wyngaard, Eds., *NATO ASI Series*, Springer Netherlands, 441–486

Siebesma, A. P., and Coauthors, 2003: A Large Eddy Simulation Intercomparison Study of Shallow Cumulus Convection. *J. Atmos. Sci.*, **60**, 1201–1219

Siebesma, A. P., P. M. M. Soares, and J. Teixeira, 2007: A Combined Eddy-Diffusivity Mass-Flux Approach for the Convective Boundary Layer. *J. Atmos. Sci.*, **64**, 1230–1248

Soares, P. M. M., P. M. A. Miranda, A. P. Siebesma, and J. Teixeira, 2004: An eddy-diffusivity/mass-flux parametrization for dry and shallow cumulus convection. *Q.J.R. Meteorol. Soc.*, **130**, 3365–3383

Stevens, B., 2000: Quasi-Steady Analysis of a PBL Model with an Eddy-Diffusivity Profile and Nonlocal Fluxes. *Mon. Wea. Rev.*, **128**, 824–836

Stevens, B., and Coauthors, 2005: Evaluation of Large-Eddy Simulations via Observations of Nocturnal Marine Stratocumulus. *Mon. Wea. Rev.*, **133**, 1443–1462

Stull, R. B., 1988: An Introduction to Boundary Layer Meteorology. Kluwer Academic, 666 pp.

Sušelj, K., T. F. Hogan, and J. Teixeira, 2014: Implementation of a Stochastic Eddy-Diffusivity/Mass-Flux Parameterization into the Navy Global Environmental Model. *Wea. Forecasting*, **29**, 1374–1390

Teixeira, J., and S. Cheinet, 2004: A Simple Mixing Length Formulation for the Eddy-Diffusivity Parameterization of Dry Convection. *Boundary-Layer Meteorology*, **110**, 435–453

Teixeira, J., and Coauthors, 2011: Tropical and Subtropical Cloud Transitions in Weather and Climate Prediction Models: The GCSS/WGNE Pacific Cross-Section Intercomparison (GPCI). *J. Climate*, **24**, 5223–5256

Telford, J. W., 1975: Turbulence, entrainment, and mixing in cloud dynamics. *Pure and Applied Geophysics*, **113**, 1067–1084

Troen, I. B., and L. Mahrt, 1986: A simple model of the atmospheric boundary layer; sensitivity to surface evaporation. *Boundary-Layer Meteorol*, **37**, 129–148

Zhang, M. H., and J. L. Lin, 1997: Constrained Variational Analysis of Sounding Data Based on Column-Integrated Budgets of Mass, Heat, Moisture, and Momentum: Approach and Application to ARM Measurements. *J. Atmos. Sci.*, **54**, 1503–1524

Zhang, M. H., J. L. Lin, R. T. Cederwall, J. J. Yio, and S. C. Xie, 2001: Objective Analysis of ARM IOP Data: Method and Sensitivity. *Mon. Wea. Rev.*, **129**, 295–311

Zilitinkevich, S. S., T. Elperin, N. Kleeorin, and I. Rogachevskii, 2007: Energy- and flux-budget (EFB) turbulence closure model for stably stratified flows. Part I: steady-state, homogeneous regimes. *Boundary-Layer Meteorol*, **125**, 167–191